PhD. THESIS

Algorithms and methods for robust geodetic kinematic positioning

Presented by
Julià Talaya i López

Supervised by
Ismael Colomina i Fosch

Tutor
Manuel Hernández-Pajares

Als meus pares,
a la meva dona i als meus fills Alba, Inés i Biel.

Contents

List of Tables

List of Figures

Chapter 1
Introduction

Airborne sensors have always been the fastest way of collecting information in extended areas. However, to produce a cartographic document a certain metric must be fulfilled; therefore, the data collected by airborne sensors must be georeferenced.

The NAVSTAR Global Positioning System, most commonly known as GPS, has played an important role in the development of high precision geodetic positioning techniques. The possibility of using the GPS constellation for kinematic geodetic positioning has provided the geodetic community with a very important tool on its goal to portrait the Earth's shape.

Over the last decade relative precisions of 10–100 mm have often been obtained with kinematic GPS. Nevertheless, the days of measuring the quality of a survey methodology by estimating the precision of some controlled tests are gone. Today, mainly because facts and reality are stubborn, we know that precision without accuracy and reliability serves no serious project.

This work focuses on the reliability of geodetic kinematic GPS positioning. Different algorithms and methods for increasing the reliability of kinematic surveys are presented. An increase in reliability implies better chances of solving correct ambiguity parameters, and more redundancy simplifies the automation of the GPS processing. Automating kinematic GPS processing reduces the need for very well trained GPS operators, as well as operational costs. The number of kinematic GPS positioning users is increasing every yea. In addition, some studies claim that there will be a lack of skilled GPS operators in the near future; companies need to avoid costly (both in terms of time and money) training periods for operators. Hence, kinematic GPS computations should be automated by using robust algorithms. And it is well-known that the key to automation is the use of reliable algorithms and that automation is the goal of every production line, from car factories to mapping companies.

This work also presents some approaches to reduce deployment costs and provide flexibility when planning a survey by using existing permanent GPS stations having a low recording rate in high dynamics kinematic GPS positioning.

1.1 Applications of geodetic kinematic positioning

Earth observation sensors have been widely used by the cartographic community to map different aspects of the Earth. In this section, some of the most commonly used mapping and geodetic airborne techniques are described to illustrate the state-of-the-art of kinematic GPS positioning through its application in sensor orientation.

1.1.1 Aerial triangulation

Aerial photography is nowadays the usual way to start the production of medium-large scale maps. A map is produced by taking observations of stereoscopic models formed by aerial photograph stereopairs. In order to preserve the metrics, the photographs forming the stereopairs must be orientated in the mapping coordinate system.

The orientation of a metric photograph is achieved by determining the coordinates of the exposure center and their attitude at the moment the photograph is taken. Aerial triangulation consists in determining the orientation parameters of a block of aerial images by using as observations the photo measurements from a set of points and the coordinates from a subset of these points called ground control points.

GPS has made three main contributions to airborne aerial triangulation: airplane navigation, determination of ground control points and determination of the projection center of images. The last one implies the use of high precision kinematic positioning.

The aerial camera provides an electrical pulse at the time of frame exposure; the GPS receiver tags the electrical signal in order to know (in GPS time) the instant at which the photograph has been taken. Once a high precision trajectory has been computed, the antenna position is interpolated at the mid-exposure time recorded by the GPS receiver. The coordinates of the antenna and the vector antenna-camera projection center are included as observations in a combined block adjustment to assist with the global determination of photo orientation parameters. The use of kinematic GPS in aerial triangulation results in a dramatic decrease in the number of ground control points when compared with classical aerial triangulation [Col89, Fri90, CHTT92, Col93, AS93].

In aerial triangulation supported by GPS, the derived GPS trajectory has some external redundancy coming from photogrammetric observations. This redundancy makes the technique very robust (in fact some systematic GPS errors can be corrected in the combined block adjustment by some parameters called drift parameters.) However, aerial triangulation supported by GPS is an exception. The rest of the applications described in this section does not have any generalized external redundancy.

1.1.2 Pushbroom sensors

As explained above, the goal of aerial triangulation is the determination of external orientation parameters. Aerial triangulation obtains external orientation parameters indirectly taking advantage of the fact that the geometry of a frame image has been frozen at the moment the image has been taken. However, there are certain types of sensors that collect information from a linear sensor containing a vector of pixels perpendicular to the line of flight and covering the area by means of the movement of the airplane while it is flying. These sensors are called pushbroom sensors or linear sensors. In the case of linear sensors, the images can be considered supraimages formed by merging hundreds or thousands of single line images. The geometry of those images is much more complex because the orientation of each single linear image must be determined prior to reconstructing the cartographic document. The orientation of these sensors is achieved by directly measuring the orientation parameters during the flight [AT00]. These sensors are hard or even

impossible to orient using indirect methods such as aerial triangulation.

The direct determination of orientation parameters (also called direct georeferencing) combines the use of inertial sensors with high precision GPS kinematic positioning. With some simplifications, it can the thought that the projection center of each line image is derived from the high precision GPS trajectory while the attitude of each line image is obtained from the gyroscopes of the inertial system attached to the head of the image sensor.

Direct georeferencing may also be used to orient frame images directly without the help of aerial triangulation [Col99]. The main advantage of using direct orientation instead of aerial triangulation is a reduction in the manpower needed to orient a project and a reduction in processing time.

On the other hand, the main disadvantage of direct georeferencing (either for pushbroom sensors or photo orientation) is that the determination of the image/line projection center mainly relies on the derived GPS trajectory; therefore, the reliability of the kinematic GPS trajectory determination is a very important issue to be addressed.

1.1.3 Mobile mapping

Mobile mapping is a technique for gathering geographical information, such as natural landmarks and the location of roads, from a moving vehicle. The developments in digital cameras, GPS and Inertial Measurement Units (IMU) positioning have led to an easier, cheaper and more accurate mobile mapping technology.

Mobile mapping surveys can be based on digital image stereopairs taken along a road. These images need to be oriented in order to extract georeferenced information from photographs. If a vehicle is collecting information at 60 km/h and a pair of images is taken every 10 m, then more than 60,000 images would be taken during a 5 hour survey. It is clear that such a high number of images cannot be oriented by using an indirect method such as aerial triangulation. The solution is to orient the images directly by integrating GPS and IMU systems.

In mobile mapping, the required accuracy can be less critical than in the case of the aerial sensors (due to the fact that the mapped objects are closer in mobile mapping than in aerial mapping surveys.) Nevertheless, the working environment can be much tougher and unpredictable than in any aerial survey. The GPS/IMU integration to georeference is based on the use of the accurate position provided by GPS to calibrate the accelerometers and gyroscopes of the inertial measurement unit. If there is a gap in the precise positioning given by GPS, then the sensors from the IMU cannot upgrade the calibration parameters and the overall orientation starts to degrade. Depending on the quality of the IMU and on the orientation requirements of the mobile mapping survey, the maximum GPS gaps that the system can tolerate range from a few seconds to a few minutes. A GPS receiver over a vehicle doing a survey will suffer satellite signal blockage or heavy multipath from the buildings and trees surrounding the roads and streets. In these circumstances, it is clear that mobile mapping users will need robust algorithms for facilitating GPS positioning of their vehicles.

1.1.4 Airborne gravimetry

Geoid determination has been one of the major challenges in geodesy in the last few centuries. There are several ways of determining the geoid. One of the most usual is by using gravity measurements. However, terrestrial gravity measurements are a very slow and expensive technique, especially in mountainous and forest areas. Airborne gravity measurements have been pursued for several years, but this technique did not really succeed until the advent of kinematic GPS positioning.

The effect of the gravity field can be observed either by a very expensive airborne gravimetry sensor, such as LaCoste&Romberg, or by a more affordable strapdown IMU. Some studies show that it is possible to obtain gravity anomalies at the level of 1-3 mGal [SW94, SLW94, Bru00]. The main idea is that gravity sensors recover the combined effect of vertical acceleration resulting from aircraft vertical motion and the Earth's gravity while high precision kinematic GPS positioning will be able to recover vertical acceleration resulting from the aircraft vertical motion. Thus, a smart combination of both allows the Earth's gravity field to be recovered.

Very precise kinematic GPS positioning is also used in the GRACE (Gravity Recovery and Climate Experiment) twin satellite mission, where the accuracy of the orbital position is at the 2–3 cm level, (for more details, see [DBBS+03]).

1.2 Precise positioning in real life applications: the actual state-of-the-art

Geodetic kinematic positioning has given an answer to the requirements of the above applications, at least locally. However, when looking at the state-of-the-art in kinematic positioning, one realizes that the unsolved problems are related to reliability and operational issues rather than precision.

Small errors in the model such as small cycle slips in phase observations or fixing ambiguity parameters to erroneous values can lead to wrong trajectories that may differ up to 0.5 m from the correct solution with formal errors below the decimeter. These solutions can be very dangerous because errors can propagate to the whole survey. Thus, in a production environment, GPS positioning robustness can be considered as the limiting factor of the survey, especially when it is not possible to check the results against an independent reference. That is the case of GPS/INS direct orientation.

Several works have shown very good precisions at long distances from reference stations [Han97], [CHPJ+99], [RL97]. However, all the prerequisites needed (setting up a network of permanent GPS stations, availability of external atmospheric models, accessibility to precise orbits, stations measuring at the same record interval ...) can be difficult to fulfill in real life applications. In the presence of bad GPS constellations, those techniques may lead to biased solutions; therefore, it is very important to make sure that everything possible has been done to guarantee the accuracy of the estimated trajectory.

The automation of GPS trajectory determination is not an easy task. On the contrary, there are several variables in a survey that (even if the survey has been carefully planned)

make very difficult to ensure a priori that a mission will be successfully computed, especially in medium and long range missions.

In centers where high precision kinematic trajectories are computed (such as Institut Cartogràfic de Catalunya), it is well-known that the processing of a kinematic survey is not an automatic calculation. The data must be analyzed by highly skilled experts with extensive knowledge of kinematic GPS processing in order to obtain a reasonably good trajectory. During the tuning of processing parameters, the specialist must change the value of the parameters related to the cutoff angle, eliminate satellites, force a new ambiguity resolution process ... As said above, parameter tuning and recomputations have two main consequences: the operator performing the high precision kinematic computation must be a well-trained specialist, and the determination of rover receiver trajectories takes a non negligible amount of time. In real life projects, both situations can be problematic.

The solution to these problems is to automate GPS trajectory determination as much as possible and, as discussed before, the key to automation is reliability. A better reliability and robustness in the algorithms allow problems to be more easily detected and, as a consequence, less interaction in the process.

By increasing reliability and automating kinematic GPS computations the time and resources needed to develop a project will be reduced.

Nowadays, as a result of the extensive use of the Internet, there are some attempts to offer Internet-based processing of GPS surveys. Several systems are already in operation for static measurements, but there is a great interest in extending the services to kinematic GPS surveys. These services can only be provided if a high degree of automation is obtained, and this is only possible with robust and reliable algorithms for GPS kinematic processing.

1.3 Contributions of this dissertation

The scope of this work does not extend to an increase in accuracy of kinematic GPS surveys, given that the developments in algorithms in the latter years have covered this issue quite satisfactorily.

The contributions of this dissertation are related to an increase in reliability of kinematic GPS processing. In real life projects, the use of more reliable algorithms and methods results in fewer interactive computations and lower probability of repeating expensive aerial surveys, and allows less skilled operators to carry out the process. The new ideas, algorithms and methodology presented in this work can be summarized as follows:

- Several ideas are presented to increase the amount of information available in kinematic GPS processing, such as using several reference stations, dynamical models for the ionosphere, global processing ... Although some of these ideas have also been presented previously, a study of the impact on the reliability of surveys has been done.

- A novel approach to use multiple kinematic receivers without adding new position parameters by making use of inertial measurements is presented. Their impact on

reliability increase has also been proven.

- In aerial surveys, GPS kinematic positioning is generally used for georeferencing data taken by airborne sensors. The use of the data observed by these sensors for facilitating GPS positioning is also part of the study. The integration of oriented photogrammetric pairs or laser distance measurements together with kinematic GPS positioning have been investigated, and have been proved very helpful in real life projects.

- Finally, the increase in reliability in new constellation scenarios (modernized GPS and Galileo) has also been analized in order to know what the situation in future scenarios will be like.

1.4 Structure of the thesis

The first part of the thesis covers Chapters 2-5, where the fundamentals of GPS processing are explained.

In Chapter 2, the principal models for GPS positioning are described together with the most usual systematic errors that can affect a kinematic survey.

Chapter 3 covers the delay that affects GPS signals when traveling through the troposphere. Some of the ways to correct that delay are also presented.

Similarly, Chapter 4 deals with the delay of GPS signals when crossing the dispersive part of the atmosphere, called ionosphere.

The basic issues covering internal and external reliability of GPS phase trajectories are explained in Chapter 5.

The main part of the work is presented in Chapters 6-8 of this thesis.

In Chapter 6, some procedures and algorithms for increasing the reliability of kinematic GPS positioning are presented.

The use of external information from oriented sensors for increasing reliability is presented in Chapter 7.

The increase in reliability when the new forth coming scenarios (modernized GPS and Galileo) are a reality is treated in Chapter 8.

Finally, the conclusions and recommendations of the work are presented in Chapters 9 and 10.

A GPS kinematic processing software has been developed to do the research presented in this thesis. The last part of the thesis contains appendix A, where the main characteristics of the software are presented.

Chapter 2
Kinematic GPS positioning

From a geodetic standpoint, the NAVSTAR-GPS is a satellite-based one-way dual-band ranging system in the L band [PS95b]. A geodetic GPS receiver delivers code and phase observations from carrier signals generated by the GPS satellites at two different frequencies f_1 and f_2

$$f_1 = 154 \times 10.23 \text{ MHz} \approx 1.57 \text{ GHz}, \; f_2 = 120 \times 10.23 \text{ MHz} \approx 1.23 \text{ GHz}$$

and whose corresponding wavelengths are

$$\lambda_1 \approx 19.0 \text{ cm}, \; \lambda_2 \approx 24.4 \text{ cm}.$$

The observations are usually referred to as L1 and L2, respectively. Two codes, C/A and P, are modulated on L1 but only the P code is modulated on L2. A navigation message containing the satellite ephemeris and the satellite clock correction parameters is also transmitted.

The GPS receiver generates a replica of the code and measures the time offset between transmission and reception of the code. This time offset multiplied by the speed of light is usually called pseudorange, code range or, simply, code observation. A more precise – though less accurate or ambiguous– observable is the carrier phase; the receiver generates a signal at the nominal frequency of the carrier phase, and then compares it to the signal received from the satellite which is not constant because of the Doppler effect induced by the relative satellite-receiver motion. The integrated Doppler shift over time is the carrier phase observable. It is worth mentioning that the original designers of the NAVSTAR-GPS program did not foresee that the integrated Doppler shift of the nominal frequency would be employed as a useful observable for high precision positioning. The carrier phase observable has no time transmission information; consequently it is affected by a bias (the initial ambiguous integer number of carrier frequency cycles is called initial ambiguity.) These ambiguities remain constant as long as the receiver maintains the lock with the satellites. The carrier phase observable plus the initial ambiguity may be ideally represented by the distance in cycles between the satellite and receiver antennas [TK98].

2.1 Models for GPS positioning

A family of closely related models for L1, L2, code and phase observations has been developed in the geodetic community [WBD+87], [HWLC94], [Lei90]. We consider here the following model for satellite s and receiver r. Concerning the notation used, a superindex

ρ_r^s (km)	$\delta\rho_r^s$ (m)	$c \cdot \delta t^s$ (m)	τ_r^s (m)	$I_r^s f_i^{-2}$ (m)	$d\rho_r^s$ (m)	multipath (m)	(m)
20200 (zenith)	2.5-10 (broadcast)	10-70 • 1 ∗	2 (zenith)	2-10 (zenith)	10	0.3-3 P	<.05 Φ

• SA on ∗ SA off

Table 2.1: Typical magnitude and variation intervals for GPS model parameters [PS95a].

s in a parameter represents that this parameter refers to a satellite s, and a subindex r in a parameter represents that this parameter refers to a receiver r.

$$\begin{array}{rcllll} \lambda_1\Phi_{1r}^s &=& \rho_r^s + c(\delta t^s - \delta T_r) + \tau_r^s & -I_r^s f_1^{-2} & +\lambda_1(N_{1r}^s + \varphi_r(t_0) - \varphi^s(t_0)), & \\ \lambda_2\Phi_{2r}^s &=& \rho_r^s + c(\delta t^s - \delta T_r) + \tau_r^s & -I_r^s f_2^{-2} & +\lambda_2(N_{2r}^s + \varphi_r(t_0) - \varphi^s(t_0)) & -d\rho_r^s \quad +b_{1r}, \\ C_{1r}^s &=& \rho_r^s + c(\delta t^s - \delta T_r) + \tau_r^s & +I_r^s f_1^{-2} & & +b_{2r}, \\ P_{2r}^s &=& \rho_r^s + c(\delta t^s - \delta T_r) + \tau_r^s & +I_r^s f_2^{-2} & & -d\rho_r^s \quad +b_{3r}, \end{array} \tag{2.1}$$

where Φ_{1r}^s, Φ_{2r}^s are the measured carrier phases and C_{1r}^s, P_{2r}^s are the measured code ranges ($\lambda_1 \cdot \Phi_{1r}^s$ and $\lambda_2 \cdot \Phi_{2r}^s$ are the carrier phase observations expressed in the same units as the pseudoranges, and may be regarded as a biased pseudorange observation;) ρ_r^s is the distance between the satellite and receiver antennas including the model for the satellite orbit; c is the speed of light in a vacuum, and δt^s, δT_r the satellite and receiver clock error, respectively; τ_r^s is the frequency independent effect of tropospheric refraction; $I_r^s f_1^{-2}$, $I_r^s f_2^{-2}$ are the first order ionospheric errors; N_{1r}^s, N_{2r}^s are the so-called integer ambiguities (integer number of cycles), and $\varphi_r(t_0)$, $\varphi^s(t_0)$ are the initial fractional phase error terms; $d\rho_r^s$ is the differential range between the L1 and L2 phase centers; b_{1r}, b_{2r} and b_{3r} are interchannel bias terms accounting for the synchronization errors of the four observations. In equations 2.1, ρ_r^s may be also written as

$$\rho_r^s = \sqrt{(X_r - X^s - \delta X^s)^2 + (Y_r - Y^s - \delta Y^s)^2 + (Z_r - Z^s - \delta Z^s)^2},$$

where (X_r, Y_r, Z_r) are the coordinates of the receiver antenna, (X^s, Y^s, Z^s) the coordinates of the satellite and $(\delta X^s, \delta Y^s, \delta Z^s)$ the possible errors of (X^s, Y^s, Z^s). In equations 2.1, ρ_r^s does not explicitly show terms for the multipath effects. It must be noted that the terms reflecting the noise of the four observed amounts are not included. Noise for phase ranges $\lambda_1 \cdot \Phi_{1r}^s$, $\lambda_2 \cdot \Phi_{2r}^s$ is at the millimeter level, for C/A-code ranges is at the meter level (although it can be better using phase smoothing techniques, [Hat82]) and for P-code ranges can be better than 0.2 m.

Typical magnitudes for some GPS model parameters are given in table 2.1, where $\delta\rho_r^s$ stands for the ephemeris error ($\delta\rho_r^s = \sqrt{\delta X^{s2} + \delta Y^{s2} + \delta Z^{s2}}$). It is known that the terms

$\varphi_r(t_0)$, $\varphi^s(t_0)$, though usually unknown, are stable at the nanosecond level [TK98]. The terms b_{1r}, b_{2r} and b_{3r} are the same for the different channels of the receiver [GY95].

The usual rule of thumb for a single observer equipped with a GPS receiver reads: by tracking at least four satellites simultaneously, it is possible to solve for the four unknowns $(X_r, Y_r, Z_r, \delta T_r)$ with an accuracy (comparing the computed and the real position of the observer) of about 10 m for X_r, Y_r ,Z_r and 30 ns for δT_r. The statement holds for a determination of the parameters X_r, Y_r ,Z_r, δT_r from a particular estimation model derived from equations 2.1. An estimation model may range from a very simplified version of equations 2.1 to the whole set of equations. The estimation model depends on the type and amount of available information/data and the type of positioning task. Thus, for a single observer performing GPS positioning in real time, the actual values of some of the parameters in the model are not known, and must therefore be predicted, approximated or even neglected, which leads to the 10 m and 30 ns mentioned above.

2.2 Differential positioning with GPS

Some of the parameters present in equations 2.1 are spatially correlated. That is the case of ionospheric, tropospheric, and ephemeris modeling parameters. Note also that δt^s –the satellite clock error– does not depend on the receiver. If there is an interest in positioning, a usual way to deal with the above parameters is either to approximate them with a priori known data or to cancel them by collecting GPS data simultaneously at a close –well surveyed– reference point. This is known as DGPS (Differential GPS), and the underlying principle is that close points are affected by nearly the same errors. In formulas, DGPS positioning is carried out by performing the so-called single or first differences between observations [WBD+87]. First differences for satellite s and receivers, say, 1 and 2 are usually written with the help of the Δ operator

$$\Delta \bullet^s_{1,2} = \bullet^s_2 - \bullet^s_1,$$

where $\bullet^s_r$, $\bullet^s_r$ stand for any of the expressions of equations 2.1 for $r = 1, 2$:

$$\begin{aligned}
\lambda_1 \Delta\Phi^s_{1_{1,2}} &= \Delta\rho^s_{1,2} - c\Delta\delta T_{1,2} + \Delta\tau^s_{1,2} - \Delta I^s_{1,2} f_1^{-2} + \lambda_1(\Delta N^s_{1_{1,2}} + \Delta\varphi_{1,2}(t_0)), \\
\lambda_2 \Delta\Phi^s_{2_{1,2}} &= \Delta\rho^s_{1,2} - c\Delta\delta T_{1,2} + \Delta\tau^s_{1,2} - \Delta I^s_{1,2} f_2^{-2} + \lambda_2(\Delta N^s_{2_{1,2}} + \Delta\varphi_{1,2}(t_0)) \\
&\quad -\Delta d\rho^s_{1,2} + \Delta b_{1_{1,2}}, \\
\Delta C^s_{1_{1,2}} &= \Delta\rho^s_{1,2} - c\Delta\delta T_{1,2} + \Delta\tau^s_{1,2} + \Delta I^s_{1,2} f_1^{-2} + \\
&\quad \Delta b_{2_{1,2}}, \\
\Delta P^s_{2_{1,2}} &= \Delta\rho^s_{1,2} - c\Delta\delta T_{1,2} + \Delta\tau^s_{1,2} + \Delta I^s_{1,2} f_2^{-2} - \\
&\quad \Delta d\rho^s_{1,2} + \Delta b_{3_{1,2}}.
\end{aligned} \tag{2.2}$$

Notice that parameters δt^s and $\varphi^s(t_0)$ vanish when single differences between receivers are formed. If the distance between the receivers is small (10–20 km), the single difference ionospheric, tropospheric and ephemeris errors $(\Delta I^s_{r1,r2}, \Delta\tau^s_{r1,r2}, \Delta\delta\rho^s_{r1,r2})$ are also small; hence, they can be neglected. In such cases, the integer ambiguities may be easily solved.

However, if the distance between receivers is longer, the residual error parameters cannot be neglected and must be taken into account.

In positioning, most times it is of no interest to solve for the single difference receiver clock error parameter $\delta T_{1,2}$ $(= \delta T_2 - \delta T_1)$, and so double differences can be performed. Double difference observations may be obtained by differentiating two single difference observations, each involving the same pair of receivers but different satellites. Double difference observations, which involve receivers i, j and satellites 1, 2, are expressed with the $\nabla\Delta$ operator

$$\nabla\Delta\bullet_{i,j}^{1,2} = \Delta\bullet_{i,j}^{2} - \Delta\bullet_{i,j}^{1}\,.$$

Then, after double differencing, equations 2.2 becomes

$$\begin{array}{rcll}
\lambda_1\cdot\nabla\Delta\Phi_{1_{1,2}}^{1,2} &=& \nabla\Delta\rho_{1,2}^{1,2} + \nabla\Delta\tau_{1,2}^{1,2} - \nabla\Delta I_{1,2}^{1,2} f_1^{-2} + \lambda_1\cdot\nabla\Delta N_{1_{1,2}}^{1,2}, & \\
\lambda_2\cdot\nabla\Delta\Phi_{2_{1,2}}^{1,2} &=& \nabla\Delta\rho_{1,2}^{1,2} + \nabla\Delta\tau_{1,2}^{1,2} - \nabla\Delta I_{1,2}^{1,2} f_2^{-2} + \lambda_2\cdot\nabla\Delta N_{2_{1,2}}^{1,2} & -\nabla\Delta d\rho_{1,2}^{1,2}, \\
\nabla\Delta C_{1_{1,2}}^{1,2} &=& \nabla\Delta\rho_{1,2}^{1,2} + \nabla\Delta\tau_{1,2}^{1,2} + \nabla\Delta I_{1,2}^{1,2} f_1^{-2}, & \\
\nabla\Delta P_{2_{1,2}}^{1,2} &=& \nabla\Delta\rho_{1,2}^{1,2} + \nabla\Delta\tau_{1,2}^{1,2} + \nabla\Delta I_{1,2}^{1,2} f_2^{-2} & -\nabla\Delta d\rho_{1,2}^{1,2}.
\end{array} \tag{2.3}$$

Performing single or double differences is a particular approach for taking advantage of the high correlation between some parameters in equations 2.1. Rather than eliminating (or gathering) these auxiliary parameters (receiver time error, instrumental delays, satellite time error, atmospheric delays $\cdots$), it is possible to estimate them. There are basically two approaches, a global approach and a local one. The global approach makes use of GPS observations spread all over the world (there is a continuous track of the satellites during the whole orbit), and some of the receivers are synchronized with an atomic clock. The strength of this set of observations makes possible a robust estimation of all the parameters present on the undifferenced equations 2.1. The local approach makes use of external information (precise ephemerides and precise satellite clocks) to solve the auxiliary parameters present on the undifferenced GPS observation model. There is a positioning technique called PPP (Precise Point Positioning) based on the undifferenced model where the positioning of a single dual frequency GPS receiver is computed using precise ephemerides and precise satellite clocks. By using PPP and positioning services based on this principle, it is possible to obtain a 10–20 cm precision in position but the lock with the satellites must be maintained for a minimum of 10–20 minutes to allow the atmospheric parameters to converge [MBSBS01], [HSG]. This restriction makes these techniques very unstable for kinematic positioning.

The ionosphere, troposphere and receiver clock parameters $(I_{ir}^{s}(t), \tau_r^s(t), \delta T_r(t))$ exhibit high temporal correlations. Hence, they can be treated as stochastic parameters in a stochastic dynamic system. These parameters will be discussed in detail in sections 3 and 4. Today, research is focused on tropospheric and ionospheric modeling; therefore, greater knowledge of signal propagation can be expected within the next few years.

In equations 2.3, the terms $\nabla\Delta N_{1_{1,2}}^{1,2}$, $\nabla\Delta N_{2_{1,2}}^{1,2}$ are referred to as the double difference ambiguities or the double difference phase integers, and play a key role in geodetic

positioning. If these parameters are solved correctly, the phase observations can be considered as highly accurate and precise pseudorange observations allowing for an accurate and precise kinematic positioning.

2.2.1 Linear phase combinations

Apart from single differences and double differences between observations of the same type, it is also possible to create linear combinations of different types of observables. Because of the dispersive nature of the ionosphere (its effect depends on the frequency of radio waves), a linear combination between the L1 observable and the L2 observable can eliminate the first order effect of the ionospheric delay. If we multiply the first equation in 2.1 by $\frac{f_1^2}{(f_1^2-f_2^2)}$ and subtract the second equation in 2.1 multiplied by $\frac{f_2^2}{(f_1^2-f_2^2)}$, we will end with a ionospheric free equation.

$$\begin{aligned}\lambda_3 \cdot \Phi_3 \quad = \quad & \rho_r^s + c \cdot (\delta t^s - \delta T_r) + \tau_r^s \qquad + \lambda_1 \cdot (N_{1r}^s + \varphi_r(t_0) - \varphi^s(t_0)) \cdot \tfrac{f_1^2}{(f_1^2-f_2^2)} \\ & + d\rho_r^s \cdot \tfrac{f_2^2}{(f_1^2-f_2^2)} - b_{1r} \cdot \tfrac{f_2^2}{(f_1^2-f_2^2)} \quad - \lambda_2 \cdot (N_{2r}^s + \varphi_r(t_0) - \varphi^s(t_0)) \cdot \tfrac{f_2^2}{(f_1^2-f_2^2)}.\end{aligned} \tag{2.4}$$

However, ionospheric free linear combinations are not the only application for linear phase combinations; in fact, different wavelengths of linear phase measurements can be used to determine the ambiguities. According to [Wüb89], the linear combination.

$$\Phi_{n,m}(t) = n\Phi_1(t) + m\Phi_2(t), \tag{2.5}$$

will have an associated wavelength

$$\lambda_{n,m} = \frac{c}{(nf_1 + mf_2)}, \tag{2.6}$$

and the integer ambiguity of the linear –not necessarily integer– phase combination will be the linear combination of the original ambiguities.

The most useful linear phase combinations used in geodetic positioning together with the associated wavelength, ionospheric scale factor V_I and the propagated noise $\sigma_{n,m}$ are shown in table 2.2 (the notation of the table is defined in equations 2.5 and 2.6.)

Linear phase combinations such as wide laning can be very useful in ambiguity resolution. If L1 and L2 phase observations are available, then the synthetic observation $L_{widelane}$ can be used in the processing instead of L1 and L2. The formal wavelength of this combination is $\approx$ 86 cm, about 4 times larger than L1 (that is why it is called wide lane combination.) Wide lane combination reduces tropospheric and ionospheric effects. However, the noise of the wide lane phase combination is six times greater than the noise of the L1 observable. Another problem of using wide lane as the final observable is that the user needs to lock at a minimum of 4 satellites simultaneously on L1 and L2 frequencies. The L2 GPS signal is weaker than the L1 signal (especially after the AS has been activated), and any loss of lock of L2 would not allow the L1 observable to be used, even if it were available. These characteristics result in extensive use of the wide lane

Signal	n	m	$\lambda_{n,m}$ cm	V_I	$\sigma_{n,m}$ mm
$L1$	1	0	19.0	0.779	3.0
$L2$	0	1	24.4	1.283	3.9
$L_{widelane}$	1	-1	86.2	-1.000	19.4
$L_{narrowlane}$	1	1	10.7	1.000	2.1
$L_{ionfree}$	–	–	≈ 5.4	0.000	10.0

Table 2.2: Linear combination of carrier phases ([See93]).

combination in intermediate steps of ambiguity resolution strategies but not as the final observable.

2.2.2 Observation synchronization

The time scale on a GPS receiver is based on inexpensive quartz clocks and the fact that simultaneous code observations of four satellite allows the clock offset to be computed between receiver time and GPS time (δT_r in equations 2.1). The quartz clock present on high precision GPS receivers can have a drift of 1 millisecond in 15 minutes, while the receiver clock offset (δT_r in 2.1) can be computed by the receiver with an accuracy of 30 nanoseconds.

Most GPS receivers make all their internal tasks based on the receiver time (internal clock). Consequently, in order to synchronize them with GPS time, the receiver keeps computing the receiver clock offset, and when the offset reaches a magnitude of 1 ms, the receiver will align its internal clock to GPS time. If a GPS receiver is collecting data at 1Hz, it will record the observations based on the receiver time, and therefore the observations will be synchronized to receiver time and not to GPS time. The observations will show some jumps at the time the receiver is aligning its internal clock to GPS time. Figure 2.1 shows a receiver clock offset (δT_r in equations 2.1) from a high quality GPS receiver. The receiver clock shows a drift that is aligned when the difference with GPS time is bigger than 1 millisecond.

Differential positioning with GPS is based on single differences formed between receivers (see equations 2.2). Single differences between receivers can be formed if both sets of observations are synchronized because most of the parameters that are cancelled out have a time dependency. As explained above, most GPS receivers take observations that are synchronized with GPS time at the millisecond level. These observations must be synchronized in a preprocessing step at a higher accuracy level. The correction applied to the synchronization preprocessing is derived from the receiver time offset and Doppler observations (sometimes Doppler observations must be derived from phase observations):

$$\Phi_r^s(t) \quad = \quad \Phi_r^s(t_r - \delta_r), \tag{2.7}$$

where

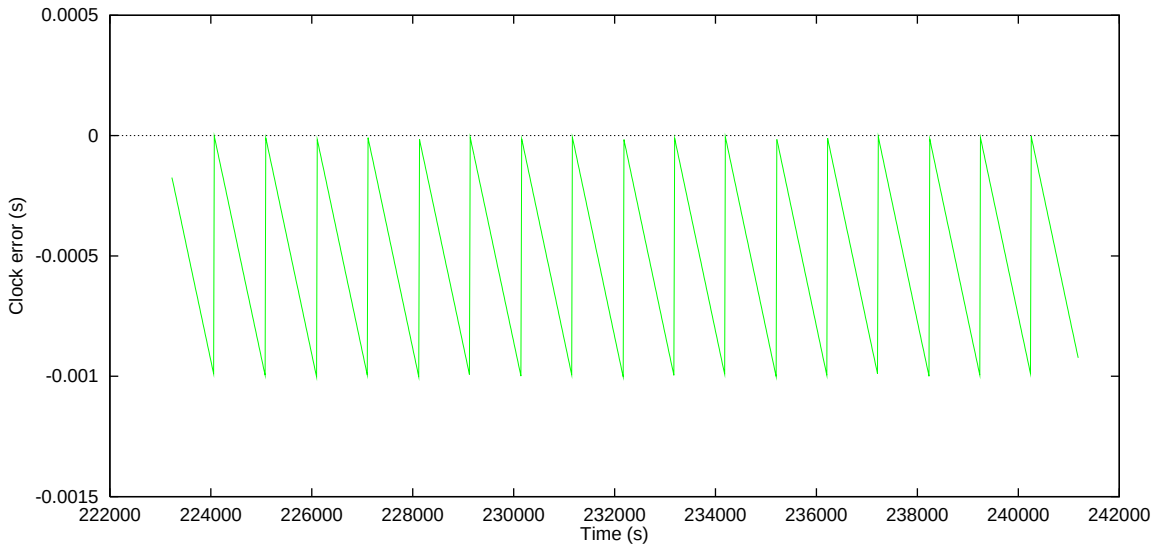

Figure 2.1: Receiver clock error.

$$\begin{aligned} \Phi_r^s(t) &= \text{phase observation at time t (GPS time),} \\ \delta_r &= \text{receiver clock error at time t,} \\ t_r &= \text{receiver time when the observation is taken.} \end{aligned} \tag{2.8}$$

Using a Taylor series development, we obtain

$$\Phi_r^s(t) = \Phi_r^s(t_r) - \dot{\Phi}_r^s(t_r) \cdot \delta_r, \tag{2.9}$$

where

$$\dot{\Phi}_r^s(t_r) = \text{Doppler observation at receiver time } t_r. \tag{2.10}$$

It must be pointed out that due to the high relative velocity between the GPS receiver and GPS satellite, the Doppler observation can reach 3000–4000 cycles in one second. Thus, an offset of 1 millisecond between GPS time and receiver time can lead to a 3–4 cycle correction on the phase observation. Figure 2.2 shows the magnitude of the phase observation for a given satellite during the same period shown in figure 2.1.

2.2.3 Cycle slip detection/correction

Another important assumption about the models used in differential positioning with GPS is that data is free from cycle slips. A cycle slip occurs when the receiver loses lock with a satellite signal. When a cycle slip is present, then carrier phase ambiguity is no longer a constant and either it must be repaired or a new ambiguity parameter must be determined. If the cycle slip is not identified, model 2.1 will no longer be true and a systematic error will be present in the trajectory determination.

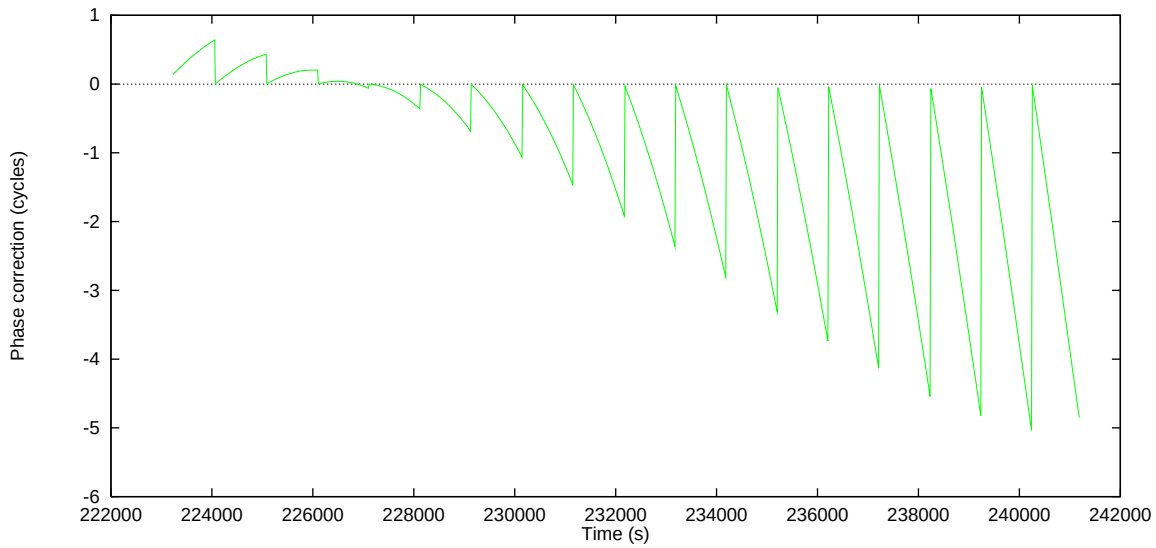

Figure 2.2: Carrier phase correction.

A cycle slip can be due to several different reasons: obstructions between the antenna and the signal path, high signal noise due to multipath or when signals from a low elevation satellite are received, interference, or receiver signal processing. Cycle slips caused by antenna obstructions are usually very easy to detect because they are a few thousands of cycles wide. However, cycle slips due to multipath and receiver signal processing can be only 1 or 2 cycles wide and are, therefore very difficult to detect, especially in kinematic operation modes.

There is a number of methods for detecting cycle slips. The usual procedures are based on the analysis of double differences, ionospheric residuals and code and carrier phase combinations. In these analysis, either a low degree polynomial is fitted to a time series of data or a dynamic model is used to detect discontinuities on phase observations.

Misdetected cycle slips are one of the most dangerous errors in GPS processing. If a cycle slip is not detected, then equations 2.3 are no longer true (since the ambiguity parameter $\nabla\Delta N^{1,2}_{2_{1,2}}$ should be corrected by the magnitude of the uncorrected cycle slip) and we are in the presence of a model error. In these cases the nominal precision of the survey, as predicted by traditional least-square estimation, will be optimistic. In Chapter 5, the ability of a survey to detect error models is described.

2.2.4 Ambiguity resolution

When a receiver locks to a GPS satellite, the initial phase observation contains an arbitrary number of whole phase cycles, i.e. the ambiguity parameters. According to equations 2.3, if four or more satellites are observed and the ambiguity parameters $(\nabla\Delta N^{i,j}_{1_{i,j}}, \nabla\Delta N^{i,j}_{1_{i,j}})$ are solved, a highly accurate antenna trajectory can be computed because the value $\lambda_1 \cdot \nabla\Delta\Phi^{1,2}_{i_{1,2}} - \lambda_1 \cdot \nabla\Delta N^{1,2}_{i_{1,2}}$ can be considered as a very precise pseudorange observation ($\sigma \approx$ few mm). The ambiguity parameters remain constant as long as the GPS receiver maintains the lock with the GPS satellite.

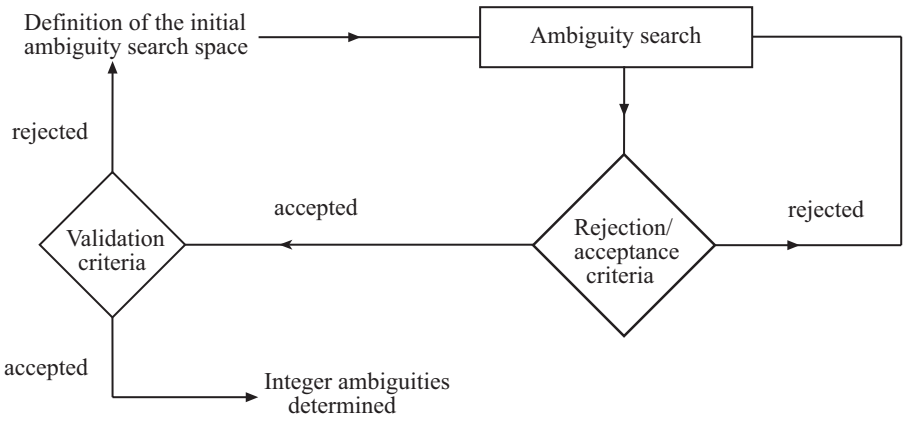

Figure 2.3: Strategy for OTF ambiguity resolution.

In short and medium distance static differential GPS positioning, where the receiver remains in the same position and observes a significant change on the satellite constellation geometry during the survey, the isolation of the integer ambiguity parameters from various errors and bias present in the observations is relatively feasible. However, in a kinematic survey the ambiguity parameters must be solved OTF (On-The-Fly) while the receiver is in motion, which is far more difficult.

As the ambiguity parameters remain constant, one may argue that the ambiguities can be solved at the beginning of the survey by performing a static session and, once the ambiguities are solved, start the kinematic mission. This statement is correct, but in real life applications, the success of the mission cannot rely on the receiver to be always tracking four or more satellites, particularly in an airborne/maritime survey, where it is not possible to restart the survey if the lock to the satellites signals is lost.

Although there are various techniques for OTF ambiguity resolution, as explained in [Abi93], they use a rather similar strategy for resolving ambiguities based on an approximation of the ambiguity parameters and their covariances. The strategy defines an ambiguity search space that is expected to contain the true ambiguity; then, the algorithm searches for the correct ambiguity applying a certain acceptance and rejection criteria, and the search process is stopped after some validation criteria are fulfilled. Different OTF algorithms apply different validation, rejection and assurance criteria. The standard strategy is displayed in figure 2.3.

As explained in 2.2.1, the use of a phase combination between L1 and L2 to increase the wavelength makes the ambiguity resolution easier.

In figure 2.4, the formal error of a kinematic survey is shown. The formal positioning error without fixing the ambiguity parameters to their integer value (their values are estimated as a real value) can be seen on the left side of the plot. As more data is available, the estimation of the ambiguity parameters is better, and therefore the formal error converges to zero. At a certain number of epochs, the information available is enough to determine the integer value of the ambiguity parameters. After fixing the ambiguities to their correct value, the formal position error makes a big improvement and remains

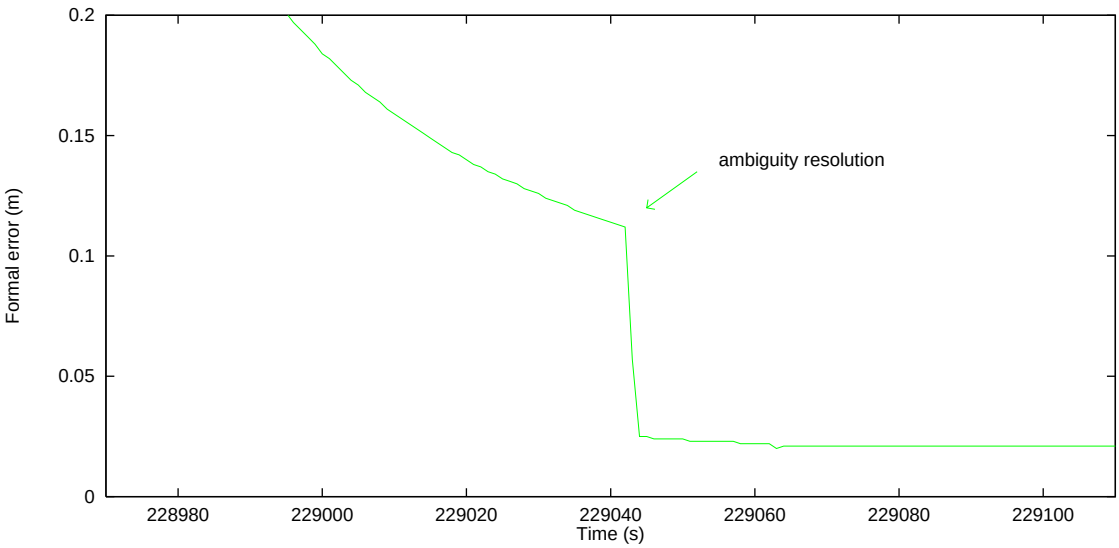

Figure 2.4: Formal error before and after ambiguity resolution.

constant for the rest of the survey at the level of the double difference carrier phase noise.

2.2.5 Ambiguity dilution of precision

Carrier phase ambiguity resolution is needed for high precision GPS positioning. Whatever the processing strategy used, at certain instant the ambiguity solving algorithm must be launched. As explained in 2.2.4, OTF algorithms are based on estimated ambiguity parameters and their covariances. A measure of the strength with which one can expect to have a successful resolution and validation of the ambiguities was introduced in [TO97]. The measure was called ADOP (Ambiguity Dilution Of Precision) and is defined as

$$ADOP = \sqrt[2n]{det\ Q_x}, \tag{2.11}$$

where $det\ Q_x$ is the determinant of the covariance matrix of the ambiguity parameters (in cycles). A value of 0.2 cycles for the ADOP is also used in [TO97] as a reference value for a successful validation of the ambiguities solved by an OTF algorithm. As a consequence, if the ADOP is lower than 0.2 we can be quite confident that the validation algorithm guarantees that the ambiguities are solved correctly.

2.3 Use of pseudorange measurements

Solutions only based on phase observations are very common in static processing. In fact, in most cases code pseudorange observations are only used in the preprocessing state for blunder detection and for receiver synchronization. However, in the parameter estimation process only phase observations are taken into account. In kinematic positioning, the situation changes dramatically. As proved in [SBE94] to obtain reasonably good results

in short flights (less than 20 minutes) the combined use of code and phase observations is a must.

Phase observations are smooth enough for kinematic precise positioning. However, errors in ambiguity resolution can lead to an unstable system with unbounded errors. On the other hand, errors in trajectories computed with pseudoranges observations are bounded but are too noisy for precise positioning and may be affected by systematic errors due to multipath measurements. There are several approaches for combining code and phase measurements in kinematic surveys in order to take advantage of the qualities of both code and phase measurements.

2.3.1 Reference trajectory

As stated above, errors in trajectories computed with pseudoranges observations are bounded but are too noisy to determine trajectories with enough accuracy. This is why some kind of average process must be applied in order to reduce the variance of the solution. The idea is to subtract the effect due to the movement of the receiver (a reference trajectory) from the pseudorange observations, resulting in static-like pseudorange observations that can be filtered or smoothed in a simple way.

The equations of the double phase differences observation at times t_k and t_{k+1} can be written as

$$\begin{aligned} \lambda_i \cdot \Delta\nabla\Phi^{s_1,s_2}_{r_1,r_2}(t_k) &= \Delta\nabla\rho^{s_1,s_2}_{r_1,r_2}(t_k) + \lambda_i \cdot \Delta\nabla N^{s_1,s_2}_{r_1,r_2} + \Delta\nabla\varepsilon^{s_1,s_2}_{r_1,r_2}(t_k), \\ \lambda_i \cdot \Delta\nabla\Phi^{s_1,s_2}_{r_1,r_2}(t_{k+1}) &= \Delta\nabla\rho^{s_1,s_2}_{r_1,r_2}(t_{k+1}) + \lambda_i \cdot \Delta\nabla N^{s_1,s_2}_{r_1,r_2} + \Delta\nabla\varepsilon^{s_1,s_2}_{r_1,r_2}(t_{k+1}), \end{aligned} \tag{2.12}$$

where ε refers to remaining residual errors.

If we subtract both equations, we obtain the so called triple differences phase observations:

$$\lambda_i \cdot \delta\Delta\nabla\Phi^{s_1,s_2}_{r_1,r_2}(t_{k,k+1}) = \delta\Delta\nabla\rho^{s_1,s_2}_{r_1,r_2}(t_{k,k+1}) + \delta\Delta\nabla\varepsilon^{s_1,s_2}_{r_1,r_2}(t_{k,k+1}), \tag{2.13}$$

where the δ operator represents

$$\delta \bullet (t_{k,k+1}) = \bullet(t_{k+1}) - \bullet(t_k).$$

It is obvious that $\delta\Delta\nabla\Phi^{s_1,s_2}_{r_1,r_2}(t_{k,k+1})$ contains, with a high degree of accuracy, the dynamic information of the survey between epochs k and k+1. As the ambiguities remain constant, if every cycle slip has been repaired and no loss of lock occurs, the parameter $N^{s_1,s_2}_{r_1,r_2}$ cancels out when triple differences are made. Since no ambiguities need to be solved, the algorithms that make use of triple differences phase observations are very robust. However, the price that must be paid is an increase of the residual noise. The philosophy of some algorithms, as those in [BH92] and [FKH96], is based on this approach. The dynamic information provided by phase measurements is subtracted from the pseudorange measurements. The residual measurement contains no dynamic information; it

can therefore be treated as a static measurement in the filtering/smoothering process to reduce the noise. Finally, a good estimation of the trajectory is obtained by adding the result of the filtering/smoothering process to the reference trajectory.

It must be pointed out that the same results are obtained using double differences between receivers and epoch instead of triple differences.

$$\lambda_i \cdot \delta\Delta\Phi^s_{r_1,r_2}(t_{k,k+1}) = \delta\Delta\rho^s_{r_1,r_2}(t_{k,k+1}) + \delta\Delta\delta T_{r_1,r_2} + \delta\Delta\varepsilon^s_{r_1,r_2}(t_{k,k+1}). \tag{2.14}$$

The solution obtained with this approach is asymptotically stable as long as the phase measurements are free from cycle slips. Accuracies of 20–40 cm are claimed in long-range aircraft positioning [BH92].

2.3.2 Combined computation

Pseudorange derived observation equations may be combined with phase derived observation equations (with the appropriate weight) in the estimation process. In such approaches, at the beginning of the survey, when ambiguities are unknown, the code information increases the convergence of the solution dramatically. However, once the survey has been initialized, i.e. after several minutes, the pseudorange derived observation equations do not have any significant influence on the result of the survey; they are only used for checking the consistency of the survey in the presence of cycle slips in phase observations.

The use of code observations has a major inconvenience; namely code measurements taken by a GPS receiver are not independent over time. Usually, GPS receivers take advantage of precise phase observations to stabilize the code observations tracking loop and smooth code measurements. Such an effect can lead to a systematic error in pseudorange-code observations. Consequently, code measurements errors may not behave as white noise with zero mean and ambiguity parameters may not converge to their correct values.

There are some works on the combination of WADGPS (Wide Area Differential GPS) corrections and high precision smoothed code information from dual frequency receivers. Dual frequency code observations correct the ionospheric delay while WADGPS corrections are used to model satellite errors (orbits and clocks). Some works like [SHN] claim to have achieved decimeter level kinematic positioning at more than 1000 km from the nearest reference station. However, they need rather large observation time spans to allow the filter convergence.

2.4 Dynamic models

The dynamics of a GPS receiver in motion may be predictable (i.g. in a satellite) or unknown (i.g. on an airplane). This information about the dynamics may be used in trajectory computation as additional information. In the case of satellite orbits, the dynamic model will be very precise while, in the airborne receiver, only some restrictions on acceleration changes can be applied.

If a Kalman filter algorithm is used in the processing software, a dynamic model must be provided as it corresponds to the transition matrix needed in the algorithm. The dynamic model includes some a priori knowledge of the system dynamics. If the knowledge is accurate and precise, it can be very helpful to reduce the noise of the solution. If the knowledge is accurate but not precise, it will have no effect on the result and it will increase the computation burden. Finally, if the a priori dynamic knowledge is wrong, the use of the dynamic model will deteriorate the solution.

For instance, in the cycle slip detection step, if the dynamic model used is able to predict the receiver position at epoch t_{i+1} from the receiver position at epoch t_i with an accuracy of 10 cm, then this information will be very valuable for detecting cycle slips in phase observations at both frequencies L1 and L2.

Several models are used in kinematic GPS positioning, some of which are very sophisticated. In airborne kinematic GPS positioning, the dynamics of the aircraft can be very complicated, especially under turbulence conditions and during turns. However, airborne surveys are usually flown under good meteorological conditions and in straight lines. Thus, the so-called PV model can be appropriated for these periods of constant speed. The process $x(t)$ will be modeled as

$$\begin{aligned} \dot{v} &= w_v, \qquad \text{(PV model)} \\ \dot{x} &= v + w_x, \end{aligned} \tag{2.15}$$

where w_v,w_x are the white noise vectors.

It is apparent that for even higher dynamics the above model is unsuited. The PVA model is then used:

$$\begin{aligned} \dot{a} &= w_a, \qquad \text{(PVA model)} \\ \dot{v} &= a + w_v, \\ \dot{x} &= v + w_x, \end{aligned} \tag{2.16}$$

where the first-order autoregressive Gauss-Markov process is often preferred for the acceleration. That is,

$$\dot{a} = -\alpha^{-1} a + w_a, \tag{2.17}$$

where α is a diagonal matrix with the time correlation parameters of the process and w_a,w_v and w_x are the vectors containing white noise variables.

Four unknowns must solved at each epoch (three for position and one for time). As stated above, airborne surveys can have a very complicated dynamics, which makes it difficult to predict the position of the aircraft. However, the drift of the receiver clock can be modeled with reasonable precision, and the dynamic model of the receiver clock can be used to overcome periods with three satellites. During these periods, the receiver clock offset will be estimated according to the dynamic model, and the position of the rover receiver will be computed using observations from three satellites. There are a number of ways to deal with the receiver clock error. $\mathbf{c(t)}$ can be modeled using a simple

model as a random walk process, either by making $\delta T_r(t) = c_1(t)$ with $\mathbf{c} = (c_1)$ or $\delta T_r(t) = c_1(t) + c_2(t) \cdot t$ with $\mathbf{c}^T = (c_1, c_2)$ and

$$\dot{\mathbf{c}} = w, \tag{2.18}$$

where $\mathbf{w}$ is the vector containing white noise variables. More elaborated models may also be used to approximate the Allan variance plots of typical crystal clocks [BH92].

2.4.1 Inertially aided GPS positioning

If accurate inertial observations are available from an IMU (Inertial Measurement Unit), a much better dynamic model can be used by resorting to the well known mechanization equations of inertial navigation. The observational errors of GPS and IMU sensors are very complementary, and therefore the integration of GPS and IMU has great advantages for both systems. GPS positioning usually works at moderate rates (1–10Hz), and thereby cannot describe the trajectory of the vehicle at higher frequencies. The noise of GPS phase positioning is moderate (1–2 cm) and has the great advantage that if ambiguities are correctly solved, the GPS positioning shows no drift. On the other hand, IMU positioning can describe the trajectory at high frequencies ($>$ 50 Hz) with very low noise, but the trajectory computed by using only IMU measurements is affected by drifts resulting from errors on the components of the IMU (gyroscopes and accelerometers). If a Fast Fourier Transformation is applied to the errors of GPS and IMU observations one can observe that GPS observations errors lie in low frequencies while IMU observations errors lie in high frequencies; therefore, it is clear that both systems complement each other.

In [Sch01] an example of the use of inertially aided RTK positioning is shown. In this example, IMU measurements are also used to bridge ambiguities in case, of short loss of lock of the GPS receiver.

2.5 Antenna phase center variations

In order to process satellite signals and obtain code and phase observations, GPS receivers have several elements for signal reception and signal processing. The first element is the GPS antenna for measuring the electromagnetic waves coming from GPS satellites.

The geometrical center of the antenna does not coincide with the electrical center of the antenna (where the signal is measured). The difference between the geometrical center and the electrical center has a constant part called antenna offset and a variable part called antenna phase center variations. As it is not possible to build a true omnidirectional antenna, the responses of the antenna to signals coming from different directions are slightly different. As a result, the electrical center of the antenna changes depending on the direction of the signal coming from the satellite, as shown in 2.5.

The antenna offset is usually provided with the GPS antenna. However, some kinematic antennas do not have any information about the value of their antenna offset, and so it must be estimated by a calibration process [RSMB95]. The values of antenna phase center variations must be estimated by a calibration process as well because they are not

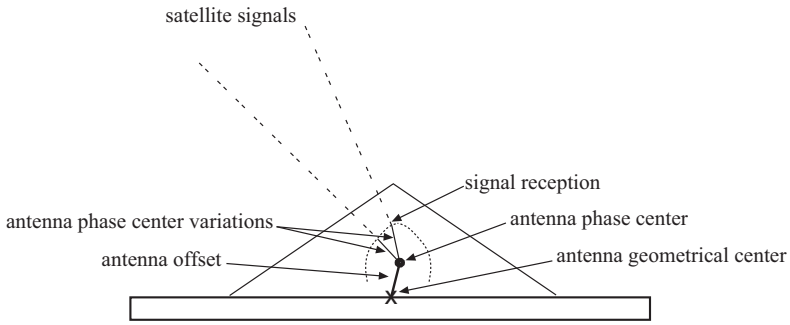

Figure 2.5: Antenna offset and antenna phase center variations.

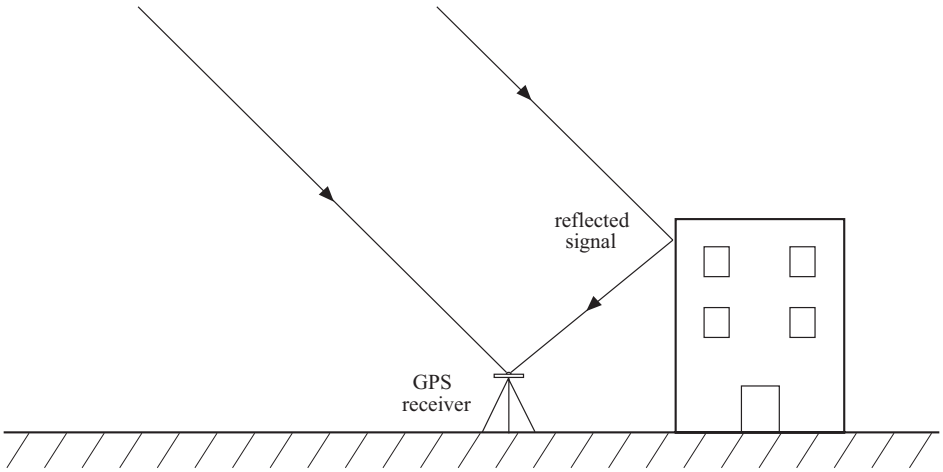

Figure 2.6: Multipath.

provided by antenna manufacturers. The antenna phase center variation is usually estimated as a function of the signal elevation but, in some cases, a function of the elevation and azimuth of the signal is adjusted. Variations of the antenna phase center can be up to 2 cm in standard GPS antennas.

2.6 Multipath

Another error source is multipath. Multipath errors are due to reflected signals from surfaces near the GPS antenna. The reflected signal interferes with the direct signal from the satellite and is read as additive noise by the GPS antenna (see figure 2.6).

In an airborne environment, the GPS antenna is surrounded by metallic parts of the aircraft; therefore, multipath can be a limiting factor for high precision kinematic GPS positioning [PS95a].

Antenna effects on measurements may be observed when comparing residuals from a zero baseline survey and a 1 meter baseline survey in a multipath environment. In a zero baseline survey, data from two receivers connected to the same antenna is combined and the corresponding residuals are obtained; in a 1 meter baseline survey, data from two

receivers with two different antennas forming a 1 meter baseline is combined, and the residuals of the double differences are obtained. In both surveys, data from receiver 1 and receiver 2 is affected by the same satellite clock, ionospheric and tropospheric errors. Moreover, in a zero baseline survey, as both receivers process the same signal coming from the same antenna, the antenna effects are the same for both receivers. Hence, the difference in magnitude of the residuals corresponds to antenna phase center variations and multipath.

According to [WM01], the multipath effect on carrier phase Φ_m can be described as follows:

$$\Phi_m = \frac{\lambda_i}{2\pi} \cdot \arctan \frac{\alpha \cdot \sin\left(\frac{d}{\lambda_i} \cdot 2\pi\right)}{1 + \alpha \cdot \cos\left(\frac{d}{\lambda_i} \cdot 2\pi\right)}, \tag{2.19}$$

where α is a damping factor taking values from 0 to 1, λ_i is the carrier phase wavelength and d is the multipath delay. If the α parameter takes the maximum value of 1, the carrier phase error can reach a magnitude of $\alpha/4$ (4.8 cm for L1 and 6.1 cm for L2). The multipath error often shows a periodic behavior of 10 to 45 minutes.

In static GPS positioning, the receiver position can be averaged for a certain period of time from minutes to hours. Due to the fact that the relative geometry between the receiver and the satellite varies, the effect of the multipath and the antenna phase center variation also changes during a survey. Consequently, the effect can be mitigated. In kinematic survey, the position of the receiver at one epoch must be determined with the observations of that epoch and cannot be averaged. Thus, the antenna phase center errors and the multipath will have a direct effect on the computed position.

The GPS constellation has a period of 1 sidereal day ($\approx$ 23 hours 56 minutes); therefore, the same constellation geometry is repeated every sidereal day at a given place. In a permanent GPS station (assuming that the scenario has not changed), the reflexions of satellite signals will be the same every sidereal day. This fact may be taken into account to determine residuals correlations between GPS observations taken 1 sidereal day apart. Several studies [WM01] have been carried out to correct multipath interference in GPS permanent stations by using the correlation of multipath effects spaced 1 sidereal day.

In the context of kinematic positioning some studies have been conducted [CRD00] to mitigate carrier phase multipath using relative carrier phase measurements from an array of closely-spaced antennas. A reduction of 47% has been obtained, but in the present state a rapid change in the environment is not possible; therefore, this technique can only be applied in low dynamics kinematic positioning. Much effort is being made by antenna designers in order to mitigate multipath effects; in consequence, big improvements can be expected in this field in the near future.

	Final (2 weeks)	**Rapid** (2 days)	**Predicted** (real time)
Ephemerides	5 cm	10 cm	50 cm
Clocks	0.3 ns	0.5 ns	150 ns
Pole	0.1 mas	0.2 mas	–
Pole Rates	0.2 mas/day	0.4 mas/day	–
UT1-UTC	50 us	300 us	–
Length of Day	30 us/day	60 us/day	–

Table 2.3: Product accuracies offered by the IGS service.

2.7 Satellite ephemerides

Most algorithms developed for kinematic GPS processing are designed to be used either in postprocessing or in real-time mode. This is why they use only broadcast orbits included in the navigation messages of GPS satellites. The current accuracy of broadcast orbits is 2–5 m (1 σ). Simulations made by Colombo [Col92] show that, in long range kinematic positioning (800 km), the precision of the trajectory will be worse by a factor of two when using 1 meter accuracy GPS orbits and worse by a factor of 10 when using 10 meter orbits (broadcast orbits). Also, a significant double difference residual improvements can be seen in [MCL95], where a 200 km range flight is processed using broadcast orbits as well as precise orbits.

The use of precise orbits such as the ones provided by the International GPS service (IGS) [Beu] may lead to a significant improvement in the trajectory determination of the rover receiver. However, IGS precise final orbits are available with a delay of about 15 days. In certain applications, this delay cannot be accepted (real time applications, fast postprocessing applications ...). Two solutions can then be applied: the use of predicted or rapid orbits, and the improvement of broadcast orbits at the same time as the trajectory computation.

IGS is offering some products such as predicted precise orbits and rapid orbits, which can be used in applications where it is not possible to wait for the IGS precise final orbits (see table 2.3). Predicted orbits are valid for the next 24 hours and can be used in real time applications. Rapid orbits are available within 24–48 hours and can be used in fast postprocessing applications. These orbits are used in several real time applications such as determination of atmospheric water vapor contents with GPS, where results need to be available within 0.5–2 hours in order to be useful for weather forecast. In [Bak98], it has been proved that, if satellite residuals are small, the results obtained with predicted orbits can be equivalent to the results obtained with IGS final orbits. As real time applications are growing within the GPS community, IGS is combining hourly files from a subset of the IGS network in order to improve predicted and rapid orbits.

Another possibility of improving the accuracy of the GPS trajectory using broadcast orbits may be to combine data from several reference stations and to perform an orbit adjustment. This approach is used by the WAAS (Wide Area Augmentation System)

concept, where GPS data from a set of GPS stations is used to derive orbital errors of GPS satellites. In [CE98], this approach is used with similar precision to the ones obtained when using precise orbits.

Some work carried out by NASA [MBSBS01] is aimed at the implementation of a Global Differential GPS (GDGPS) system to provide global real-time positioning with a precision of less than 10 cm in horizontal and 20 cm in vertical. The service gathers data from a world network of dual frequency GPS receivers in real time. Once the data has been collected, the service computes real time precise orbits and clocks for all GPS satellites and disseminates the information using IGDG (Internet-based Global Differential GPS). Users must have a dual frequency receiver to correct ionospheric errors. As users can be either static or kinematic, this level of precision can be enough for most kinematic airborne surveying missions, where an accuracy of 10–20 cm fulfills the requirements for sensor orientation. However, in order to correct ionospheric errors, a convergence time is needed. The need for a convergence time, together with unmodeled tropospheric errors, will be a problem in missions where continuous loss of lock may happen, such as large scale photogrammetric flights.

2.8 Summary

In this Chapter, we have presented the GPS basic observables: pseudorange and carrier phase. GPS observation equations for kinematic GPS positioning are described, and an explanation of all significant terms is provided.

In section 2, techniques for differential GPS positioning have been introduced, and the single and double difference GPS models have been derived. Linear phase combinations have been also reviewed by presenting the most useful phase combination used in geodetic positioning. The basic procedures for observation normalization (cycle slip detection and observation synchronization) have also been explained. The GPS ambiguity fixing (estimation and validation) problem for high precision carrier phase positioning have been formulated together with a measure of the strength with which one can expect to have a successful resolution of the ambiguities.

The use of pseudorange observations as well as carrier phase observations for high precision kinematic GPS positioning has been mentioned in section 3. Section 4 presents a study on the use of dynamic models to assist in trajectory determination of a moving GPS receiver.

Sections 5 and 6 have pointed out the problem of receiving GPS signals due to antenna phase center variations and to the environment (multipath).

The errors caused by the wrong determination of the GPS satellites ephemerides have been dealt with at the end of this Chapter.

Tropospheric and ionospheric delays are particularly problematic for kinematic positioning. Therefore, they will be covered in more detail in the following chapters.

Chapter 3
Tropospheric delay

The troposphere is the part of the Earth's atmosphere that extends from the ground to a height of 12–40 km. The propagation speed of GPS signals in the troposphere and in the vacuum is different. As a result, the signals experience a delay when crossing the troposphere on their way from the satellite to the receiver.

Tropospheric delay can be divided into a dry and a wet component. Dry air is responsible for the dry component while the water vapor content is responsible for wet delay. Total delay at the zenith direction ranges from 1.5 to 2.5 meters. Dry delay can account for more than 90% of the total delay whereas wet delay accounts for the remaining 10%.

Estimation of total/residual tropospheric delay has been widely employed in static geodetic GPS. As explained in equations 2.1, the observation equation used for deriving tropospheric parameters may be written as

$$\lambda_i \cdot \Phi_r^s = \rho_r^s + c \cdot (\delta t^s - \delta T_r) + \tau_r^s \quad - I_r^s f_i^{-2} \quad + \lambda_i \cdot (N_r^s + \varphi_r(t_0) - \varphi^s(t_0)), \tag{3.1}$$

where

$$\begin{array}{rcl}
\lambda_i & = & L_i \text{ wavelength,} \\
\Phi_r^s & = & \text{phase observable,} \\
\rho_r^s & = & \text{geometric distance (receiver - satellite),} \\
c & = & \text{light speed,} \\
\delta t^s & = & \text{satellite clock error,} \\
T_r & = & \text{receiver clock error,} \\
\tau_r^s & = & \text{tropospheric delay between satellite s and receiver r,} \\
I_r^s & = & \text{ionospheric delay between satellite s and receiver r,} \\
f_i & = & L_i \text{ frequency,} \\
N_r^s & = & \text{initial ambiguous integer number of cycles between satellite s} \\
 & & \text{and receiver r,} \\
\varphi_r(t_0) & = & \text{initial receiver fractional phase error,} \\
\varphi^s(t_0) & = & \text{initial satellite fractional phase error.}
\end{array} \tag{3.2}$$

Tropospheric delay errors are becoming well understood in geodetic static positioning [Ou96]. After many years of research tropospheric models have been developed to such an extent that they can compete with Water Vapor Radiometers (WVR) and radio sounders on the determination of the water vapor content.

The usual way of dealing with the troposphere is to determine a zenith delay that will be common to all satellites and apply a scale factor that will take into account the satellite elevation with respect to the GPS station. The scale factor is called mapping function; hence the τ_r^s term in 3.1 is split into two terms:

$$\tau_r^s = Map_r^s \cdot Trop_r. \tag{3.3}$$

The mapping function is usually a function of satellite elevation, but it may also contain information about the receiver position. A very simplified mapping function can be

$$Map_r^s = 1/cos(z_r^s), \tag{3.4}$$

where z is the zenith angle of the satellite.

The term $Trop_r$ only depends on the station and has a strong temporal correlation. In static positioning, good results are obtained if this value is kept constant for time periods of 1–3 hours.

When the residual tropospheric delay is estimated, the tropospheric parameter $Trop_r$ is divided into two components: $Trop_{std}$ will take into account the tropospheric delay assuming standard atmosphere models, and $Trop_{unk}$ will parameterize the delay due to the differences between the standard atmosphere and the real atmosphere:

$$Trop \;\; = \;\; Trop_{std} + Trop_{unk}. \tag{3.5}$$

There are several models for deriving standard atmosphere delay such as Saastamoinen [Saa73], Hopfield, Blak ..., some of which are based on surface meteorological values. When no standard atmosphere model is used, then $Trop_{std} = 0$ and $Trop_{unk}$ will solve for the total tropospheric delay.

As wet tropospheric delay is very difficult to model and has a different behavior from dry delay, sometimes total tropospheric delay is divided into dry delay (determined by standard models) and wet delay (estimated in the computations). In such cases, two mapping functions such as the Niell mapping functions [Nie96] are used for translating the tropospheric delay from its zenith value into the actual receiver-satellite geometry.

$$Trop \;\; = \;\; Dry_{Map} \cdot Dry_{Trop_{std}} + Wet_{Map} \cdot Wet_{Trop_{unk}}, \tag{3.6}$$

where

$$\begin{aligned}
Trop &= \text{total tropospheric delay,} \\
Dry_{Map} &= \text{mapping function corresponding to dry delay,} \\
Dry_{Trop_{std}} &= \text{tropospheric zenith dry delay computed with standard} \\
&\quad \text{atmospheric parameters,} \\
Wet_{Map} &= \text{mapping function corresponding to wet delay,} \\
Wet_{Trop_{unk}} &= \text{tropospheric zenith wet delay (unknown).}
\end{aligned} \tag{3.7}$$

However, little has been studied in the particular case where a receiver is in motion and the altitude difference between the kinematic receiver and the reference station is usually big, sometimes reaching 10 km.

Experience from GPS static positioning suggests that kinematic tropospheric delay may be approached in two different ways: the use of extended standard atmospheric values and the estimation of total/residual tropospheric delay.

3.1 Extended standard atmosphere models

As stated above, the standard atmospheric models used for $Trop_{std}$ determination are based on surface meteorological values (pressure, temperature, humidity). When no reliable surface meteorological data is available, standard atmosphere surface values must be applied. These models can take into account either hydrostatic path delay plus wet path delay or only dry tropospheric delay.

In order to take advantage of these models in an airborne environment, the standard atmosphere must also be defined in its vertical profile. In [CL96], [CL97], a series of models for determination of a 3-dimensional standard atmosphere is proposed. Such extended models are also proposed for use in the FAA's (Federal Aviation Administration) WAAS (Wide Area Augmentation System).

At low altitudes, the most critical parameter is the water vapor gradient (clouds are proof that water vapor is not homogeneously spread in height.) At high altitudes ($\approx$ 10 km), there is very little water vapor left but the temperature gradient becomes the critical parameter, from which the amount of atmosphere still lying above the aircraft is computed.

When meteorological conditions are not standard (thermal inversions, cold front...) residual tropospheric delay can still play an important role by limiting the accuracy of GPS surveys.

The operational altitudes of airborne Earth observation sensors range from 500 to 10000 meters above ground depending on the desired data resolution, precision and ground coverage. At low altitudes, the tropospheric effect is usually similar to that suffered by the reference station. However, when flying at high altitudes, the tropospheric effect suffered by the reference station can be very different from that on the airborne receiver because the GPS signal has traveled a significant different portion of troposphere. For this reason, the tropospheric model for airborne applications must take into account the differential portion of troposphere that satellite signals need to travel from GPS satellites to airborne and ground receivers.

3.2 Tropospheric delay estimation

Redundancy on GPS computations (when more than 4 satellites are available) can be used for determination of tropospheric delay. However, there are several points that hinder such a determination.

Although there is some redundancy in GPS computations, correlation between all the parameters is very high, and it is even possible to have an overparameterized problem (the problem can be even worse if ionospheric parameters are also estimated.) Hence, the general approach is to use a standard model as a first approximation and to estimate the residual tropospheric error with some constraints.

The usual approaches for tropospheric parameter estimation are determination of a stepwise function or adjustment of some stochastic model epoch by epoch. Although the use of a stochastic model seems to be capable of a better modeling, experience in static tests shows that both techniques show a similar performance with respect to positioning accuracy [TK98].

If the distance between receivers is shorter than 100 km, the satellites are seen by the receivers with a similar elevation. Therefore, the values of the mapping function are very correlated, making it very difficult to decouple the tropospheric parameters from both sites. Thus, it is usual to fix the tropospheric delay from one of the stations (reference station) and estimate only the tropospheric parameters from the rover receiver.

As GPS signals are blocked by the Earth, GPS observations can only be made from satellites above the horizon. Therefore, the vertical component is much weaker than horizontal components. For instance, tropospheric errors propagate into position errors mainly in the vertical component. For tropospheric parameter determination, it is advantageous to have observations close to the horizon; however, as these rays have crossed much more troposphere than the rays coming from the zenith, they are much noisier, and therefore of little use for positioning. A common cutoff angle used in GPS positioning is 15 degrees.

The approach implemented in the software developed for this thesis can be divided into two steps. In the first step, predicted zenith tropospheric delays from kinematic and reference receivers are computed by a standard atmospheric model and applied to each satellite observation by using a mapping function. The second step consists in adding a scale factor to be estimated in the computation. This scale factor is applied to the total tropospheric delay affecting every observation from the kinematic receiver. Let $\nabla\Delta\tau_{k,r}^{s_1,s_2}$ be the double difference tropospheric delay from satellites s_1 and s_2 and receivers k and r obtained from 2.3. Then, $\nabla\Delta\tau_{k,r}^{s_1,s_2}$ can be decomposed into

$$\nabla\Delta\tau_{k,r}^{s_1,s_2} = \tau_k^{s_1} - \tau_k^{s_2} - \tau_r^{s_1} + \tau_r^{s_2}, \tag{3.8}$$

where

$$\begin{aligned}
\nabla\Delta\tau_{k,r}^{s_1,s_2} &= \text{double difference total tropospheric delay,} \\
\tau_k^{s_1} &= \text{total tropospheric delay from receiver } k \text{ and satellite } s_1, \\
\tau_k^{s_2} &= \text{total tropospheric delay from receiver } k \text{ and satellite } s_2, \\
\tau_r^{s_1} &= \text{total tropospheric delay from receiver } r \text{ and satellite } s_1, \\
\tau_r^{s_2} &= \text{total tropospheric delay from receiver } r \text{ and satellite } s_2.
\end{aligned} \tag{3.9}$$

Considering k a scale factor correcting the tropospheric delays from the kinematic

receiver, the double difference tropospheric delay applied to the double difference observation is

$$\nabla\Delta\tau_{k,r}^{s_1,s_2} = k \cdot (\tau_k^{s_1} - \tau_k^{s_2}) - \tau_r^{s_1} + \tau_r^{s_2}. \tag{3.10}$$

The scale factor k is estimated in the trajectory determination. This tropospheric parameter is estimated as a stochastic variable following a random walk pattern while the τ_i^j terms are derived from the combination of a standard atmospheric model and a mapping function.

3.3 Summary

This Chapter explains the delay that GPS signals suffer when crossing the part of the atmosphere called troposphere. The usual way of modeling tropospheric delay, that is, by dividing the slant delay into a zenith delay and a mapping function is also covered. Finally, the approach used in the software developed for this thesis is presented.

Chapter 4
Ionospheric delay

The ionosphere is the region of the Earth's atmosphere that extends from 50 km to 1000–2000 km. In this part of the atmosphere, ionizing radiation, mainly coming from the sun, causes free electrons to exist. The ionosphere is a dispersive medium for radio waves, so their effect depends on the frequency of the radio wave. The ionosphere produces an advance in carrier phase observations and a delay in code observations. The magnitude of the advance/delay in meters caused by the ionosphere is given in equation 4.1, where the '+' sign is used for code observations and the '–' sign is used for phase observations:

$$\text{ionospheric delay} \approx \mp \frac{40.3}{f_i^2} TEC, \tag{4.1}$$

where f_i is the carrier frequency and TEC is defined as the total number of electrons that are contained in a column with cross-sectional area of 1 m^2 (1 TEC unit = 10^{16} el/m^2) along the signal path between the satellite and the receiver. Ionospheric delay can reach 10 meters in the zenith direction, and even 30 meters under severe conditions.

As the main cause of ionospheric activity is the radiation coming from the sun, any increase in solar activity will generate more ionizing radiation (TEC), and therefore a rise in ionospheric delay. The number of sun spots is an indicator of solar activity; thus, an increase in the number of observed sun spots will cause more ionospheric activity. Since the beginning, the number of observed sun spots has shown an eleven year periodicity; accordingly, the magnitude of the ionospheric delay suffered by GPS signals also has an eleven year periodicity.

As GPS is a dual frequency ranging system, it can take advantage of the dispersive nature of the ionosphere to correct its effect. If P_1 and Φ_1 are code and phase measurements on the L1 frequency, and P_2 and Φ_2 are code and phase measurements on the L2 frequency then, according to equations 2.1, one can compute,

$$I = \frac{f_1^2 \cdot f_2^2}{f_2^2 - f_1^2} \cdot (P_1 - P_2) + b_2 - b_3, \tag{4.2}$$

$$I = \frac{f_1^2 \cdot f_2^2}{f_2^2 - f_1^2} \cdot (\lambda_2 \cdot \Phi_2 - \lambda_1 \cdot \Phi_1 - (\lambda_2 \cdot N_2 - \lambda_1 \cdot N_1)) - b_1. \tag{4.3}$$

However, due to the noise of code measurements, especially after AS has been switched on, the ionospheric delay obtained in equation 4.2 is not precise enough to be used for removing the ionospheric bias of phase measurements.

In practice, N_1 and N_2 cannot be determined; only double difference ambiguity parameters can be determined, but equation 4.3 may be used for cycle slip detection. According

to its geometric free condition, any cycle slip in data will appear as a sudden change in I, and therefore, analyzing the dynamics of I makes it possible to detect cycle slips in data.

Ionospheric delays, like tropospheric delays, show a spatial and temporal correlation. If double difference observations are processed, the temporal correlation can be modeled as a random walk (see figure 6.23) by using stochastic parameters. With regard to spatial correlation, it is known that ionospheric delays show a high correlation in distance. Determination of the correct ionospheric correlations between data recorded by different reference receivers has not been fully studied and it is not widely applied in multireference station computation. It is also beyond the scope of this work to investigate ionospheric temporal and spatial correlations.

Ionospheric errors have been identified as an accuracy limiting factor for kinematic positioning where low redundancy is present. In kinematic trajectory determination, the survey can present continuous loss of lock mainly due to blockage of GPS signals during maneuvers (it must be pointed out that in RTK surveys the distance of operation is restricted to 10–20 km due to differential ionospheric delays.)

To handle ionospheric delay, two approaches can be used: to process a ionospheric free combination of the primary observables or to use/compute ionospheric models.

4.1 Use of ionospheric free combination

According to equations 2.1, it is possible to make a combination of L1 and L2 phase observations to obtain a ionospheric free pseudo-observation usually called L3:

$$\lambda_3 \cdot \Phi_3 = \lambda_1 \cdot \Phi_1 \cdot \frac{f_1^2}{(f_1^2 - f_2^2)} - \lambda_2 \cdot \Phi_2 \cdot \frac{f_2^2}{(f_1^2 - f_2^2)}. \tag{4.4}$$

The observation equation of the ionospheric free phase combination will be

$$\begin{aligned} \lambda_3 \cdot \Phi_3 \;=\; & \rho_r^s + c \cdot (\delta t^s - \delta T_r) + \tau_r^s \quad && +\lambda_1 \cdot (N_{1r}^s + \varphi_r(t_0) - \varphi^s(t_0)) \cdot \tfrac{f_1^2}{(f_1^2 - f_2^2)} \\ & + d\rho_r^s \cdot \tfrac{f_2^2}{(f_1^2 - f_2^2)} - b_{1r} \cdot \tfrac{f_2^2}{(f_1^2 - f_2^2)} && -\lambda_2 \cdot (N_{2r}^s + \varphi_r(t_0) - \varphi^s(t_0)) \cdot \tfrac{f_2^2}{(f_1^2 - f_2^2)}. \end{aligned} \tag{4.5}$$

In the double difference combination the ionospheric free combination will be of the form

$$\begin{aligned} \lambda_3 \cdot \nabla\Delta\Phi_{3_{1,2}}^{1,2} \;=\; & \nabla\Delta\rho_{1,2}^{1,2} + \nabla\Delta\tau_{1,2}^{1,2} \quad && +\lambda_1 \cdot \nabla\Delta N_{1_{1,2}}^{1,2} \cdot \tfrac{f_1^2}{(f_1^2 - f_2^2)} \\ & - \nabla\Delta d\rho_{1,2}^{1,2} \cdot \tfrac{f_2^2}{(f_1^2 - f_2^2)} && -\lambda_2 \cdot \nabla\Delta N_{2_{1,2}}^{1,2} \cdot \tfrac{f_2^2}{(f_1^2 - f_2^2)}, \end{aligned} \tag{4.6}$$

where the ionospheric first order term has vanished.

The use of ionospheric free combination faces two problems. The first one is that the integer nature of double difference ambiguities $\nabla\Delta N_1$ and $\nabla\Delta N_2$ is lost. Double difference ionospheric free combination creates a new parameter to be estimated $\nabla\Delta N_3$, which follows the relation

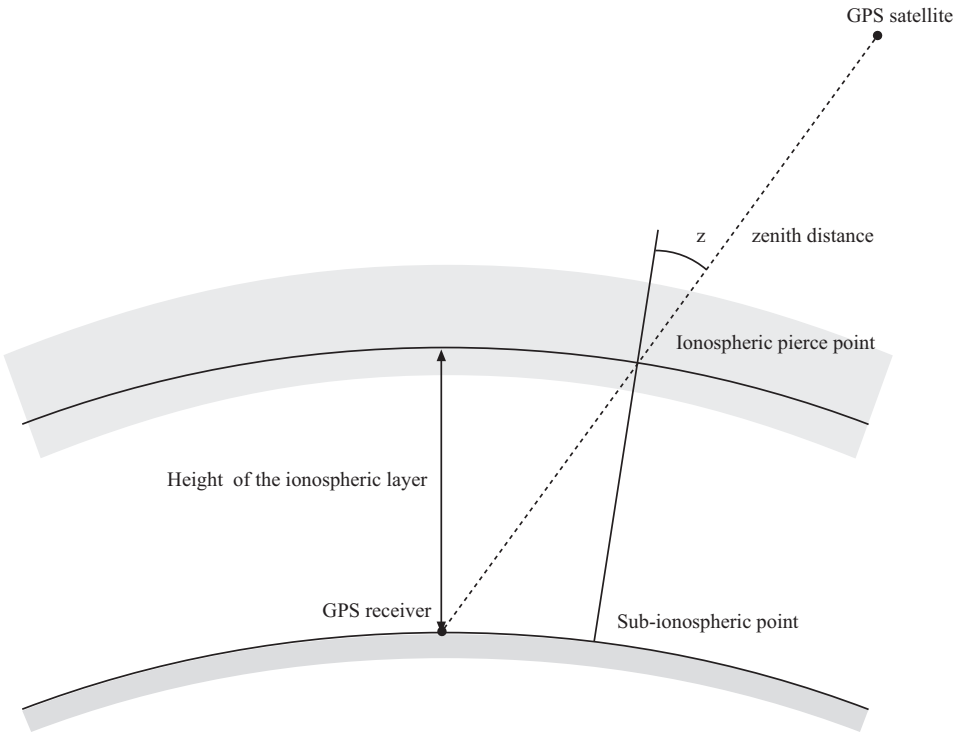

Figure 4.1: Ionospheric single layer and subionospheric point.

$$\nabla\Delta N_3 = \nabla\Delta N_1 \cdot factor_1 - \nabla\Delta N_2 \cdot factor_2. \tag{4.7}$$

The factors $factor_2$ and $factor_1$ are not integers so the ionospheric free ambiguity parameter will not keep the integer nature of the L1 and L2 ambiguities. The fact that the integer nature is lost makes impossible the exact determination of the $\nabla\Delta N_3$ parameters, and therefore they must be estimated approximately as real numbers.

The second problem of using ionospheric free combination in kinematic positioning is that, to form ionospheric free combination, a number of satellites must be tracked in both frequencies. Due to the AS, the quality of the L2 signal is worse than the quality of the L1 signal, so it is usual to have frequent losses of lock in L2 in kinematic environments. Therefore, if 5 satellites are being tracked continuously in the L1 frequency and there is a loss of lock in two satellites in the L2 frequency, then it might be impossible to compute the trajectory using ionospheric free combination.

4.2 Ionospheric models

In a first approximation, is it possible to consider the ionosphere as an infinitesimal single layer lying at 350–400 km above the Earth's surface. The ray path of the signal sent by the satellite to the receiver crosses this layer at a point called subionospheric point, (see figure 4.1).

The observation of a satellite from a reference station provides information about the

ionosphere at the ionospheric pierce point. Combining all the observations from different satellites, different reference stations and different times, it is possible to build a model of ionospheric delays in the GPS signal. This approach is used by several scientific groups that provide daily ionospheric models, for example gAGE/UPC [HPJS99] and CODE [SBM+95].

The use of precise ionospheric models would allow double difference ionospheric effects to be externally determined. Moreover, it would be possible to apply the model described in 2.3 fixing the double difference ionospheric parameters $\nabla\Delta I^{1,2}_{1,2}$ to the values derived from the model. In this case, the trajectory determination would be in the same situation as if the reference station were less than 10 km from the rover receiver. The resolution of ambiguities in that situation would be much easier and the robustness of the solution would be very high. However, the daily global ionospheric models provided are not precise enough to neglect the ionospheric effects. In fact, the difference between the double difference ionospheric prediction by the model and the real double difference ionospheric value can be bigger than one L1 cycle. Nevertheless, these global models may be used to help stochastic ionospheric parameters determine double difference ionospheric values. The more accurate the model, the more weight to the stochastic ionospheric parameters may be given.

A critical issue in the accuracy of ionospheric models is the possibility of predicting $\nabla\Delta I \cdot \frac{f_2^2-f_1^2}{f_1^2 \cdot f_2^2}$ with an error of less than 2.7 cm (half the distance of one L2 cycle minus one L1 cycle). As explained in chapter 2, the usual way of solving ambiguities in kinematic positioning is to solve the L5 ambiguities (with a wavelength of $\approx$ 86 cm) first and then attempt to solve L1 and L2 ambiguities. Once the L5 ambiguities have been solved, there exists a relation that relates the L1 and L2 ambiguities:

$$\nabla\Delta N_5 = \nabla\Delta N_1 - \nabla\Delta N_2. \tag{4.8}$$

Then, if a precise ionospheric model is available, we can combine equations 4.3 and 4.8 to obtain

$$\nabla\Delta I = \frac{f_1^2 \cdot f_2^2}{f_2^2 - f_1^2} \cdot (\lambda_2 \cdot \nabla\Delta\Phi_2 - \lambda_1 \cdot \nabla\Delta\Phi_1 - (\lambda_2 \cdot (\nabla\Delta N_1 - \nabla\Delta N_5) - \lambda_1 \cdot \nabla\Delta N_1), \tag{4.9}$$

where $\nabla\Delta\Phi_1$ and $\nabla\Delta\Phi_2$ are observations, $\nabla\Delta I$ is given by the model and $\nabla\Delta N_5$ has already been computed. The unknown $\nabla\Delta N_1$ will then be expressed as

$$\nabla\Delta N_1 = (-\nabla\Delta I \cdot \frac{f_2^2 - f_1^2}{f_1^2 \cdot f_2^2} + \lambda_2 \cdot \nabla\Delta\Phi_2 - \lambda_1 \cdot \nabla\Delta\Phi_1 + \lambda_2 \cdot \nabla\Delta N_5)/(\lambda_2 - \lambda_1). \tag{4.10}$$

Therefore, as the double difference phase observation noise is at the level of 0.5 cm, it can be seen that if the value of $\nabla\Delta N_1$ is determined by rounding the real value of 4.10, the determination of the L1 ambiguity will be correct as long as the error of $\nabla\Delta I \cdot \frac{f_2^2-f_1^2}{f_1^2 \cdot f_2^2}$ is less than $(\lambda_2 - \lambda_1)/2 \approx 2.7$ cm.

High precision regional area ionospheric models are being studied to increase the applicability of ionospheric models in ambiguity resolution at more than 100 km from

the reference station [CHPJ+99], [Odi02]. These high precision ionospheric models are a key element in regional area Real Time Kinematic positioning.

As will be explained in 6.2.1, the strategy implemented in the software developed for this thesis is a combination of ionospheric models (if available) to correct part of the ionospehric delay and the use of one stochastic parameter per satellite pair to correct the residual part of the ionospheric delay.

4.3 Summary

The principal limiting factor for high precision long range kinematic GPS positioning is ionospehric delay. As explained in this Chapter, the two main approaches to the problem are the use of the ionospheric free carrier phase combination and the use of ionospheric models completed with stochastic parameters.

Chapter 5
Reliability

In kinematic positioning, the quality of results is usually measured by the precision of the trajectory. Although the precision of estimates is very important it measures only the error propagation of the model used and is expressed by the a posteriori covariance matrix of the trajectory. However, the reliability of the survey also needs to be checked. The reliability describes the survey's ability to check for the presence of modeling errors [TK98].

The employed models usually consist of two parts, a functional part and a stochastic part. The functional part describes the relations between observations and unknowns while the stochastic part models the expected uncertainty of data. If the model does not match the physical reality, then it is said to be biased.

The precision will measure the amount of variability in parameters providing that there are no errors in the model (unbiased model). For this reason, several tests need to be carried out to perform a model validation. These tests will have the associated probability error (significance and power of the test). Assuming that the hypothesis H_0 is that the model is correct, then a Type I error will occur if the null hypothesis is rejected despite being true. The probability of Type I error is called the level of significance of the test and is usually represented by α. Type II error occurs when the hypothesis H_0 is accepted while in fact it is false. Type II error is the most harmful of the possible errors because we accept the model despite not being valid, (see table 5.1). When the model has a bias (which has not been detected), the formal precision obtained by the a posteriori covariance matrix does no longer represent the variability of the solution around its mean.

In a factory environment, Type I and Type II errors may also be identified as producer and consumer risks. Let us imagine that a factory makes tubes of a certain diameter D; the factory's quality control department will test the tubes diameter (H_0: the tube has a diameter D). Making a Type I error is a risk for the producer because a correct tube is rejected (with the consequent loss of money). Making a Type II error is a risk for the consumer because he is buying a tube with the wrong diameter (also with the consequent loss of money). If our factory makes trajectories, a Type I error will force us to recompute

		Null hypothesis	
		True	False
Decision	Accept H_0	$\surd$	*Type II error*
	Reject H_0	*Type I error*	$\surd$

Table 5.1: Hypothesis Test

the trajectory trying to find an error (i.e. cycle slip) while in fact the trajectory is correct. Making a Type II error, we will deliver the wrong trajectory to the end user, for instance a photogrammetrist, with unpredictable consequences such as the generation of maps with the wrong metric.

Type I errors and Type II errors cannot be minimized at the same time. Fixing the confidence level of Type I errors, the strength of the model will determine the confidence region of Type II errors (also called power of the hypothesis test). A measure of this confidence is provided by reliability.

As explained in [TK98] in a recursive computation (Kalman filter) the null and alternative hypotheses will be

$$\begin{array}{lrcl} H_o: & y_k & = & A_k x_k + e_k, \\ & & \text{versus} & \\ H_a: & y_k & = & A_k x_k + e_k + C_k \Delta, \end{array} \tag{5.1}$$

where

$$\begin{array}{rcl} y_k & = & \text{vector of observables of time epoch k,} \\ x_k & = & \text{vector of parameters,} \\ A_k & = & \text{design matrix,} \\ e_k & = & \text{vector of measurement noise,} \\ c_k\Delta & = & \text{error model.} \end{array} \tag{5.2}$$

5.1 Internal reliability

As explained above, internal reliability is a measure of the capability of the system to detect blunders with a given probability. Internal reliability does not depend on observations or residuals. It can be computed once the configuration of the system (satellite constellation, reference and rover station location) is known.

Given a functional error $C_k\Delta$, it is possible to compute the probability of detecting a given error but, instead of computing the power of the test, sometimes it is more useful to compute the minimum size of the error that can be detected with a probability β. This value is known as Minimal Detectable Bias (MDB) [Teu98]. The MDB is determined by

$$|\Delta| = \sqrt{\frac{\lambda_0}{{c_k}^t Q_{v_k}^{-1} c_k}}, \tag{5.3}$$

where

$$\begin{array}{rcl} \Delta & = & \text{Minimal Detectable Bias,} \\ \lambda_0 & = & \text{non-centrality parameter,} \\ c_k & = & \text{vector defining error model,} \\ Q_{v_k}^{-1} & = & \text{covariance matrix of residuals.} \end{array} \tag{5.4}$$

The value of the non-centrality parameter λ_0 is a function of the level of significance of the test α and the power of the test β. Common values used in geodetic applications are $\alpha = 0.001$ and $\beta = 0.20$, which leads to $\lambda_0 \approx 17$.

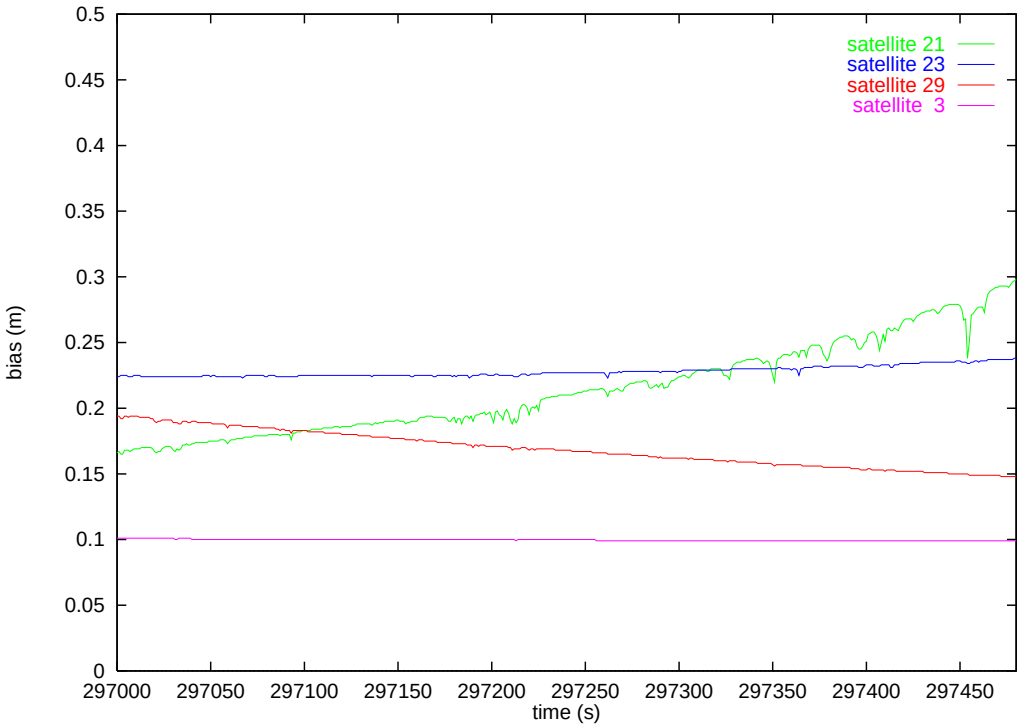

Figure 5.1: Internal reliability

Vector c_k will define the error model that is being tested. Thus, in order to compute the MDB of the jth observation, vector c_k will take the form $(0, 0, ..., 0, 1, 0, ..., 0, 0)^t$ with the 1 placed at the jth row.

Figure 5.1 shows an example of the Minimal Detectable Bias of phase observations from different satellites in a real survey. As the geometry of the satellites at the time of the flight was not very favorable, the MDB exceeds the magnitude of 1 cycle, which means that a cycle slip of 1 cycle on satellite 23, for instance, will not be detected by the survey.

5.2 External reliability

External reliability is the impact of undetectable biases on computed parameters. Good internal reliability does not imply an acceptable influence on the position computation. It is desirable that the influence of the Minimal Detectable Bias on parameters (external reliability) is kept under certain limits in order to guarantee a reasonable confidence in the result of the survey. When computing the reliability of a survey, first the MDB of the observations (internal reliability) is computed and then the influence of each of the marginally detectable errors on the parameters (external reliability).

In figure 5.2, the effect on the position of an error equivalent to the Minimal Detectable Bias plotted in 5.1 is shown. The same bias applied to different observations does not always have the same impact on computed parameters. Notice that while satellite 21 has a lower MDB than satellite 23, its effect on the trajectory (external reliability) is greater.

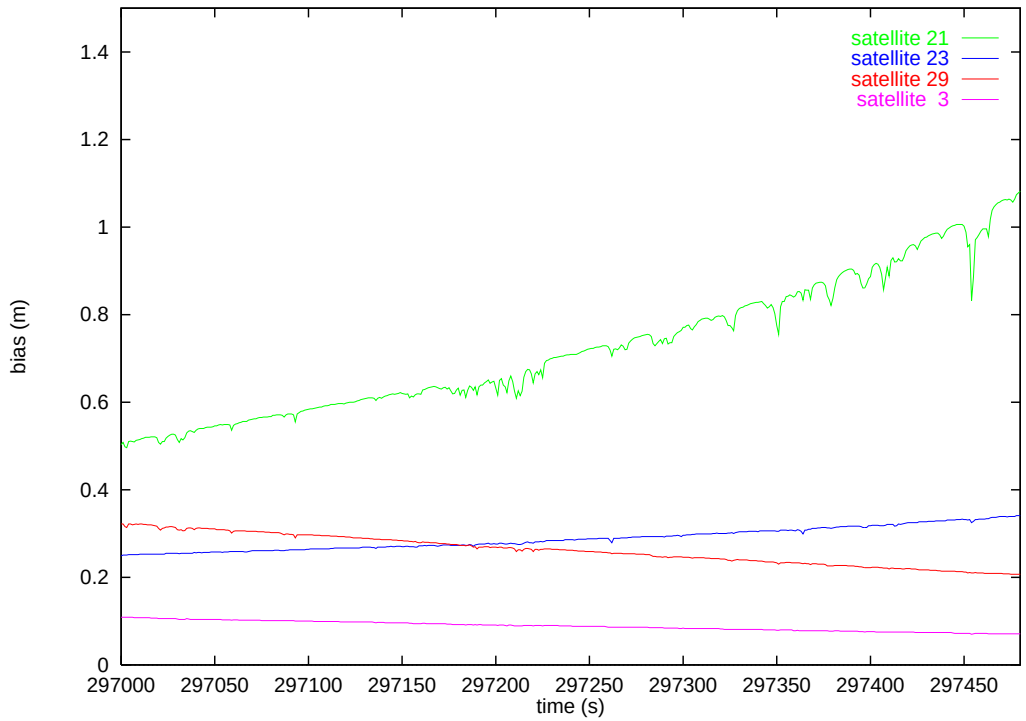

Figure 5.2: External reliability

Very few works have been done concerning internal and external reliability in GPS positioning [BCT94] is an example where the reliability issue is studied in an aerial triangulation block with GPS aerial control. This kind of studies should be done more frequently in order to assess the robustness of the algorithms used in georeferencing.

5.3 Summary

In this Chapter, the principal concepts of reliability have been presented. In particular, the concepts of internal and external reliability have been explained with some examples in the context of GPS kinematic positioning.

Chapter 6
Improving reliability of kinematic surveys

As already stated, when looking at the state-of-the-art in kinematic positioning applied to Earth observation missions, unlike precision, an important issue not fully studied is reliability rather than precision.

This work studies different ideas, both on algorithms and receiver configurations, in order to improve the robustness of kinematic surveys, especially airborne kinematic positioning.

In order to test all the different approaches a GPS kinematic software has been developed. The software is based on double difference GPS observations and a Kalman filter estimation algorithm. The main characteristics of the software development are described in appendix A. The development of a GPS kinematic processing software was required because it is difficult to do research using the available commercial software. Most of the times the algorithms used by commercial software are not described and even elementary statistical information is not available for all the observations, parameters and residuals treated in the computation.

6.1 Global processing

When using an algorithm based on Kalman filtering, the computation of a kinematic trajectory can be performed either by filtering the data to obtain the best solution employing all the data up to the current epoch of processing, or by smoothing the trajectory with the data from the whole survey to estimate the position at each epoch. The formal error of a filtered solution is high at the beginning of the survey and converges to a certain value as the process is running and more data is used in the computation.

As explained in [Gel74], [BH92], an optimal smoother can be thought of as a combination of two optimal filters, one forward filter that processes all the data taken before a given epoch t and a backward filter that processes all the data taken after the given epoch t. Considering the following notation:

$$\begin{array}{ll} \hat{x}_f & \text{forward estimate at epoch } t, \\ P_f & \text{forward error covariance at epoch } t, \\ & \\ \hat{x}_b & \text{backward estimate at epoch } t, \\ P_b & \text{backward error covariance at epoch } t, \\ & \\ \hat{x}(t/T) & \text{smoothed estimate at epoch } t, \\ P(t/T) & \text{smoothed error covariance at epoch } t, \end{array} \tag{6.1}$$

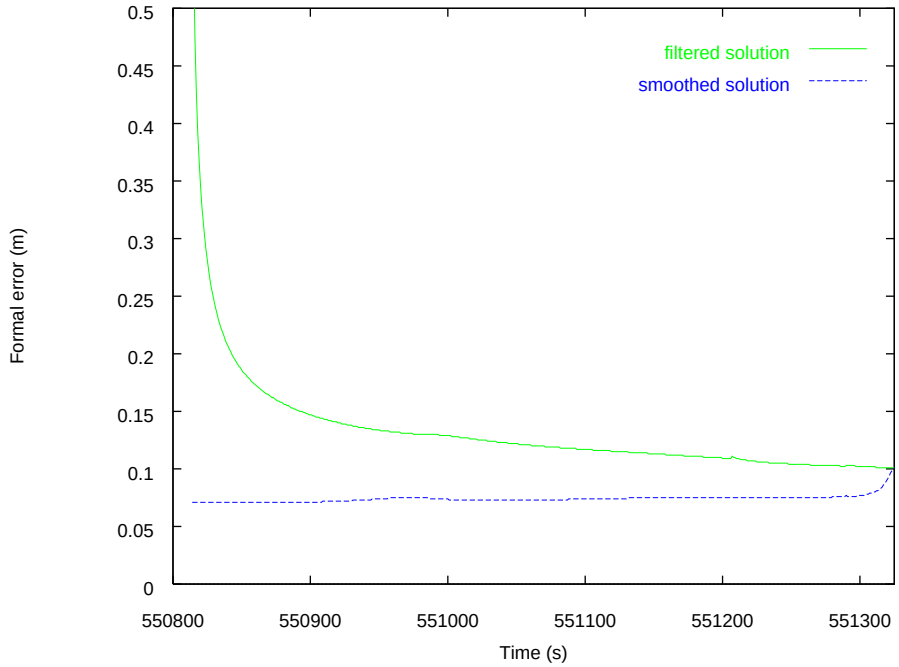

Figure 6.1: Formal error of a trajectory: filtered solution versus smoothed solution.

the smoothed solution is

$$\begin{aligned} P(t/T) &= \frac{1}{\frac{1}{P_f}+\frac{1}{P_b}} = \frac{P_b P_f}{P_b + P_f}, \\ \hat{x}(t/T) &= P(t/T)(\frac{\hat{x}_f}{P_f} + \frac{\hat{x}_b}{P_b}). \end{aligned} \tag{6.2}$$

From equations 6.2 it is easy to see that $P(t/T)$ is always lower than the forward error covariance. This is also evident from the fact that the smoothed solution has been obtained processing more information than the filtered solution. In figure 6.1, the formal error of a trajectory can be observed using a filtered solution and a smoothed solution. Note that the value of convergence depends on several factors (geometry of the satellites in view, multipath, residual modeling errors ...).

Kinematic GPS positioning may be performed in real time or in postprocessing depending on the applications. Filtered solutions have some advantages; for example, the possibility of computing the receiver trajectory in real time allows for a certain number of applications usually related to navigation. However, in most applications it is preferable to have a reliable solution to a fast solution. Hence, smoothed solutions should the preferred ones in non navigation applications.

As explained in Chapter 2, if the correct integer ambiguity parameters are solved, kinematic GPS positioning provides very precise trajectories. If the survey has no static initialization for ambiguity determination, then OTF (On-The-Fly) techniques must be used. Although OTF is sometimes used as a synonym of RTK (Real Time Kinematic), there is a difference between them. OTF techniques aim to determine the correct integer

ambiguity parameter while the receiver is moving; this can be done either in real time or in postprocessing. RTK is used to define a survey where the correct ambiguities are solved in real time, and therefore the precise trajectory is also obtained in real time. RTK surveys use OTF techniques to solve ambiguities. It is clear that if an OTF algorithm is used in postprocessing, its chances of finding the correct ambiguity parameters increase when a better initial estimation of the ambiguity parameters is used. Therefore, it is always preferable to use OTF algorithms in the smoothed solution rather than in the filtered one.

6.1.1 Implementation

The implementation of a global processing in a postprocessing kinematic GPS software is quite simple. First, a forward filtering of the whole survey is performed keeping the ambiguity as free floating parameters. Then, a backwards filtering and a trajectory smoothing can be carried out. The formal accuracy of smoothed ambiguity parameters is lower than that of the filtered ones.

In figure 6.2, the formal accuracy of a set of L1 ambiguity filtered parameters of different satellites is shown. In the validation phase, OTF algorithms have some acceptance/rejection criteria; these criteria usually depend on the formal accuracy of the float ambiguity. For example, if the acceptance criteria require that the formal accuracy of the float ambiguity should be lower than 0.2 m, then the OTF algorithm will not be able to validate any proposed ambiguity parameters within the first two thirds of the survey. If the proposed global solution is used, the formal accuracies of the L1 ambiguity parameters improve dramatically (see figure 6.3). Hence, if the float ambiguity parameters of the smoothed solution are used, their formal error is always lower than the limit imposed by the acceptance/rejection criteria. Therefore, the OTF algorithm can validate the ambiguity parameters at any stage of the survey and not only in the last third of the survey, thus providing more flexibility during trajectory computation.

It is suggested that this flexibility be used for selecting an optimal epoch to trigger OTF algorithms, which increases the chances of solving the correct ambiguity parameters. The capacity to solve ambiguities is highly correlated with the distance to the reference station. As a rule of thumb in a kinematic survey, ambiguities can be solved if the survey is carried out within 15–25 km from the reference station. The possibility of triggering the OTF algorithms at any stage of the survey is very important in high dynamics kinematic surveys, since chances of solving the ambiguities increases if the ambiguities are solved at the time when the kinematic receiver is closer to the reference station. During the forward filtering of the trajectory, the software determines the time at which the kinematic receiver is closest to the reference station. Then, in the smoothed solution, the software is ready to trigger the OTF algorithm at the shortest distance to the reference station.

We can conclude that, in trajectory computation, a global processing approach is very helpful for the convergence of ambiguity parameters and the stabilization of auxiliary parameters, thus obtaining better formal accuracies of float ambiguity parameters. The improvement in the statistics of estimated ambiguity parameters adds flexibility to fix phase ambiguities at the part of the flight closest to the GPS reference station. Solving

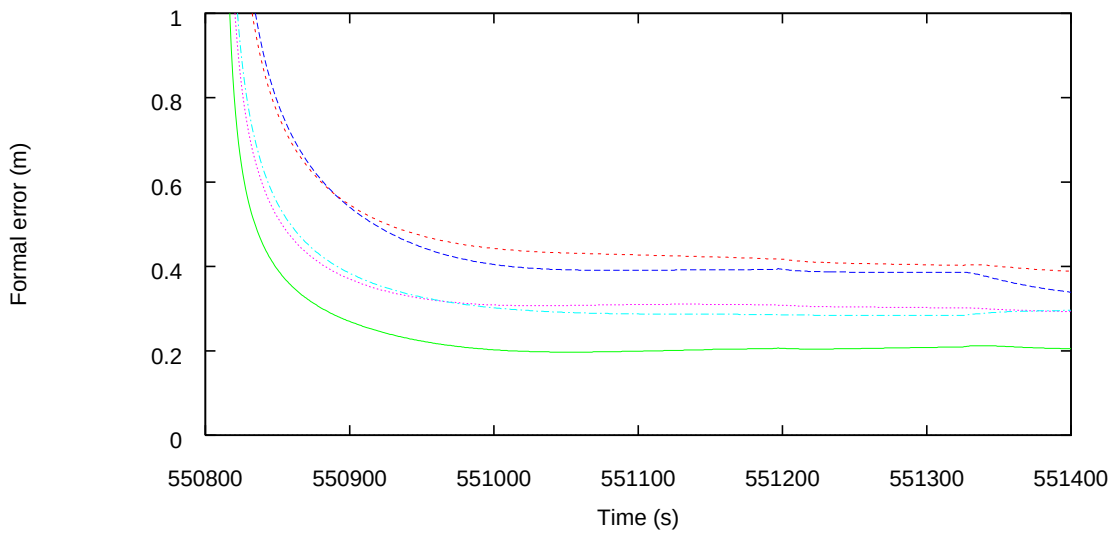

Figure 6.2: Formal precision of L1 ambiguity parameters (filtered).

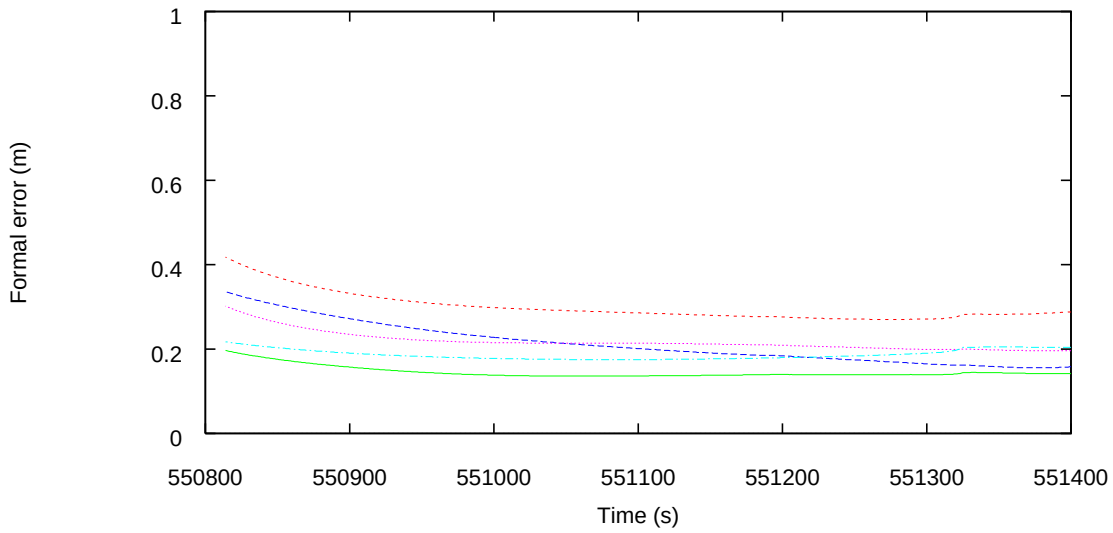

Figure 6.3: Formal precision of L1 ambiguity parameters (smoothed).

ambiguities close to the GPS reference station boosts the chances of finding the right values because the signal traveling from the satellite to rover and reference GPS receivers crosses a very similar portion of the atmosphere, and spatial errors (ionospheric, tropospheric and orbital errors) are much more correlated. If a double difference approach is used, the corresponding differential errors ($\nabla\Delta I^s_{ir}(t), \nabla\Delta\tau^s_r(t), \nabla\Delta\delta\rho$ in equations 2.3) are closer to zero.

The plotted photogrammetric flight of figure 6.4 illustrates the above concept. At the point when the distance between the aircraft and the reference station is smaller (27 km) the algorithms trying to solve the ambiguities have much fewer residual errors, and therefore much better chances of selecting the correct set of ambiguities, especially if compared to the point where the aircraft is farthest from the reference station (121 km). Thus, it is clear that a global processing and selecting the epoch to solve ambiguities provides a significant processing advantage.

6.2 Ionospheric modeling

The ionosphere is one of the limiting factors for ambiguity resolution, and therefore for precise kinematic positioning. As explained in Chapter 4, there are several ways to address the problem. The use of dual frequency receivers is mandatory if the distance to the reference station is more than 10 km. Dual frequency data may be combined obtaining a ionospheric free synthetic observable; however, as the associated ambiguity is not an integer number, it is not possible to solve the ambiguities. Use of global models or determination of local models from data collected by networks of reference GPS stations may help to solve the problem. Producing locals models instead of using ionospheric free combination has yielded excellent results in specific tests, [CHPJ+99], [HPJSC99], where the ionospheric model was produced at more than 100 km from the nearest reference station and with the required precision to solve ambiguities. However, in real life applications there are certain situations where it is not possible to rely on these models, for example surveys in areas with few permanent GPS stations or when a fast kinematic trajectory must be computed ([CTB95]) and it is not possible to wait for the models produced by third parties. Therefore, a robust kinematic algorithm must also be able to estimate ionospheric parameters to solve the correct ambiguities.

6.2.1 Stochastic ionospheric parameters

Stochastic ionospheric parameters for modeling the ionospheric effect can be utilized to obtain reasonable results in kinematic positioning. A new state is included on the state vector to account for the effect of $\nabla\Delta I^{1,2}_{1,2}$ in equations 2.3.

Although the ionosphere has a high spatial correlation, the distances between subionospheric points (described in Chapter 4) from one station may be longer than 2000 km at 15 degrees elevation. Therefore, in order to model the delay with the required accuracy one parameter is added in the state vector for each satellite-station pair. If double differences observations are used, each $\nabla\Delta I^{1,2}_{1,2}$ will be estimated by a different state.

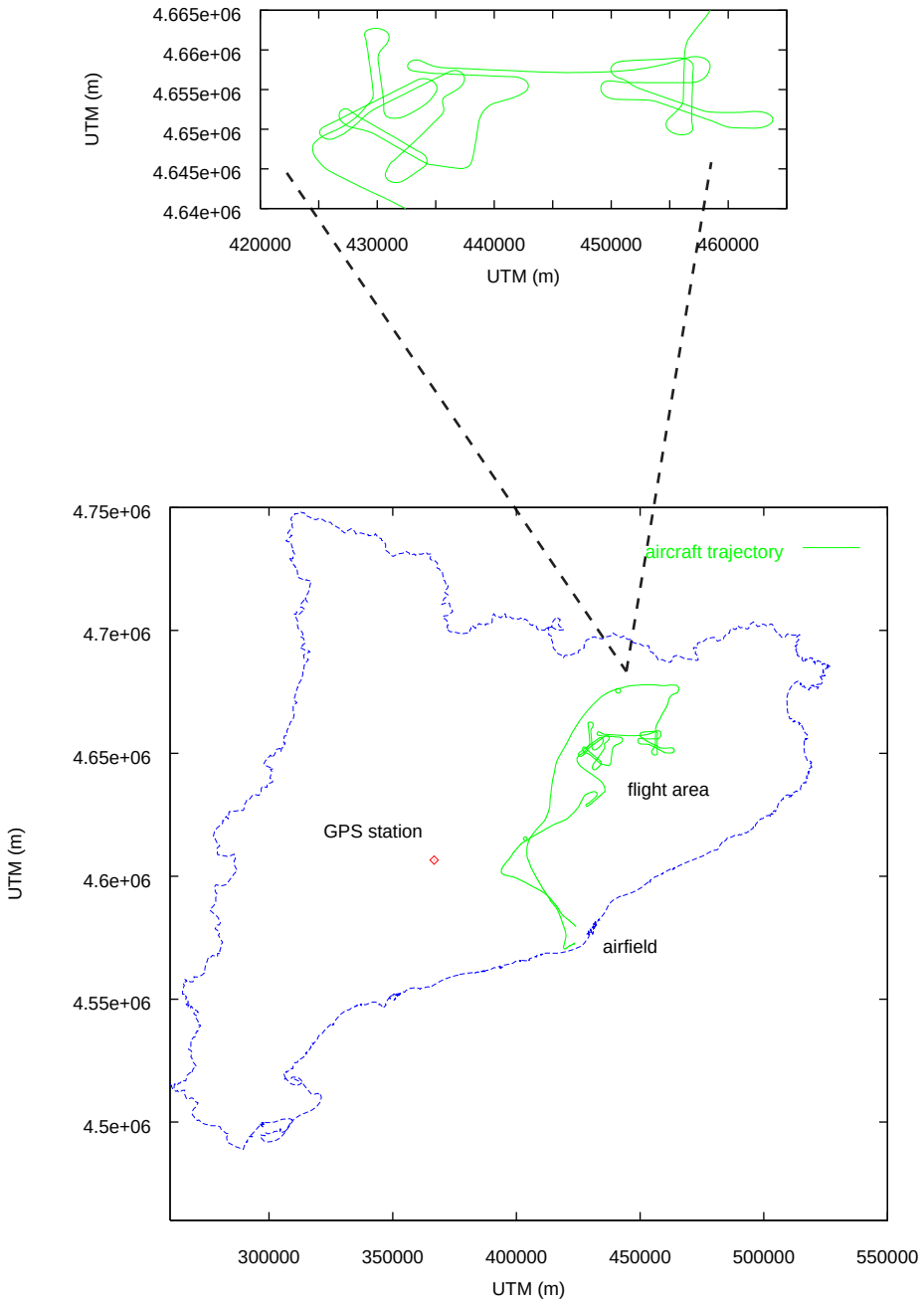

Figure 6.4: Aircraft trajectory of a large scale photogrammetric flight.

Temporal correlation of the ionosphere plays an important role in the definition of the system noise. Let S_i be the stochastic ionospheric state (random walk) that models the ionospheric effect $\nabla\Delta I^{1,2}_{1,2}$. Then, the dynamics of this state is

$$\dot{S}_{i_{t+1}} = w, \tag{6.3}$$

where w is a random variable of zero mean and standard deviation σ (white noise). The value assigned to the σ in the random variable is determined by the expected temporal correlation. It should be pointed out that if the σ is chosen as ∞ and dual frequency observations are processed, the system is equivalent to a ionospheric free pseudo-observation process. On the other hand, if a ionospheric model is applied and the value of $\nabla\Delta I^{1,2}_{1,2}$ is known at every epoch, then the σ of the random variable w is zero and the stochastic ionospheric parameters are only deterministic parameters.

The use of stochastic ionospheric parameters removes the restriction of requiring continuous observations of at least 4 satellites on L1 and L2 frequencies simultaneously [Fri98]. The information provided by the L1 and L2 observations allows stochastic ionospheric parameters to model the temporal variation of double difference ionospheric corrections, providing that the appropriate weights have been applied. Then, in time spans where L2 data is not available, the stochastic ionospheric parameters assist in modeling ionospheric effects.

If only L1 an L2 phase observations are processed in a double difference approach and ionospheric, tropospheric, ephemeris and instrumental errors are neglected, then for a receiver satellite pair equations 2.3 read:

$$\begin{aligned} \lambda_1 \cdot \nabla\Delta\Phi^{r,s}_{1_{f,m}} &= \nabla\Delta\rho^{r,s}_{f,m} + \lambda_1 \cdot \nabla\Delta N^{r,s}_{1_{f,m}}, \\ \lambda_2 \cdot \nabla\Delta\Phi^{r,s}_{2_{f,m}} &= \nabla\Delta\rho^{r,s}_{f,m} + \lambda_2 \cdot \nabla\Delta N^{r,s}_{2_{f,m}}, \end{aligned} \tag{6.4}$$

where

$$\begin{aligned} \nabla\Delta\rho^{r,s}_{f,m} = & \sqrt{(X_m - X^s)^2 + (Y_m - Y^s)^2 + (Z_m - Z^s)^2} \quad - \\ & \sqrt{(X_f - X^s)^2 + (Y_f - Y^s)^2 + (Z_f - Z^s)^2} \quad + \\ & \sqrt{(X_f - X^r)^2 + (Y_f - Y^r)^2 + (Z_f - Z^r)^2} \quad - \\ & \sqrt{(X_m - X^r)^2 + (Y_m - Y^r)^2 + (Z_m - Z^r)^2}. \end{aligned} \tag{6.5}$$

In equations 6.4, $\nabla\Delta\Phi^{r,s}_{1_{f,m}}$ and $\nabla\Delta\Phi^{r,s}_{2_{f,m}}$ are the (L1,L2) double difference satellite observations, (X_f,Y_f,Z_f) are the known coordinates of the reference station, (X^r,Y^r,Z^r) is the reference satellite position derived from the broadcast ephemeris and (X^s,Y^s,Z^s) the coordinates of satellite s derived from the broadcast ephemeris. Therefore, the unknowns of equation 6.4 are the position of the moving receiver (X_m,Y_m,Z_m) and the ambiguities $\nabla\Delta N^{r,s}_{1_{f,m}}$ and $\nabla\Delta N^{r,s}_{2_{f,m}}$.

The inclusion of stochastic ionospheric parameters adds one unknown per epoch and per satellite observed, so equations 6.4 read:

$$\begin{aligned} \lambda_1 \cdot \nabla\Delta\Phi^{r,s}_{1_{f,m}} &= \nabla\Delta\rho^{r,s}_{f,m} + \lambda_1 \cdot \nabla\Delta N^{r,s}_{1_{f,m}} - \nabla\Delta I^{r,s}_{f,m} f_1^{-2}, \\ \lambda_2 \cdot \nabla\Delta\Phi^{r,s}_{2_{f,m}} &= \nabla\Delta\rho^{r,s}_{f,m} + \lambda_2 \cdot \nabla\Delta N^{r,s}_{2_{f,m}} - \nabla\Delta I^{r,s}_{f,m} f_2^{-2}. \end{aligned} \tag{6.6}$$

In this equation, the unknowns to be estimated are the same as in equations 6.4 plus the additional stochastic parameter $\nabla\Delta I^{r,s}_{f,m}$. The convergence of these new parameters may be very slow because they are correlated with the ambiguity parameters (see equations 6.6). Fortunately, the correlation time of each stochastic process is different. Solving for ionospheric parameters together with ambiguity parameters may therefore require large time spans of observation to be processed (up to one hour). Loss of lock of some satellites and the addition of new ambiguity parameters make the convergence even more difficult.

In the case of postprocessing computation, the solution can be smoothed with forward and backward filters. Thus, if the session is long enough to allow the ionospheric parameters to converge, the smoothed solution is valid for the entire survey. If a real time solution must be obtained, the backward filter cannot be used. Then, the solution is not acceptable before the convergence of the stochastic ionospheric parameters, in which case a non-negligible initialization time must be given at the beginning of the survey.

6.2.2 Implementation

To implement ionospheric stochastic parameters in the postprocessing software, a new parameter must be added to the state vector for each satellite in view. This new parameter does not represent the ionospheric delay for one receiver-satellite observation but the double difference ionospheric delay ($\nabla\Delta I^{r,s}_{f,m}$). A new parameter for each station pair (f,m) and for each satellite pair (r,s) is therefore added to the state vector.

The ionospheric parameter can be estimated as a random walk or, considering the spatial and temporal correlation of ionospheric delays, it can be modeled as a Gauss-Markov process with a variance depending on the epoch interval and distance between both receivers.

The fact that new parameters are estimating double difference ionospheric delays implies that if there is a change in the reference satellite, a new set of parameters should be computed. The software must transform the parameters referred to reference satellite r_1 ($\nabla\Delta I^{r_1,s_1}_{f,m}, \nabla\Delta I^{r_1,s_2}_{f,m}, \nabla\Delta I^{r_1,s_3}_{f,m}, \nabla\Delta I^{r_1,s_4}_{f,m} \ldots$) into double difference ionospheric delays referred to the new reference satellite. For example, if the new reference satellite is s_1, the ionospheric parameters can be easily transformed as follows:

$$\begin{aligned} \nabla\Delta I^{s_1,r_1}_{f,m} &= -\nabla\Delta I^{r_1,s_1}_{f,m}, \\ \nabla\Delta I^{s_1,s_2}_{f,m} &= \nabla\Delta I^{r_1,s_2}_{f,m} - \nabla\Delta I^{r_1,s_1}_{f,m}, \\ \nabla\Delta I^{s_1,s_3}_{f,m} &= \nabla\Delta I^{r_1,s_3}_{f,m} - \nabla\Delta I^{r_1,s_1}_{f,m}, \\ \nabla\Delta I^{s_1,s_4}_{f,m} &= \nabla\Delta I^{r_1,s_4}_{f,m} - \nabla\Delta I^{r_1,s_1}_{f,m}, \\ &\ldots \end{aligned} \tag{6.7}$$

In order to apply the parameter transformations shown in 6.7 after a change in the reference satellite, the software must ensure that the new and the old reference satellites

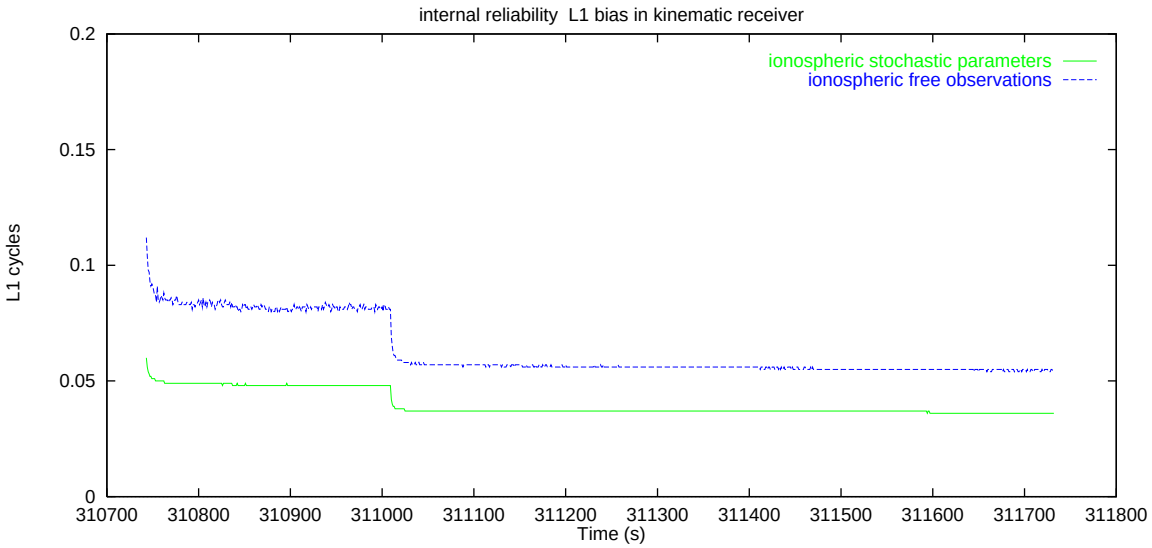

Figure 6.5: MDB using a ionospheric free observable and stochastic ionospheric parameters

are present simultaneously for at least one epoch. If that is not the case the value $\nabla\Delta I_{f,m}^{r_1,s_1}$ does not exist and it is therefore not possible to apply 6.7; then, new parameters need to be estimated.

Data from a real survey has been used to study the increase in reliability introduced by stochastic ionospheric parameters. In figure 6.5 the MDB (corresponding to the L1 observable of satellite prn 9) when ionospheric free observables are used is compared to the MDB when ionospheric stochastic parameters are adjusted. It can be seen that there is an improvement of about 35% in the MDB. The jump in the plot is due to the fact that a new satellite has risen above the cutoff angle. More satellites in view imply a better constellation and, a better chance of detecting a bias (lower MDB).

If available, global or regional ionospheric models can be easily used (without changing the state vector) by adding the following pseudo-observations:

$$\nabla\Delta I_{f,m}^{r,s} = ion_{model}(m,s) - ion_{model}(f,s) + ion_{model}(f,r) - ion_{model}(m,r), \tag{6.8}$$

where $ion_{model}(i,j)$ is the ionospheric delay given by the model corresponding to the signal path from satellite j to receiver i. These pseudo-observations are utilized in the computation with a weight depending on the accuracy of the ionospheric model employed. If a very precise regional model is used, the weight is very high and the stochastic ionospheric parameters remain fixed to the values provided by the model. If a general low precision ionospheric model is used, then the pseudo-observations 6.8 would be employed with a very low weight and would have little effect on the trajectory computation.

6.3 Multiple reference receivers

Another possibility of incrementing the robustness of surveys is to increase the number of reference receivers. Processing more than one reference receiver raises the number of observations, which is the best way to increase reliability. As has been mentioned before, the objective of a reference receiver is to cancel out/mitigate common errors with the kinematic receiver. Some common errors (mainly ionospheric and tropospheric errors) show a high spatial correlation while other errors (satellite clocks) are not spatially correlated and have very similar effects on all observers regardless of their location. The fact that a set of reference receivers is covering a certain area can be used for eliminating/mitigating the spatial correlated errors over that area and that should be done whenever possible. Some works have been carried out [Raq98], [Wei97], [Fot00] to study the benefits of multiple reference receivers.

When double difference phase observations from a network of reference receivers are used, the correct correlations must be taken into account.

Let $\nabla\Delta\Phi_{k,r_i}^{s_j,s_r}$ be a double difference observation where

$$\begin{array}{lcl} \Phi_k^{s_j} & = & \text{phase observation from satellite j and kinematic receiver,} \\ \Phi_k^{s_r} & = & \text{phase observation from reference satellite and kinematic receiver,} \\ \Phi_{r_i}^{s_j} & = & \text{phase observation from satellite j and reference receiver i,} \\ \Phi_{r_i}^{s_r} & = & \text{phase observation from reference satellite and reference receiver i,} \end{array} \tag{6.9}$$

with the associated variance $\varsigma_k^{s_j}$, $\varsigma_k^{s_r}$, $\varsigma_{r_i}^{s_j}$, $\varsigma_{r_i}^{s_r}$.

If a kinematic receiver and a reference station (r_1) are observing a constellation of 5 satellites, then the covariance matrix associated to double difference observations is

$$\begin{pmatrix} \varsigma_k^{s_1}+\varsigma_k^{s_r}+\varsigma_{r_1}^{s_1}+\varsigma_{r_1}^{s_r} & \varsigma_{r_1}^{s_r}+\varsigma_k^{s_r} & \varsigma_{r_1}^{s_r}+\varsigma_k^{s_r} & \varsigma_{r_1}^{s_r}+\varsigma_k^{s_r} \\ \varsigma_{r_1}^{s_r}+\varsigma_k^{s_r} & \varsigma_k^{s_2}+\varsigma_k^{s_r}+\varsigma_{r_1}^{s_2}+\varsigma_{r_1}^{s_r} & \varsigma_{r_1}^{s_r}+\varsigma_k^{s_r} & \varsigma_{r_1}^{s_r}+\varsigma_k^{s_r} \\ \varsigma_{r_1}^{s_r}+\varsigma_k^{s_r} & \varsigma_{r_1}^{s_r}+\varsigma_k^{s_r} & \varsigma_k^{s_3}+\varsigma_k^{s_r}+\varsigma_{r_1}^{s_3}+\varsigma_{r_1}^{s_r} & \varsigma_{r_1}^{s_r}+\varsigma_k^{s_r} \\ \varsigma_{r_1}^{s_r}+\varsigma_k^{s_r} & \varsigma_{r_1}^{s_r}+\varsigma_k^{s_r} & \varsigma_{r_1}^{s_r}+\varsigma_k^{s_r} & \varsigma_k^{s_4}+\varsigma_k^{s_r}+\varsigma_{r_1}^{s_4}+\varsigma_{r_1}^{s_r} \end{pmatrix} \tag{6.10}$$

If we have a second reference receiver (r_2) and we build double difference observations between the kinematic receiver and this reference receiver (r_2), then the covariance matrix from the double difference observations is

$$\begin{pmatrix} \varsigma_k^{s_1}+\varsigma_k^{s_r}+\varsigma_{r_2}^{s_1}+\varsigma_{r_2}^{s_r} & \varsigma_{r_2}^{s_r}+\varsigma_k^{s_r} & \varsigma_{r_2}^{s_r}+\varsigma_k^{s_r} & \varsigma_{r_2}^{s_r}+\varsigma_k^{s_r} \\ \varsigma_{r_2}^{s_r}+\varsigma_k^{s_r} & \varsigma_k^{s_2}+\varsigma_k^{s_r}+\varsigma_{r_2}^{s_2}+\varsigma_{r_2}^{s_r} & \varsigma_{r_2}^{s_r}+\varsigma_k^{s_r} & \varsigma_{r_2}^{s_r}+\varsigma_k^{s_r} \\ \varsigma_{r_2}^{s_r}+\varsigma_k^{s_r} & \varsigma_{r_2}^{s_r}+\varsigma_k^{s_r} & \varsigma_k^{s_3}+\varsigma_k^{s_r}+\varsigma_{r_2}^{s_3}+\varsigma_{r_2}^{s_r} & \varsigma_{r_2}^{s_r}+\varsigma_k^{s_r} \\ \varsigma_{r_2}^{s_r}+\varsigma_k^{s_r} & \varsigma_{r_2}^{s_r}+\varsigma_k^{s_r} & \varsigma_{r_2}^{s_r}+\varsigma_k^{s_r} & \varsigma_k^{s_4}+\varsigma_k^{s_r}+\varsigma_{r_2}^{s_4}+\varsigma_{r_2}^{s_r} \end{pmatrix} \tag{6.11}$$

If we want to process both sets of double difference observations at the same time (kinematic-reference$_1$ and kinematic-reference$_2$), it is clear that they will be correlated (the observations measured by the kinematic receiver are used on both sets of double difference

data). Thereby, this correlation should be determined and used in the computation. Take, for example, the case of a survey with one kinematic receiver and two reference receivers (r_1 and r_2). The associated covariance matrix for double difference GPS observations is

$$\begin{pmatrix}
\nabla\Delta\varsigma_{k,r_1}^{s_1,s_r} & \Delta\varsigma_{k,r_1}^{s_r} & \Delta\varsigma_{k,r_1}^{s_r} & \Delta\varsigma_{k,r_1}^{s_r} & \nabla\varsigma_k^{s_1,s_r} & \varsigma_k^{s_r} & \varsigma_k^{s_r} & \varsigma_k^{s_r} \\
\Delta\varsigma_{k,r_1}^{s_r} & \nabla\Delta\varsigma_{k,r_1}^{s_2,s_r} & \Delta\varsigma_{k,r_1}^{s_r} & \Delta\varsigma_{k,r_1}^{s_r} & \varsigma_k^{s_r} & \nabla\varsigma_k^{s_2,s_r} & \varsigma_k^{s_r} & \varsigma_k^{s_r} \\
\Delta\varsigma_{k,r_1}^{s_r} & \Delta\varsigma_{k,r_1}^{s_r} & \nabla\Delta\varsigma_{k,r_1}^{s_3,s_r} & \Delta\varsigma_{k,r_1}^{s_r} & \varsigma_k^{s_r} & \varsigma_k^{s_r} & \nabla\varsigma_k^{s_3,s_r} & \varsigma_k^{s_r} \\
\Delta\varsigma_{k,r_1}^{s_r} & \Delta\varsigma_{k,r_1}^{s_r} & \Delta\varsigma_{k,r_1}^{s_r} & \nabla\Delta\varsigma_{k,r_1}^{s_4,s_r} & \varsigma_k^{s_r} & \varsigma_k^{s_r} & \varsigma_k^{s_r} & \nabla\varsigma_k^{s_4,s_r} \\
\nabla\varsigma_k^{s_1,s_r} & \varsigma_k^{s_r} & \varsigma_k^{s_r} & \varsigma_k^{s_r} & \nabla\Delta\varsigma_{k,r_2}^{s_1,s_r} & \Delta\varsigma_{k,r_2}^{s_r} & \Delta\varsigma_{k,r_2}^{s_r} & \Delta\varsigma_{k,r_2}^{s_r} \\
\varsigma_k^{s_r} & \nabla\varsigma_k^{s_2,s_r} & \varsigma_k^{s_r} & \varsigma_k^{s_r} & \Delta\varsigma_{k,r_2}^{s_r} & \nabla\Delta\varsigma_{k,r_2}^{s_2,s_r} & \Delta\varsigma_{k,r_2}^{s_r} & \Delta\varsigma_{k,r_2}^{s_r} \\
\varsigma_k^{s_r} & \varsigma_k^{s_r} & \nabla\varsigma_k^{s_3,s_r} & \varsigma_k^{s_r} & \Delta\varsigma_{k,r_2}^{s_r} & \Delta\varsigma_{k,r_2}^{s_r} & \nabla\Delta\varsigma_{k,r_2}^{s_3,s_r} & \Delta\varsigma_{k,r_2}^{s_r} \\
\varsigma_k^{s_r} & \varsigma_k^{s_r} & \varsigma_k^{s_r} & \nabla\varsigma_k^{s_4,s_r} & \Delta\varsigma_{k,r_2}^{s_r} & \Delta\varsigma_{k,r_2}^{s_r} & \Delta\varsigma_{k,r_2}^{s_r} & \nabla\Delta\varsigma_{k,r_2}^{s_4,s_r}
\end{pmatrix} \tag{6.12}$$

where

$$\begin{aligned}
\nabla\varsigma_k^{s_i,s_r} &= \varsigma_k^{s_i} + \varsigma_k^{s_r}, \\
\Delta\varsigma_{k,r_i}^{s_r} &= \varsigma_{r_i}^{s_r} + \varsigma_k^{s_r}, \\
\nabla\Delta\varsigma_{k,r_i}^{s_j,s_r} &= \varsigma_k^{s_j} + \varsigma_k^{s_r} + \varsigma_{r_i}^{s_j} + \varsigma_{r_i}^{s_r}.
\end{aligned} \tag{6.13}$$

Another advantage of using multiple reference stations is the possibility of applying multipath reduction techniques that take advantage of the fact that the environment of the permanent reference stations remains unalterable while the geometry of the GPS constellation has a period of approximately 23 hours 56 minutes. Comparing phase residuals observed one day apart it is possible to mitigate the effect of the multipath.

6.3.1 Ambiguity constraints

In order to obtain a precise kinematic positioning, it is necessary to decorrelate the ambiguity parameters from other effects, mainly tropospheric and ionospheric errors, and as a consequence to obtain the precise trajectory of the rover receiver. As explained above, when a network of reference receivers is used it is possible to add more double difference observations in the kinematic computation (using the appropriate correlations). However, for each new double difference phase observation utilized in the adjustment, a new ambiguity parameter must be solved. Thus, if the use of a network of reference receivers is adding n extra double difference phase observations, then n additional ambiguity parameters must be solved.

In order to take full advantage of the network of reference receivers, it is advisable to preprocess the double difference observations between reference receivers, and making use of their known precise coordinates, solve the corresponding ambiguities. Then, in kinematic computations the solved ambiguities between reference stations can be used as a constraint to help in the decorrelation between atmospheric effects and ambiguity parameters [Tal00].

Using the notation from equations 2.1:

$$\begin{aligned}
\lambda_1 \cdot \nabla\Delta\Phi^{s_1,s_r}_{1_{k,r_1}} &= \nabla\Delta\rho^{s_1,s_r}_{k,r_1} + \nabla\Delta\tau^{s_1,s_r}_{k,r_1} - \nabla\Delta I^{s_1,s_r}_{k,r_1} f_1^{-2} + \lambda_1 \cdot \nabla\Delta N^{s_1,s_r}_{1_{k,r_1}}, \\
\lambda_1 \cdot \nabla\Delta\Phi^{s_1,s_r}_{1_{k,r_2}} &= \nabla\Delta\rho^{s_1,s_r}_{k,r_2} + \nabla\Delta\tau^{s_1,s_r}_{k,r_2} - \nabla\Delta I^{s_1,s_r}_{k,r_2} f_1^{-2} + \lambda_1 \cdot \nabla\Delta N^{s_1,s_r}_{1_{k,r_2}},
\end{aligned} \tag{6.14}$$

with $\nabla\Delta\Phi^{s_1,s_r}_{1_{k,r_1}}, \nabla\Delta\Phi^{s_1,s_r}_{1_{k,r_2}}$ being two L1 double difference observations between satellites (s_1, s_r), a kinematic receiver k and two reference receivers (r_1, r_2). As explained above, there are two ambiguity parameters that need to be solved: $\nabla\Delta N^{s_1,s_r}_{1_{k,r_1}}$ and $\nabla\Delta N^{s_1,s_r}_{1_{k,r_2}}$.

The L1 double difference observation $\nabla\Delta\Phi^{s_1,s_r}_{1_{r_1,r_2}}$ between reference receivers r_1 and r_2 can also be made. However, this observation is not independent of the observations used in 6.14 as the following relation holds:

$$\nabla\Delta\Phi^{s_1,s_r}_{1_{r_1,r_2}} = \nabla\Delta\Phi^{s_1,s_r}_{1_{k,r_2}} - \nabla\Delta\Phi^{s_1,s_r}_{1_{k,r_1}}. \tag{6.15}$$

If the double difference L1 observations $\nabla\Delta\Phi^{s_1,s_r}_{1_{r_1,r_2}}$ between the reference stations are processed taking into account that the coordinates of the reference stations are known, then all the ambiguity parameters corresponding to the double difference observations between reference stations can be solved. Once these ambiguity parameters are solved, they can be used in the determination of the kinematic trajectory as a constraint. For each satellite pair and for each independent reference receiver pair, the following constraint is added in the computation:

$$\begin{aligned}
\lambda_1 \cdot \nabla\Delta\Phi^{s_1,s_r}_{1_{k,r_1}} &= \nabla\Delta\rho^{s_1,s_r}_{k,r_1} + \nabla\Delta\tau^{s_1,s_r}_{k,r_1} - \nabla\Delta I^{s_1,s_r}_{k,r_1} f_1^{-2} + \lambda_1 \cdot \nabla\Delta N^{s_1,s_r}_{1_{k,r_1}}, \\
\lambda_1 \cdot \nabla\Delta\Phi^{s_1,s_r}_{1_{k,r_2}} &= \nabla\Delta\rho^{s_1,s_r}_{k,r_2} + \nabla\Delta\tau^{s_1,s_r}_{k,r_2} - \nabla\Delta I^{s_1,s_r}_{k,r_2} f_1^{-2} + \lambda_1 \cdot \nabla\Delta N^{s_1,s_r}_{1_{k,r_2}}, \\
\nabla\Delta N^{s_1,s_r}_{1_{r_1,r_2}} &= \nabla\Delta N^{s_1,s_r}_{1_{k,r_2}} - \nabla\Delta N^{s_1,s_r}_{1_{k,r_1}},
\end{aligned} \tag{6.16}$$

with $\nabla\Delta N^{s_1,s_r}_{1_{r_1,r_2}}$ being the known ambiguity parameters corresponding to the double difference observations from satellites (s_1, s_r) and receivers (r_1, r_2).

The same reasoning can be applied to the L2 frequency.

Once the constraints are added in the computation, it is clear that the use of a network of reference receivers does not increase the number of ambiguity parameters to be solved. If the ambiguities related to the double difference observations between the kinematic and reference receiver r_1 are taken as the basic ambiguities, then every new double difference observation between the kinematic receiver and reference receiver r_n incorporates a new ambiguity and a new constraint (provided that the ambiguities between reference receivers 1 and n are known).

If a network of reference receivers is available, solving such a high number of extra equations or constraints can be a very computer demanding task. In this case, it is enough to select a subset of reference stations surrounding the area of interest, for example, three stations provided the moving receiver lie inside the triangle defined by the reference stations.

6.3.2 Ionospheric constraints

If the ionospheric stochastic parameters described in 6.2.1 are used, the approach described in the previous section can also be used for constraining ionospheric stochastic parameters. In this case, double difference observations between reference stations must be preprocessed in order to determine the double difference ionospheric error $\nabla\Delta I^{s_1,s_r}_{r_1,r_2}$ between reference stations. As the coordinates from reference stations are precisely known and the coordinates of satellites are also precisely known (in particular if precise ephemerides are used), the value of $\nabla\Delta\rho^{s_1,s_r}_{r_1,r_2}$ may be accurately determined. A look at the double difference observation equations between a pair of reference stations (equation 6.17), shows that once the ambiguity parameters are solved, it is not difficult to compute the values of the ionospheric $\nabla\Delta I^{s_1,s_r}_{r_1,r_2}$ and tropospheric $\nabla\Delta\tau^{s_1,s_r}_{r_1,r_2}$ parameters:

$$\begin{aligned}
\lambda_1\cdot\nabla\Delta\Phi^{s_1,s_r}_{1_{r_1,r_2}} &= \nabla\Delta\rho^{s_1,s_r}_{r_1,r_2}+\nabla\Delta\tau^{s_1,s_r}_{r_1,r_2}-\nabla\Delta I^{s_1,s_r}_{r_1,r_2}f_1^{-2}+\lambda_1\cdot\nabla\Delta N^{s_1,s_r}_{1_{r_1,r_2}},\\
\lambda_2\cdot\nabla\Delta\Phi^{s_1,s_r}_{2_{r_1,r_2}} &= \nabla\Delta\rho^{s_1,s_r}_{r_1,r_2}+\nabla\Delta\tau^{s_1,s_r}_{r_1,r_2}-\nabla\Delta I^{s_1,s_r}_{r_1,r_2}f_2^{-2}+\lambda_2\cdot\nabla\Delta N^{s_1,s_r}_{2_{r_1,r_2}}.
\end{aligned} \tag{6.17}$$

This information can be used in kinematic processing and a similar relation to 6.16 holds for ionospheric parameters. The constraint to be applied is described in equation 6.18. The use of multiple reference stations does not increase the number of ionospheric parameters to be solved:

$$\nabla\Delta I^{s_1,s_r}_{1_{r_1,r_2}} = \nabla\Delta I^{s_1,s_r}_{1_{k,r_2}}-\nabla\Delta I^{s_1,s_r}_{1_{k,r_1}}. \tag{6.18}$$

6.3.3 Tropospheric constraints

As in to the previous sections, preprocessing data between reference stations also allows the double difference tropospheric parameter $\nabla\Delta\tau^{s_1,s_r}_{r_1,r_2}$ to be accurately known.

However, the use of this information in kinematic preprocessing is slightly more complicated although the relation used for double difference ionospheric and double difference ambiguity parameters also holds for the double difference tropospheric parameter (see equation 6.19), this constraint cannot be applied directly.

$$\nabla\Delta\tau^{s_1,s_r}_{r_1,r_2} = \nabla\Delta\tau^{s_1,s_r}_{k,r_2}-\nabla\Delta\tau^{s_1,s_r}_{k,r_1}. \tag{6.19}$$

As explained in Chapter 3, the usual way to treat the tropospheric effect is to estimate a differential tropospheric parameter per station pair and to apply a mapping function to compute the effect of the troposphere on a given satellite. Therefore, the estimated parameter is not a double difference tropospheric delay $\nabla\Delta\tau^{s_1,s_r}_{r_1,r_2}$ but the differential zenith tropospheric delay τ_{r_1,r_2}. The double difference tropospheric delay can be derived by using the following equation:

$$\nabla\Delta\tau^{s_1,s_r}_{r_1,r_2} = (map(r_1,s_1)-map(r_1,s_r)-(map(r_2,s_1)+map(r_2,s_r))\cdot\tau_{r_1,r_2}, \tag{6.20}$$

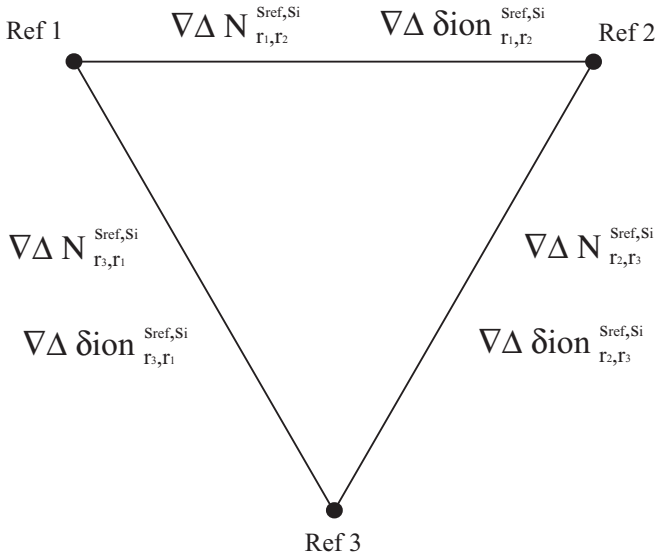

Figure 6.6: 1st step in a multiple reference station computation

where $map(r_i, s_i)$ is the mapping function from satellite s_i observed at site r_i, and τ_{r_i,r_j} is the differential tropospheric parameter computed in the processing.

By substituting relation 6.20 in equation 6.19, we obtain the following relation:

$$\begin{array}{ll} (map(r_1,s_1) - map(r_1,s_r) - (map(r_2,s_1) + map(r_2,s_r)) \cdot \tau_{r_1,r_2} & = \\ (map(k,s_1) - map(k,s_r) - (map(r_2,s_1) + map(r_2,s_r)) \cdot \tau_{k,r_2} & - \\ (map(k,s_1) - map(k,s_r) - (map(r_1,s_1) + map(r_1,s_r)) \cdot \tau_{k,r_1}. & \end{array} \tag{6.21}$$

In this constraint the value of the mapping functions $map(r_i, s_j)$ is known and the value of the tropospheric zenith delay $\tau_{n,m}$ corresponds to the parameters estimated in the state vector. Therefore, when processing a kinematic GPS trajectory using two reference stations r_1, r_2, the corresponding differential tropospheric delays $\tau_{k,r_1}, \tau_{k,r_2}$ are included in the state vector. However, as the differential tropospheric delay between reference stations τ_{r_1,r_2} is computed in the first step, equation 6.21 can be used either to add a new equation in the computation or to eliminate one unknown.

6.3.4 Implementation

The best way to implement a multiple reference station computation making use of the ambiguity, ionospheric and tropospheric constraints is by doing a two-step process. In the first step, the double difference computations between reference stations are made, fixing the precisely known stations coordinates and solving the ambiguity, ionospheric and tropospheric parameters, (see figure 6.6). All this information can be stored in a file for later use in the computation of different kinematic surveys in the area covered by the network of reference stations.

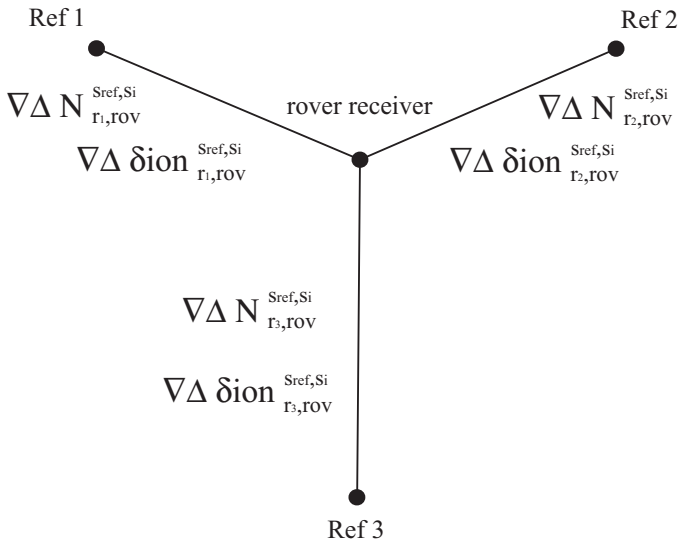

Figure 6.7: 2st step in a multiple reference station computation

The second step will consist in the trajectory determination by generating all the double difference observations between the kinematic receiver and the network of permanent stations, (see figure 6.7). The corresponding double difference ambiguity, ionospheric and tropospheric parameters from the reference stations are read at each epoch from the file generated in the first step and applied in the computations as constraints of the state vector parameters, according to equations 6.16, 6.18, 6.21.

To solve the ambiguity parameters, the software determines the epoch at which the survey is closest to a reference station. Once the smoothed trajectory has been computed up to the closest epoch, the OTF algorithm is triggered. If the postprocessing software is able to solve the ambiguity parameters corresponding to the closest reference station, then all the ambiguity parameters between the kinematic receiver and all the reference stations are automatically solved applying the ambiguity constraints.

A real life photogrammetric flight was used to study the increase in robustness with a network of permanent receivers. The survey was made over Olot and three permanent GPS stations surrounded the area, (see figure 6.8). This study has been presented in [Tal00].

It is clear that the use of multiple reference receivers increases the redundancy of reference GPS data dramatically, rendering the system much more robust against bias on observables from a reference station. A study of MDB in the presence of a bias on the measurement of a reference station can be seen in figure 6.9. This plot shows the double difference L1 observable internal reliability (for a particular satellite) of a small interval of the Olot flight. The corresponding external reliability can be observed in figure 6.10. In that particular part of the flight, an increase of 60%–90% in reliability is observed when a network of permanent GPS stations is utilized.

If the bias occurs on satellite m in the kinematic GPS receiver, the bias affects all the double difference observations between the kinematic receiver and all the reference

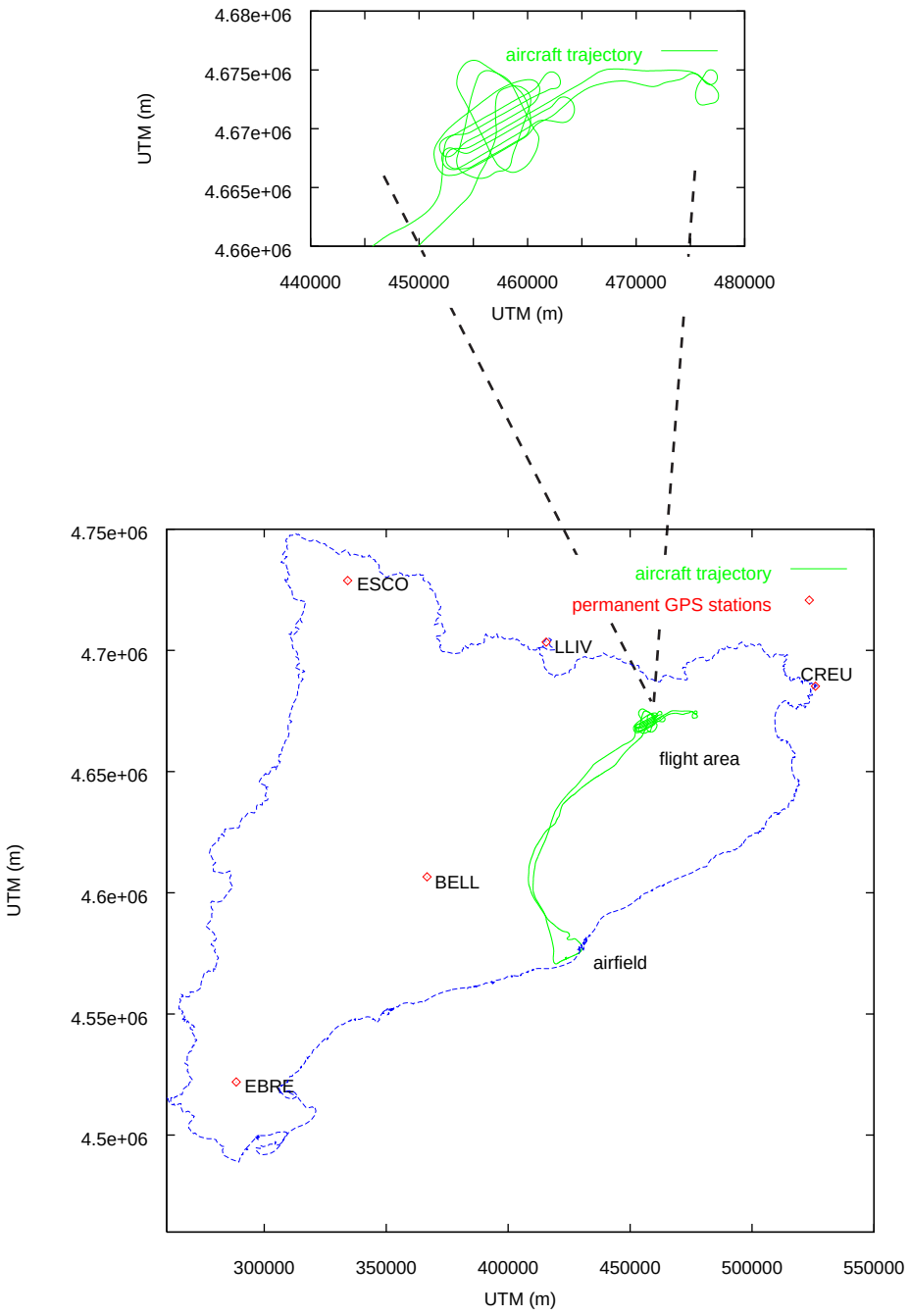

Figure 6.8: Olot flight path

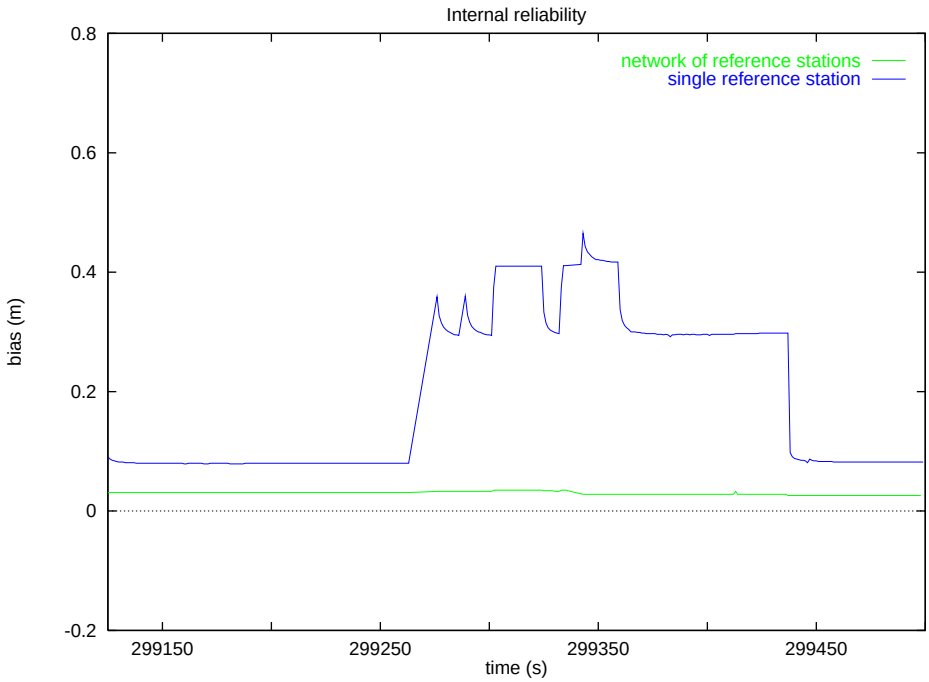

Figure 6.9: Internal reliability: bias in one reference receiver

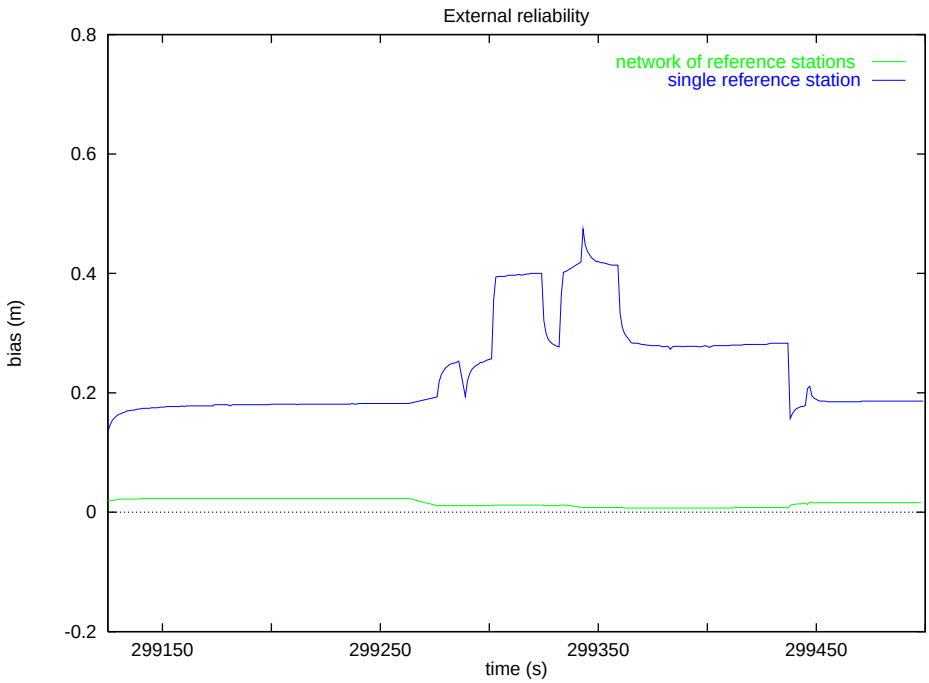

Figure 6.10: External reliability: bias in one reference receiver

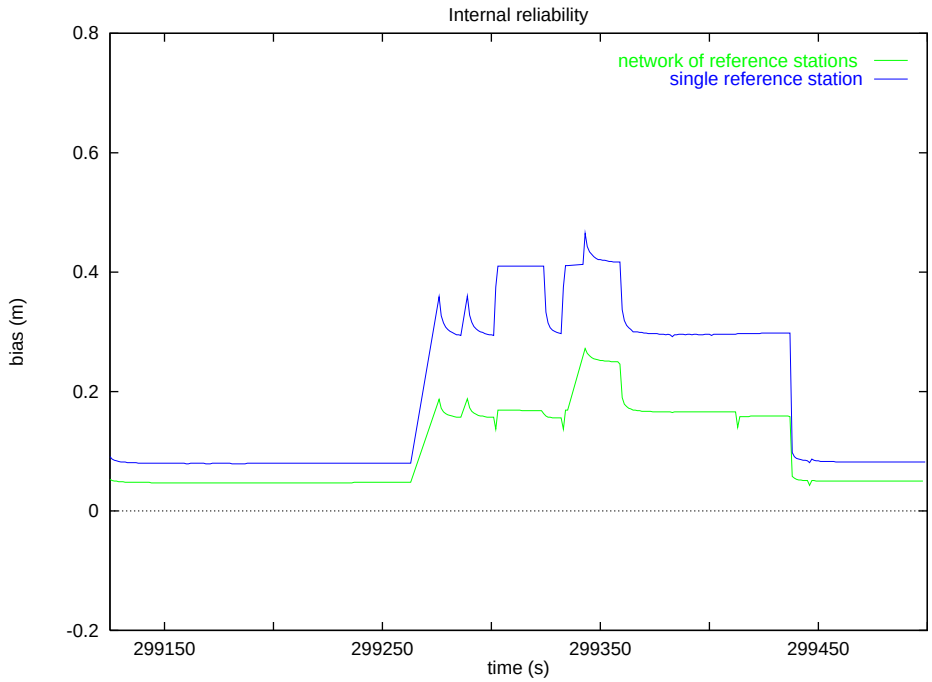

Figure 6.11: Internal reliability: bias in the kinematic receiver (L1 observable)

stations where this satellite m is present. Therefore, the improvement in robustness is not as dramatic as in the previous case, yet it increases by a factor of 30%–40%, as can be seen in figures 6.11 and 6.12.

In case a simultaneous bias occurs in the kinematic receiver in the L1 and L2 observables, the bias also affects all the double difference observations generated using that data. In this case, the L2 observable cannot *control* the L1 observable. Consequently, the magnitudes of the internal and external reliability are much bigger than in the previous cases (see figures 6.13 and 6.14. This kind of simultaneous bias in the L1 and L2 observables is not usual but can sometimes be found from in GPS data.

6.4 Multiple kinematic receivers

As explained in the previous section, the use of multiple reference GPS stations has several advantages in cycle slip detection, multipath mitigation and ionospheric modeling. However, like static receivers, kinematic receivers can also have observation problems (multipath, cycle slip, occlusions . . .). Multipath can be much worse in kinematic receivers because a place with no obstructions is carefully chosen for the location of a reference station, and the antennas are choke ring antennas, or equivalent performance patterns, designed for multipath reduction. This is not the case of the airborne antenna, since the antenna is installed over the metal surface of the airplane body and the site is not optimal from the multipath and occlusions point of view. The tail and the wings of the airplane can block the signal coming from the satellite, during the turns, causing the antenna to work under high multipath conditions, (see figure 6.15). Some antenna models designed

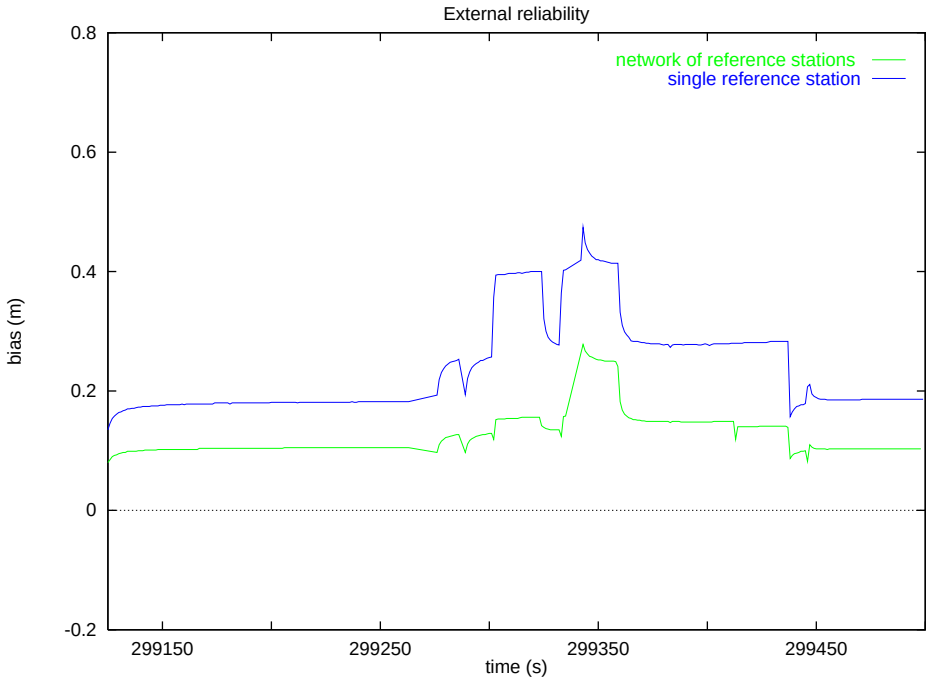

Figure 6.12: External reliability: bias in the kinematic receiver (L1 observable)

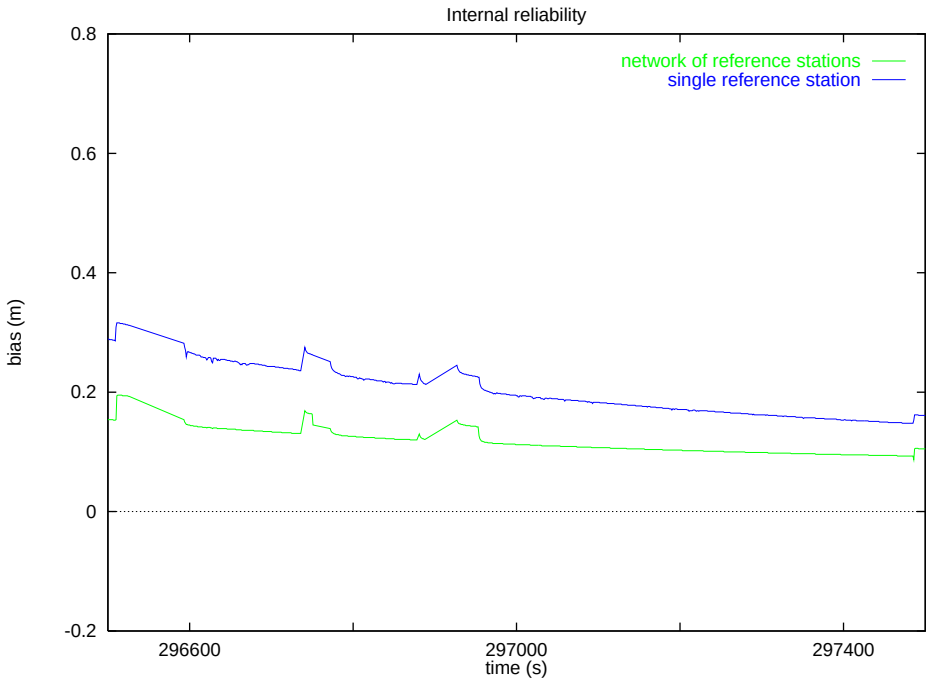

Figure 6.13: Internal reliability: bias in the kinematic receiver (L1 and L2 observables)

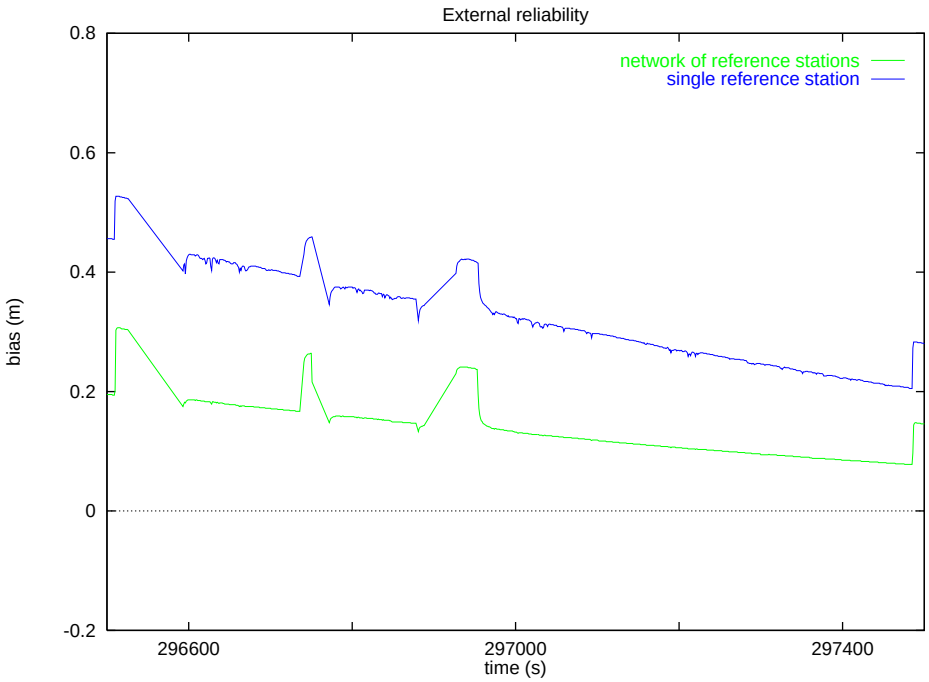

Figure 6.14: External reliability: bias in the kinematic receiver (L1 and L2 observables)

for multipath mitigation, such as choke ring antennas, may not be used in an airborne environment because an antenna must have an aerodynamic shape to be installed on the fuselage. Recent antenna designs, based on clusters of small antennas, are much more multipath resistant than the classical kinematic ones. Therefore, further advances in this field can be expected in the near future.

It is clear that the working environment of the kinematic antenna is not optimal and may have some problems when GPS signals are observed. In order to improve the performance of a kinematic receiver and to mitigate some of the observation problems (multipath, cycle slip and occlusions), it is possible to install another receiver that works with an independent antenna on the airplane.

The measurements of the secondary antenna are highly independent of the measurements of the primary antenna. A first approach is to use that information to compute an independent trajectory of the airplane. The comparisons with the primary trajectory can provide some information on the quality of the computation [SC94]. However, it is better to use this information to improve the quality of the trajectory.

In principle, the advantage is clear; the more observations in the computation, the more reliable the solution. The additional observation cannot be used directly in the computation of the main parameters (coordinates of the primary airborne antenna) because the GPS observations from the secondary kinematic receiver are referred to the coordinates of the secondary antenna. Consequently, some relations between the two kinematic antennas must be found in order to use the observations from the secondary receiver in the computations.

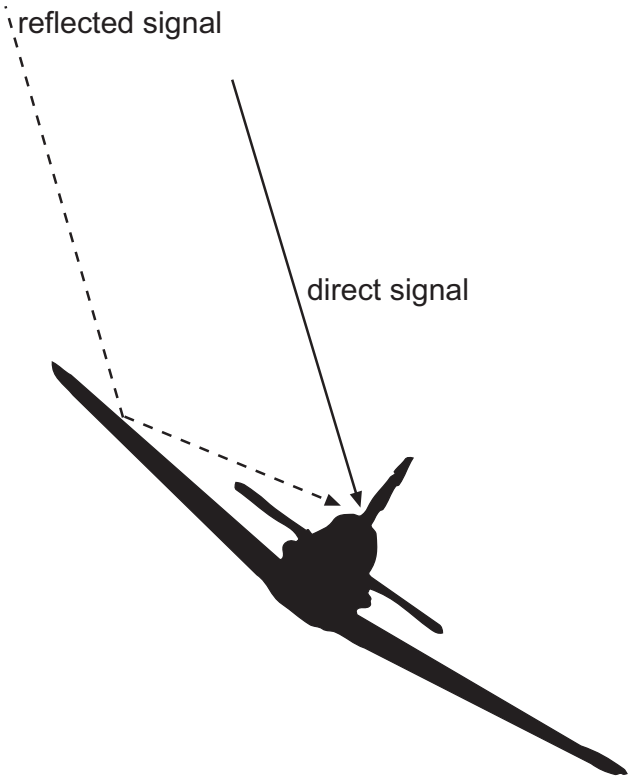

Figure 6.15: Multipath environment of an airborne antenna.

6.4.1 Distance constraint

The vector (in an Earth Center Earth Fixed ECEF reference system) between the two kinematic antennas is not constant: its orientation keeps changing while airplane is moving. However, it is clear that the distance remains invariant during the survey and can be accurately measured. Therefore, a first approach to relate the observation of the primary and secondary receiver is to incorporate a distance constraint in computations.

Let $(X_{k_1}, Y_{k_1}, Z_{k_1})$ be the coordinates of the primary airborne antenna, $(X_{k_2}, Y_{k_2}, Z_{k_2})$ the coordinates of the secondary airborne antenna and δ_{k_1,k_2} the measured distance between the primary and secondary airborne antennas.

The observation model of the primary antenna (see equation 6.22) is a function of the coordinates of this antenna (unknown), the GPS observations collected by the primary kinematic receiver, the GPS observations measured by the reference receiver and other parameters such as the coordinates of the reference station, satellites ...

$$
\begin{aligned}
\lambda_i \cdot \nabla\Delta\Phi^{s_j,s_r}_{i_{k_1,r}} &= \nabla\Delta\rho^{s_j,s_r}_{k_1,r} + \nabla\Delta\tau^{s_j,s_r}_{k,r} - \nabla\Delta I^{s_j,s_r}_{k,r} f_i^{-2} + \lambda_i \cdot \nabla\Delta N^{s_j,s_r}_{i_{k_1,r}}, \\
\nabla\Delta\rho^{s_j,s_r}_{k_1,r} &= \sqrt{(X_r - X^s_j)^2 + (Y_r - Y^s_j)^2 + (Z_r - Z^s_j)^2} - \\
&\quad \sqrt{(X_{k_1} - X^s_j)^2 + (Y_{k_1} - Y^s_j)^2 + (Z_{k_1} - Z^s_j)^2} + \\
&\quad \sqrt{(X_{k_1} - X^s_r)^2 + (Y_{k_1} - Y^s_r)^2 + (Z_{k_1} - Z^s_r)^2} - \\
&\quad \sqrt{(X_r - X^s_r)^2 + (Y_r - Y^s_r)^2 + (Z_r - Z^s_r)^2}.
\end{aligned} \tag{6.22}
$$

Similarly, the observation model of the secondary antenna (see equation 6.23) is a function of the coordinates of this antenna (also unknown), the GPS observations measured by the secondary receiver, the GPS observations collected by the reference receiver and other parameters such as the coordinates of the reference station, satellites ...

$$
\begin{aligned}
\lambda_i \cdot \nabla\Delta\Phi^{s_j,s_r}_{i_{k_2,r}} &= \nabla\Delta\rho^{s_j,s_r}_{k_2,r} + \nabla\Delta\tau^{s_j,s_r}_{k,r} - \nabla\Delta I^{s_j,s_r}_{k,r} f_i^{-2} + \lambda_i \cdot \nabla\Delta N^{s_j,s_r}_{i_{k_2,r}}, \\
\nabla\Delta\rho^{s_j,s_r}_{k_2,r} &= \sqrt{(X_r - X^s_j)^2 + (Y_r - Y^s_j)^2 + (Z_r - Z^s_j)^2} - \\
&\quad \sqrt{(X_{k_2} - X^s_j)^2 + (Y_{k_2} - Y^s_j)^2 + (Z_{k_2} - Z^s_j)^2} + \\
&\quad \sqrt{(X_{k_2} - X^s_r)^2 + (Y_{k_2} - Y^s_r)^2 + (Z_{k_2} - Z^s_r)^2} - \\
&\quad \sqrt{(X_r - X^s_r)^2 + (Y_r - Y^s_r)^2 + (Z_r - Z^s_r)^2}.
\end{aligned} \tag{6.23}
$$

Finally, the observation model of the combination of both antennas obtained after fixing the distance between them is:

$$
\begin{aligned}
\lambda_i \cdot \nabla\Delta\Phi^{s_j,s_r}_{i_{k_1,r}} &= \nabla\Delta\rho^{s_j,s_r}_{k_1,r} + \nabla\Delta\tau^{s_j,s_r}_{k,r} - \nabla\Delta I^{s_j,s_r}_{k,r} f_i^{-2} + \lambda_i \cdot \nabla\Delta N^{s_j,s_r}_{i_{k_1,r}}, \\
\lambda_i \cdot \nabla\Delta\Phi^{s_j,s_r}_{i_{k_2,r}} &= \nabla\Delta\rho^{s_j,s_r}_{k_2,r} + \nabla\Delta\tau^{s_j,s_r}_{k,r} - \nabla\Delta I^{s_j,s_r}_{k,r} f_i^{-2} + \lambda_i \cdot \nabla\Delta N^{s_j,s_r}_{i_{k_2,r}}, \\
\nabla\Delta\rho^{s_j,s_r}_{k_1,r} &= \sqrt{(X_r - X^s_j)^2 + (Y_r - Y^s_j)^2 + (Z_r - Z^s_j)^2} - \\
&\quad \sqrt{(X_{k_1} - X^s_j)^2 + (Y_{k_1} - Y^s_j)^2 + (Z_{k_1} - Z^s_j)^2} + \\
&\quad \sqrt{(X_{k_1} - X^s_r)^2 + (Y_{k_1} - Y^s_r)^2 + (Z_{k_1} - Z^s_r)^2} - \\
&\quad \sqrt{(X_r - X^s_r)^2 + (Y_r - Y^s_r)^2 + (Z_r - Z^s_r)^2} \\
\nabla\Delta\rho^{s_j,s_r}_{k_2,r} &= \sqrt{(X_r - X^s_j)^2 + (Y_r - Y^s_j)^2 + (Z_r - Z^s_j)^2} - \\
&\quad \sqrt{(X_{k_2} - X^s_j)^2 + (Y_{k_2} - Y^s_j)^2 + (Z_{k_2} - Z^s_j)^2} + \\
&\quad \sqrt{(X_{k_2} - X^s_r)^2 + (Y_{k_2} - Y^s_r)^2 + (Z_{k_2} - Z^s_r)^2} - \\
&\quad \sqrt{(X_r - X^s_r)^2 + (Y_r - Y^s_r)^2 + (Z_r - Z^s_r)^2} \\
\delta_{k_1,k_2} &= \sqrt{(X_{k_1} - X_{k_2})^2 + (Y_{k_1} - Y_{k_2})^2 + (Z_{k_1} - Z_{k_2})^2},
\end{aligned} \tag{6.24}
$$

where δ_{k_1,k_2} is the distance between both kinematic antennas. This distance must be measured/calibrated before the flight using survey methods.

Double difference observations from both kinematic receivers share spatial correlated parameters such as tropospheric and ionospheric delays (for antennas spaced a few decimeters apart, it is clear that the signal path from the satellite to both kinematic antennas is practically the same.) However, the ambiguity parameters must be solved independently for each airborne antenna. Notice that although some observations are added to the computation, the same extra parameters have also been added to the state vector.

This technique has been applied in some tests such as [SC94] where the geometric constraint was used to compare different multi receiver computations.

6.4.2 Vector constraint

The situation would be much better if the observations of the secondary receiver could be used directly in the observation model of the primary kinematic antenna without adding new parameters to be solved (the case of $\nabla\Delta N^{s_i,s_r}_{j_{k_2,r}}$ in equation 6.24). System 6.24 would be much more robust if the only unknown coordinates were the position of the primary kinematic antenna. The system would then have additional observations coming from the secondary kinematic receiver, but not extra unknowns to be solved. This is possible if the vector between $(X_{k_2}, Y_{k_2}, Z_{k_2})$ and $(X_{k_1}, Y_{k_1}, Z_{k_1})$ is known at every epoch of the flight. This situation is clearly more advantageous; the same number of parameters must be solved but additional observations provided by the secondary antenna are available in the computation. The extra information is very helpful to increase the robustness of the solution, minimizing the effect of systematic errors (undetected cycle slips, multipath ...).

The atmospheric delays (ionospheric and tropospheric delays) and the effect of orbital errors can be considered identical if the two antennas are spaced a few decimeters apart. If the vector between antennas is known at every epoch, the coordinates of the secondary kinematic receiver are a function of the coordinates of the primary kinematic receiver. If double difference observations are processed, the clock errors (from satellites and from receivers) are cancelled. As a consequence, the only remaining extra parameters are the double difference ambiguity parameters $\nabla\Delta N^{s_i,s_r}_{j_{k_2,r}}$ and the coordinates of the secondary kinematic receiver. These parameters can also be easily computed.

Let the operator $\nabla\Delta\Phi^m_n$ be

$$\begin{aligned}
\nabla\Delta\Phi^{s_i,s_r}_{j_{k_1,r}} &= \text{double difference phase observation from primary kinematic receiver,}\\
\nabla\Delta\Phi^{s_i,s_r}_{j_{k_2,r}} &= \text{double difference phase observation from secondary kinematic receiver,}\\
\nabla\Delta\rho^{s_i,s_r}_{k_1,k_2} &= \text{double difference distance between satellites and kinematic antennas,}
\end{aligned} \tag{6.25}$$

with

$$\begin{aligned}
\nabla\Delta\rho^{s_i,s_r}_{k_1,k_2} = {} & \sqrt{(X_{k_2}-X^s_i)^2+(Y_{k_2}-Y^s_i)^2+(Z_{k_2}-Z^s_i)^2} \quad -\\
& \sqrt{(X_{k_1}-X^s_i)^2+(Y_{k_1}-Y^s_i)^2+(Z_{k_1}-Z^s_i)^2} \quad +\\
& \sqrt{(X_{k_1}-X^s_r)^2+(Y_{k_1}-Y^s_r)^2+(Z_{k_1}-Z^s_r)^2} \quad -\\
& \sqrt{(X_{k_2}-X^s_r)^2+(Y_{k_2}-Y^s_r)^2+(Z_{k_2}-Z^s_r)^2},
\end{aligned} \tag{6.26}$$

where $(X_{k_1}, Y_{k_1}, Z_{k_1})$ and $(X_{k_2}, Y_{k_2}, Z_{k_2})$ are the coordinates of the primary and secondary antennas and (X_r^s, Y_r^s, Z_r^s) and (X_i^s, Y_i^s, Z_i^s) are the coordinates of the reference satellite and satellite i. In a kinematic environment, the positions of the primary antenna and secondary antenna $(X_{k_1}, Y_{k_1}, Z_{k_1})$, $(X_{k_2}, Y_{k_2}, Z_{k_2})$ are unknown, so in principle $\nabla\Delta\rho_{k_1,k_2}^{s_i,s_r}$ cannot be computed. However, if the vector between the kinematic antennas $k_1 -> k_2 = \upsilon_{(k_2,k_1)}$ is known and the position of the primary antenna is estimated within a few meters (easy to archive using code positioning), value $\nabla\Delta\rho_{k_1,k_2}^{s_i,s_r}$ may be computed with enough precision (< 1 mm).

By definition, the double difference $\nabla\Delta\rho_{k_1,k_2}^{s_i,s_r}$ receiver satellite distance can be decomposed into the substraction of two single difference receiver satellite distances (equation 6.27). Hence, it is enough to prove that the single difference receiver satellite distance $\Delta\rho_{k_1,k_1+\upsilon_{(k_2,k_1)}}^{s_m}$ can be precisely computed even if there are some errors in the coordinates of k_1.

$$\nabla\Delta\rho_{k_1,k_1+\upsilon_{(k_2,k_1)}}^{s_i,s_r} = \Delta\rho_{k_1,k_1+\upsilon_{(k_2,k_1)}}^{s_i} - \Delta\rho_{k_1,k_1+\upsilon_{(k_2,k_1)}}^{s_r}. \tag{6.27}$$

The errors in $\Delta\rho_{k_1,k_1+\upsilon_{(k_2,k_1)}}^{s_m}$ caused by approximating the coordinates of receiver k_1 are defined as

$$\varepsilon \;=\; \Delta\rho_{k_1,k_1+\upsilon_{(k_2,k_1)}}^{s_m} - \Delta\rho_{k_1+\xi,k_1+\upsilon_{(k_2,k_1)}+\xi}^{s_m}, \tag{6.28}$$

where $\xi = (\xi_x, \xi_y, \xi_z)$ are the errors in the coordinates of the primary receiver k_1. Parameter $\Delta\rho_{k_1+\xi,k_1+\upsilon_{(k_2,k_1)}+\xi}^{s_m}$ can also be written as

$$\begin{aligned}&\Delta\rho_{k_1+\xi,k_1+\upsilon_{(k_2,k_1)}+\xi}^{s_m} = \\ &\sqrt{(X_{k_1} + \xi_x - X_m^s)^2 + (Y_{k_1} + \xi_y - Y_m^s)^2 + (Z_{k_1} + \xi_z - Z_m^s)^2} - \\ &\sqrt{(X_{k_1+\upsilon_{(k_2,k_1)}} + \xi_x - X_m^s)^2 + (Y_{k_1+\upsilon_{(k_2,k_1)}} + \xi_y - Y_m^s)^2 + (Z_{k_1+\upsilon_{(k_2,k_1)}} + \xi_z - Z_m^s)^2}.\end{aligned} \tag{6.29}$$

By transferring the coordinates error (ξ_x, ξ_y, ξ_z) as an error in the satellite coordinates, (see equation 6.30), we can conclude that for the computation of the single difference receiver satellite distance $\Delta\rho_{k_1,k_1+\upsilon_{(k_2,k_1)}}^{s_m}$, an error in the satellite coordinates is equivalent to an error in the primary receiver coordinates k_1. As a consequence, the error induced by ξ in 6.29 is equivalent to an error in the satellite ephemeris:

$$\begin{aligned}&\Delta\rho_{k_1+\xi,k_1+\upsilon_{(k_2,k_1)}+\xi}^{s_m} = \\ &\sqrt{(X_{k_1} - (X_m^s - \xi_x))^2 + (Y_{k_1} - (Y_m^s - \xi_y))^2 + (Z_{k_1} - (Z_m^s - \xi_z))^2} - \\ &\sqrt{(X_{k_1+\upsilon_{(k_2,k_1)}} - (X_m^s - \xi_x))^2 + (Y_{k_1+\upsilon_{(k_2,k_1)}} - (Y_m^s - \xi_y))^2 + (Z_{k_1+\upsilon_{(k_2,k_1)}} - (Z_m^s - \xi_z))^2}.\end{aligned} \tag{6.30}$$

Errors caused by orbits have already been studied. According to [HSF], a rule of thumb for computing the effect of an orbital error is

$$\text{Error} = \frac{\text{Baseline length}}{\text{Distance beween satellite and survey area}} \cdot \text{Orbital error} \tag{6.31}$$

In our case, the baseline is less than 5 meters, the error committed when estimating the primary antenna coordinates can be considered also less than 5 meters and the distance between the satellite and GPS antennas is about 25 000 km. Consequently, the error induced by the wrong determination of the primary antenna coordinates is three orders of magnitude lower than the noise of double difference observations. This shows that the value of $\nabla\Delta\rho^{s_i,s_r}_{k_1,k_2}$ can be computed with the required accuracy.

Then, for every epoch, the double difference ambiguity parameters for a given satellite corresponding to the primary receiver and secondary receiver can be computed by

$$\nabla\Delta N^{s_i,s_r}_{j_{k_1,k_2}} = ROUND(\nabla\Delta\Phi^{s_i,s_r}_{j_{k_2,r}} - \nabla\Delta\Phi^{s_i,s_r}_{j_{k_1,r}} - \nabla\Delta\rho^{s_i,s_r}_{k_1,k_2}/\lambda_j), \tag{6.32}$$

where ROUND(X) is the nearest integer value of variable X.

As the three components used in equation 6.32 are observed or computed with an accuracy of a few millimeters, there is no problem in computing the double difference ambiguity parameter $\nabla\Delta N^{s_i,s_r}_{j_{k_1,k_2}}$.

We can conclude that if two kinematic antennas are used and the vector between both antennas (in the WGS84 system) is known, it is possible to add more observations in the trajectory computation without adding new unknowns. The robustness of the solution is thus increased. The remaining question is how to compute the vector between both antennas independently of the GPS observations.

Computation of the vector between primary and secondary kinematic antennas

A vector is defined by a distance (modulus) and two angles (direction) in the space. Obviously, if the antennas are mounted on the aircraft fuselage, the distance between the primary and the secondary antenna is fixed but that is not the case for the direction of the vector. The direction of the vector between two antennas mounted on the aircraft fuselage depends on the attitude of the airplane and can be derived from the angles of the body of the airplane in an ECEF (Earth Center Earth Fixed) system. The best sensor for the determination of angular magnitudes is clearly an Inertial Measurement Unit (IMU) [SW95]. The usual attitude parameterization in navigation (after the IMU data integration) is roll, pitch and heading (Φ, Θ, Ψ).

If the vector between both antennas at an initial time T_0 is known and an IMU sensor is installed in the airplane, the vector between kinematic antennas can be determined at any stage of the flight by using the following formula:

$$\upsilon_{e\,(k_2,k_1)}(t) = r^e_n(\lambda,\phi)_t r^n_b(\Phi,\Theta,\Psi)_t r^b_c(d)\upsilon_{c\,(k_2,k_1)}, \tag{6.33}$$

where

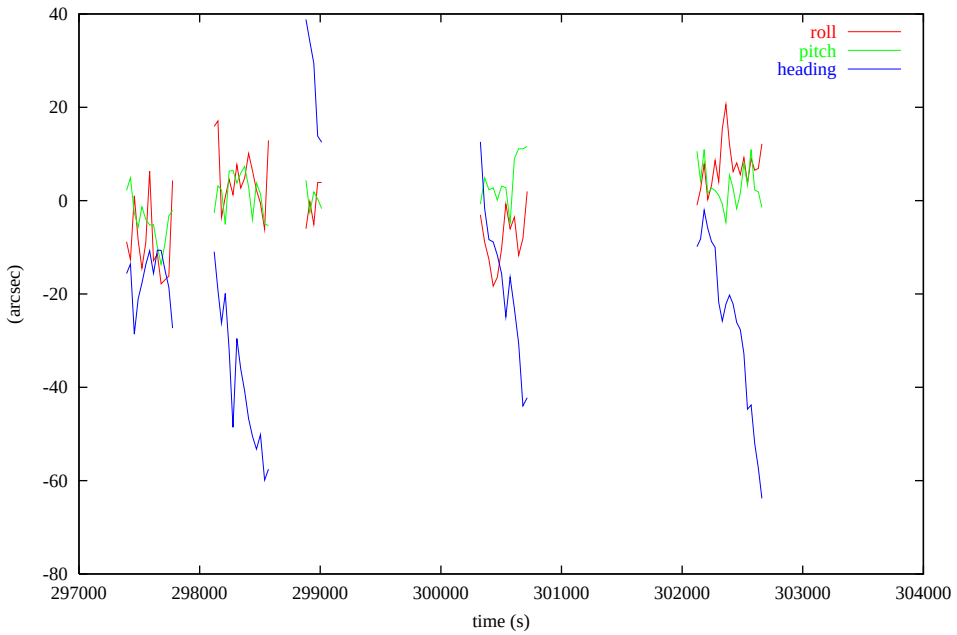

Figure 6.16: Empirical precision of the matrix $r_b^n(\Phi, \Theta, \Psi)$ derived from IMU data.

$$
\begin{array}{rcl}
v_{e\,(k_2,k_1)}(t) & = & \text{vector between kinematic antennas at time t in an ECEF frame,} \\
r_n^e(\lambda, \phi)_t & = & \text{matrix depending on the geographical position } \lambda, \phi \text{ at time t,} \\
r_b^n(\Phi, \Theta, \Psi)_t & = & \text{attitude provided by the IMU (Roll} = \Phi, \text{ Pitch=}\Theta, \text{ Heading} = \Psi) \\
 & & \text{at time t,} \\
r_c^b(d) & = & \text{misalignment matrix between the IMU frame and aircraft frame,} \\
v_{c\,(k_2,k_1)} & = & \text{vector between kinematic antennas in the aircraft frame.}
\end{array}
\tag{6.34}
$$

The photogrammetric community has been using IMU sensors to assist with camara orientation for a few years now. The empirical precision (comparison between IMU derived angular parameters of an aerial metric camera and those derived from aerial triangulation, [Cra99]) ranges from 10 to 120 arcseconds, as shown in figure 6.16 (more details can be found in [ABT01].)

Accurate determination of vector $v_{e\,(k_2,k_1)}(t)$ results from the combination of the precision of vector $v_{c\,(k_2,k_1)}$ (a few millimeters) and the errors of the rotation matrix $r_b^n(\Phi, \Theta, \Psi)_t$ (< 2 arcmin) multiplied by the distance between antennas (in the order of 1 m). Therefore, an upper bound of the total budget of the error is ≈ 5 mm. This value is good enough to determine the double difference ambiguity parameters between kinematic antennas ($\nabla\Delta N_{j k_1,k_2}^{s_i,s_r}$ in equation 6.32).

Appendix B shows the photogrammetric approach for the determination of the vector between master and kinematic antennas.

Implementation

As the second kinematic receiver-antenna has a different hardware, the noise of the observation caused by the receiver instrumentation is independent of the instrumental noise generated by the primary receiver-antenna. Therefore, processing the observations of two kinematic receivers using the vector constraint approach (derived from IMU measurements) leads to an increase in reliability of the survey with no increase in the parameters to be computed. Raising the number of phase observations also allows the observation noise to be reduced, especially in environments with heavy multipath ≈ 3 cm ([WM01]).

The implementation of the vector constraint approach has been carried out in two steps. The first step covers the determination of the vector between GPS antennas at each epoch of the flight. This is achieved by performing an initial trajectory computation (a float ambiguity trajectory determination is accurate enough) and a processing of the IMU measurements. By using the initial trajectory, the computed rotation matrix and the initial offsets (misalignment matrix and vector offset in equation 6.33), it is possible to compute the vector between kinematic antennas (in an ECEF reference system) at each epoch of the flight. The second step covers the generation of all the double difference phase observations between kinematic receivers and reference receivers. At each epoch, for each double difference observation measured by the secondary kinematic receiver (k_2), the following observation equation is used in the computation:

$$\lambda_i \cdot \nabla\Delta\Phi_{i_{k_2,r}}^{s_j,s_r} = \nabla\Delta\rho_{k_2,r}^{s_j,s_r} + \nabla\Delta\tau_{k,r}^{s_j,s_r} - \nabla\Delta I_{k,r}^{s_j,s_r} f_i^{-2} + \lambda_i \cdot (\nabla\Delta N_{i_{k_1,r}}^{s_j,s_r} - \nabla\Delta N_{j_{k_1,k_2}}^{s_j,s_r}),$$

$$\begin{aligned}\nabla\Delta\rho_{k_2,r}^{s_j,s_r} = {} & \sqrt{(X_r - X_j^s)^2 + (Y_r - Y_j^s)^2 + (Z_r - Z_j^s)^2} - \\ & \sqrt{(X_{k_1} + v_{(k_2,k_1)}x - X_j^s)^2 + (Y_{k_1} + v_{(k_2,k_1)}y - Y_j^s)^2 + (Z_{k_1} + v_{(k_2,k_1)}z - Z_j^s)^2} + \\ & \sqrt{(X_{k_1} + v_{(k_2,k_1)}x - X_r^s)^2 + (Y_{k_1} + v_{(k_2,k_1)}y - Y_r^s)^2 + (Z_{k_1} + v_{(k_2,k_1)}z - Z_r^s)^2} - \\ & \sqrt{(X_r - X_r^s)^2 + (Y_r - Y_r^s)^2 + (Z_r - Z_r^s)^2},\end{aligned} \tag{6.35}$$

where $\nabla\Delta\rho_{k_2,r}^{s_j,s_r}$ is computed by making use of the vector between the primary antenna and the secondary antenna; $\nabla\Delta\tau_{k,r}^{s_j,s_r}$ and $\nabla\Delta I_{k,r}^{s_j,s_r}$ are the parameters absorbing atmospheric delays (from primary and secondary receivers); $\nabla\Delta N_{j_{k_1,k_2}}^{s_j,s_r}$ is the ambiguity parameter between the primary and the secondary antennas (computed using equation 6.32); finally, $\nabla\Delta N_{i_{k_1,r}}^{s_j,s_r}$ are the unknown double difference ambiguity parameters between the primary antenna and the reference station.

When double difference phase observations from two kinematic antennas and one reference receiver are used, the correlation between the two sets of double difference phase observations must be taken into account (see equations 6.12 and 6.13). Indeed, the best approach would be to merge the observations from two reference receivers and two kinematic receivers and process the observations as two independent sets of double difference observations with the vector constraint approach.

In figure 6.17, the minimum detectable bias (MDB) of different satellites is shown using a single kinematic receiver (solid line) and using two kinematic receivers applying the vector constraint approach (dashed line). In this particular case, an increase of 58% is observed. It must be mentioned that in this example the constellation was not opti-

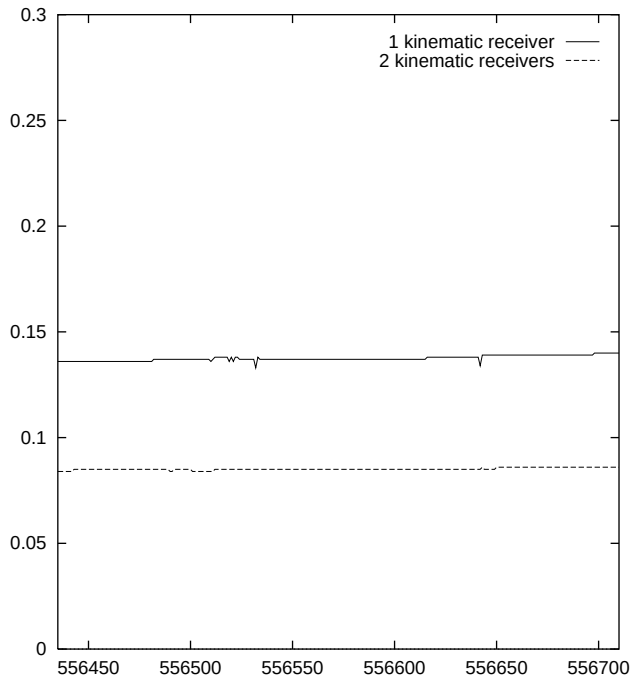

Figure 6.17: Minimum detectable bias using a single kinematic antenna and two kinematic antennas (vector constraint).

IMU noise	IMU angular accuracy	error in vector determination
0.01 deg/$\sqrt{h}$	0.008 deg	140 ppm
0.07 deg/$\sqrt{h}$	0.015 deg	262 ppm
0.15 deg/$\sqrt{h}$	0.035 deg	611 ppm
0.20 deg/$\sqrt{h}$	0.080 deg	1400 ppm

Table 6.1: Error in the determination of the vector between kinematic antennas.

mal. The constellation of GPS satellites usually shows a better configuration, and the improvements observed in the MDB are more moderate. However, the selected example is not a simulation; it is real data taken from a real flight. In real life applications it must be possible to process this kind of flights with acceptable accuracy and reliability.

The accuracy of the IMU must be considered when the weights are applied to the observations of the secondary kinematic receiver. The vector between the primary and secondary kinematic receivers computed by a low cost/precision IMU will be less accurate, and therefore parameter $\nabla\Delta\rho_{k_1,k_2}^{s_i,s_r}$ will have a non negligible error. Table 6.1 showns the error in ppm (parts per million) in the vector determination as a function of the IMU drift and the error in the determination of the angular parameters after calibration of the sensor.

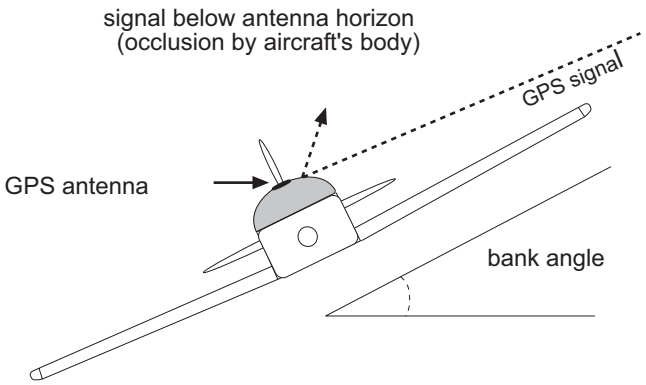

Figure 6.18: Occlusions of satellite signals during turns.

6.4.3 Overcoming satellite occlusions

An aircraft usually flies parallel strips in order to survey a certain area. Between two parallel strips the aircraft makes big turns by inclining its wings. Bank angles during turns are responsible for loss of lock to low elevation satellite signals due to occlusions by the wings or body of the aircraft (see figure 6.18). The magnitude of the baking angles is plotted in figure 6.19 for a specific flight. As can be observed, the inclination of the aircraft during turns is bigger than 20 degrees, and in certain epochs it can reach 60 degrees; therefore, signals from satellites with a lower than 20-40 degree elevation may be blocked by the aircraft during turns.

If some satellites are lost during turns, their ambiguity parameters must be solved again, increasing the number of unknowns to be adjusted by the filter and making the filter weaker. That is especially important if the same satellites are lost at each turn, leaving only a few minutes to solve the corresponding ambiguity parameters.

In order to strengthen the filter and allow the ambiguity parameters to converge, two expensive solutions are used: to fly with more than 6 satellites over 20 degrees or to fly with very low bank angles (10-20 degrees). There are only a few windows with more than 6 satellites over 20 degrees and the productivity of the airborne sensor is dramatically reduced if this option is chosen; on the other hand, flying with low bank angles increases the amount time necessary to make a turn, thus reducing the productivity of the airborne sensor.

The ideal solution is to fly with no constellation or bank angle restriction and to fill the gap in low elevation satellite observations during turns when they are occluded. Hence, the same ambiguity parameters would be valid for the whole survey regardless of the loss of lock during turns. Having a single set of ambiguity parameters to be estimated for the whole survey results in fewer unknowns to be estimated and strengthens the filter solution.

Some works have been carried out to try to bridge the gaps during satellite outages by using IMU data. However, due to the drift affecting IMU observations this solution is only valid for short outages ($\approx$ 1 minute) while turns may last several minutes.

The idea proposed in this section is to place antennas on both sides of the aircraft to

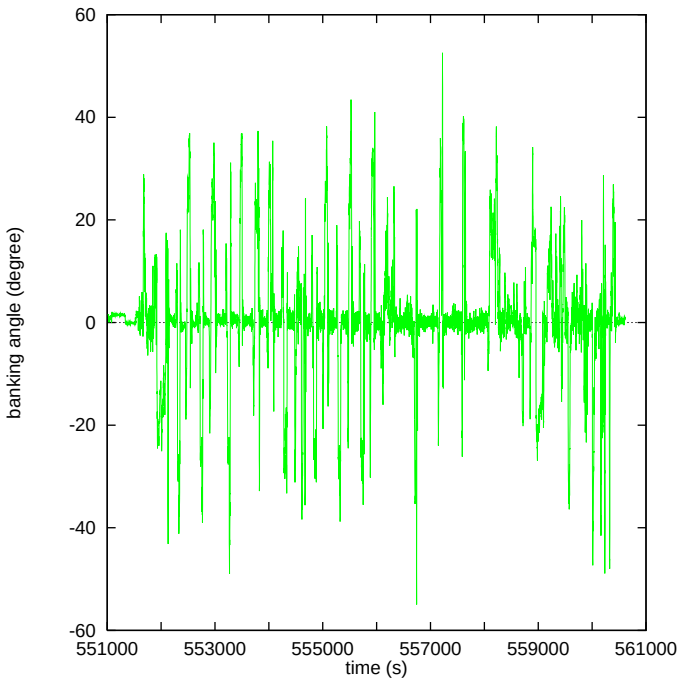

Figure 6.19: Bank angles during aircraft turns.

observe low elevation satellites during turns (see figure 6.20), and to apply equation 6.32 to translate the observations taken by the side antennas to the primary antenna making a synthetic observable.

Let us assume that during a turn there is a high elevation satellite that is continuously observed by the primary antenna (k_1) and a lateral one (k_2). Let (s_r) be the high elevation satellite and (s_i) the 20 degree elevation satellite that is lost. Before the turn (while satellites s_r and s_i are being observed by both antennas), equation 6.32 can be used to determine the ambiguity parameter $\nabla\Delta N^{s_i,s_r}_{jk_1,k_2}$ that is kept fixed during the turn. Then, at each epoch, the following equation can be applied to determine the double difference observation at the primary antenna:

$$\nabla\Delta\Phi^{s_i,s_r}_{jk_1,r} = \nabla\Delta\Phi^{s_i,s_r}_{jk_2,r} - \nabla\Delta N^{s_i,s_r}_{jk_1,k_2} - \nabla\Delta\rho^{s_i,s_r}_{k_1,k_2}/\lambda_j, \tag{6.36}$$

where $\nabla\Delta\rho^{s_i,s_r}_{k_1,k_2}$ is derived, as in 6.4.2, by using the IMU angular information. Simplifying the observations from the reference stations in both $\nabla\Delta\Phi^{s_i,s_r}_{jk_1,r}$ and $\nabla\Delta\Phi^{s_i,s_r}_{jk_2,r}$, the following equation is obtained:

$$\nabla\Phi^{s_i,s_r}_{jk_1} = \nabla\Phi^{s_i,s_r}_{jk_2} - \nabla\Delta N^{s_i,s_r}_{jk_1,k_2} - \nabla\Delta\rho^{s_i,s_r}_{k_1,k_2}/\lambda_j. \tag{6.37}$$

As the observation to satellite s_r from the primary antenna is available, the synthetic observation from the primary antenna to satellite s_i for frequency j is

$$\Phi^{s_i}_{jk_1} = \Phi^{s_r}_{jk_1} + \nabla\Phi^{s_i,s_r}_{jk_2} - \nabla\Delta N^{s_i,s_r}_{jk_1,k_2} - \nabla\Delta\rho^{s_i,s_r}_{k_1,k_2}/\lambda_j. \tag{6.38}$$

After the turn, the primary antenna recovers the lock to satellite s_i and, in order to

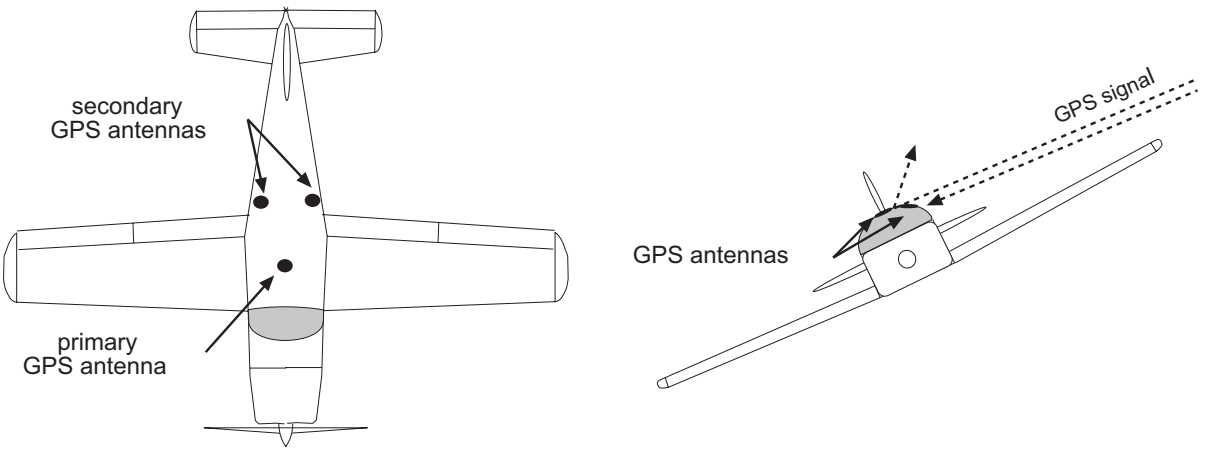

Figure 6.20: 3 antenna configuration to mitigate satellite occlusions.

maintain the ambiguity constant, the following factor (F) must be added to subsequent observations to that satellite:

$$F = \Phi_{j_{k_1}}^{s_i}(t) - \overline{\Phi_{j_{k_1}}^{s_i}(t)}, \tag{6.39}$$

where $\overline{\Phi_{j_{k_1}}^{s_i}(t)}$ is the observation from the primary antenna to satellite s_i at time t (short after the turn) and $\Phi_{j_{k_1}}^{s_i}(t)$ is the synthetic observation derived from 6.38.

A flight with two antennas was used to prove that the determination explained in 6.38 is possible. During a part of the flight, the observations from satellite 15 (with a 20 degree elevation) corresponding to the primary antenna were derived by using the observations to the same satellite from the secondary antenna, the IMU data and applying equation 6.38. Figure 6.21 shows the difference when comparing the synthetic value with the real value. The RMS of the differences is 0.034 cycles. Although this value is higher than the observation precision, it is accurate enough to bridge the gap of satellite occlusions during turns. It must be kept in mind that the airborne sensor does not usually collect data when turns are made between parallel strips. Hence, whether the precision of the trajectory is slightly reduced during turns it of little importance.

In this sample, both antennas were located at the top of the aircraft. As a consequence, the two-antenna flight was not used for overcoming satellite blockages; yet it was an empirical example of the feasibility of this approach.

To implement this approach, a careful study of the aircraft geometry must be carried out in order to decide the number and location of side antennas needed to guarantee a continuous tracking of GPS satellites during turns.

6.5 Using existing permanent GPS networks

In the previous sections it has been shown that the use of more than one reference GPS station increases the robustness of the computations dramatically. In section 6.3, the possibility of using data recorded by permanent GPS networks in geodetic kinematic

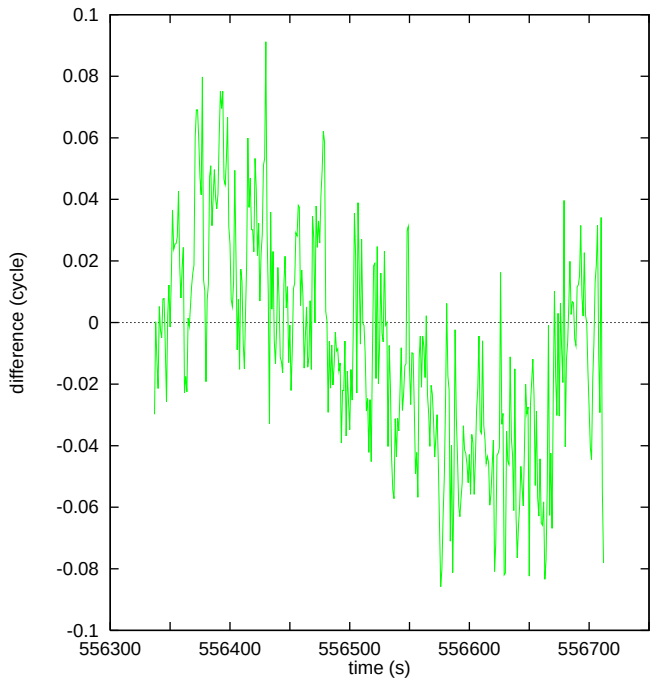

Figure 6.21: Difference between synthetic and real phase observations.

positioning has been studied. As permanent GPS networks are being deployed over the globe by geodetic institutes ([TB99]), their impact on kinematic positioning must be fully understood, particularly if the deployment cost is to be kept as low as possible.

When a kinematic survey (especially an airborne mission) is carried out the goal of kinematic positioning is to reconstruct the trajectory of the rover receiver as precisely as possible. According to the principles of GPS kinematic positioning if no IMU is used it is only possible to compute the position of the rover receiver at the time the GPS observations have been recorded and then interpolate the receiver trajectory at the desired times. In high dynamic environments, the interpolation of the trajectory can lead to a non negligible error source; for instance, the kinematic positions of a receiver on a standard surveying airplane flying at 200 knots and recording data at 1 Hz will be spaced about 100 m apart. In addition, its velocity can vary more than 2 m/s from one epoch to the next. A photogrammetric airplane can fly at 100 m/s and, depending on the photo scale, the projection center must be determined with 5–10 cm accuracy. It is clear that interpolating the trajectory using 1 Hz data will not fulfill the requirements for some applications, especially under turbulence conditions. The only way to reduce the interpolation error in GPS positioning is to increase the recording rate of the rover receiver (nowadays there are some receivers capable of recording GPS observations at 10–20 Hz.)

Now the integration of GPS/INS sensors is not balanced as the usual recording rate of inertial sensors is 50–1600 Hz compared to the 1–20 Hz of GPS receivers. Thus, having access to GPS observations at higher rates would improve sensor integration.

In the last few years there has been a significant increase in the use of GPS by Low Earth Satellites (LEOs) to determine their orbits. As in the above case, the high dynamics

of the LEOs also demands for higher recording rates.

The GPS community relies on the network of permanent GPS stations spread over the world to perform their GPS computations. However, as the standard user of GPS reference stations only needs one observation every 15–30 s, most of them record data at such rates, a small subset of the global network is recording data at 1 Hz and very few are capable of recording data at higher rates. The requirement to have GPS reference stations recording data at higher frequencies than 1 Hz is difficult to fulfill because the continuous GPS reference stations already in operation are not capable of recording data at higher frequencies than 1 Hz and very high dynamic applications are not important enough to justify the deployment or upgrading of the current GPS reference stations network in order to collect 300 to 1000 times more data.

The current trend is to broadcast the GPS observations observed by reference stations in order to allow the user to perform real time GPS kinematic positioning. The bandwidth required to transmit GPS information at 1 Hz is between 4800 to 9600 bps; at 20 Hz the capacity required would be unaffordable. Hence, it is necessary to define procedures for using data from a GPS reference stations network recording data at low frequency in high dynamics GPS kinematic computation.

According to the models explained in previous sections, double difference GPS positioning requires the simultaneous observation of GPS satellites at the reference and the rover receivers. The data from the kinematic receiver contains information about the trajectory of the receivers and is affected by ephemeris, ionospheric, tropospheric, satellite and receiver clock errors, and as the reference receiver is located at a known position, the data observed by this receiver is affected only by ephemeris, ionospheric, tropospheric, satellite and receiver clock errors. Double difference GPS positioning cancels common errors and allows the kinematic GPS trajectory to be determined.

However, if the dynamics of each of the components of GPS carrier phase observations is analyzed, then it is possible to determine the optimal recording rate of the reference and rover receivers.

Although the satellite dynamics is very high (3–4 km/s), the error due to the ephemeris arc used in the position computation changes very smoothly because the dynamics of the satellite is already included in the computation of broadcast/precise orbits. The models for determining the acceleration acting on GPS satellites (gravity field, radiation pressure ...) are very accurate; thus, the remaining perturbing acceleration introduces only smooth changes in the trajectory of the satellite. Figure 6.22 shows a graphical example of low dynamic ephemeris errors.

Tropospheric errors have also a very high temporal correlation; in fact it is common to use tropospheric random walk process noise in the order of only 3.10^{-8} m^2/s, which allows very smooth changes. In addition, double difference ionospheric corrections have generally a smooth variation in mid-latitudes (see figure 6.23). In the equatorial region, scintillation effects (irregularities in the Earth's ionosphere) can produce rapid changes in the received signal; however, even in these cases if dual frequency data is used these effect will be reasonably bounded.

The dynamics of satellite clock errors is very difficult to model because they can be

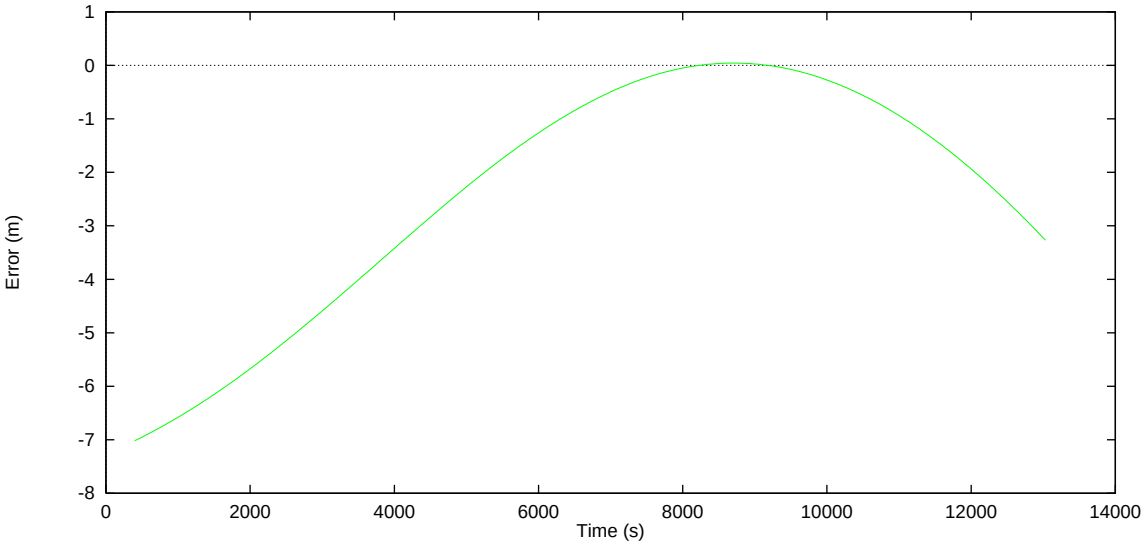

Figure 6.22: Satellite ephemeris error (broadcast versus precise ephemeris)

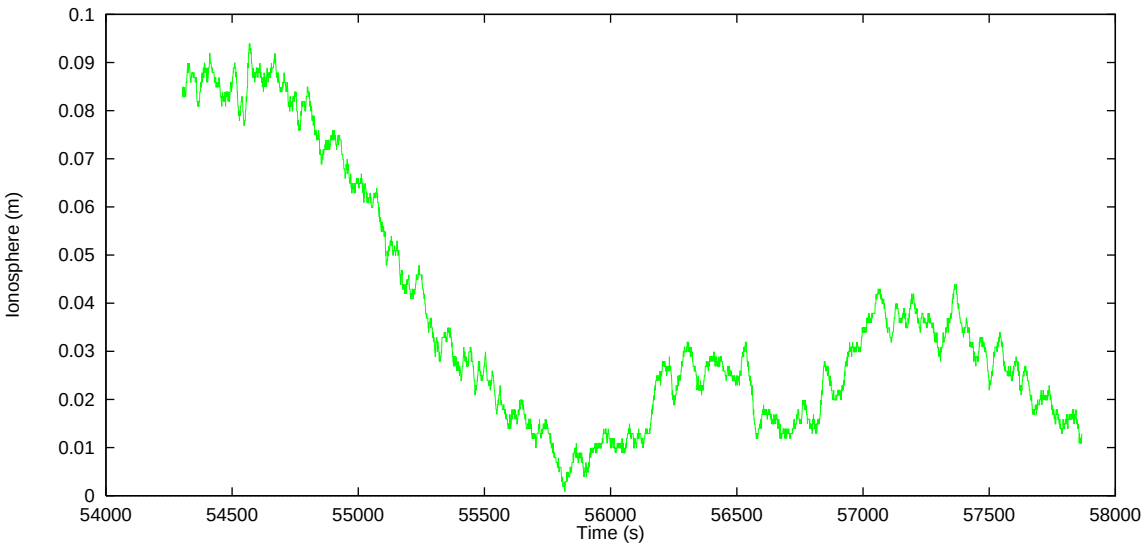

Figure 6.23: Double difference ionospheric effect.

affected by Selective Availability, and no information is provided about the nature of the SA effect. If SA is activated at nominal levels, the dynamics of the satellite clock error have an acceleration of 0.0037 m/s^2 (1σ) [RTCfMsscN98]. After 10 s the predicted satellite clock error due to SA is therefore expected to grow 0.2 m. However, if the value of the satellite clock error is known, for example at epoch 0 s and at epoch 20 s the interpolated value at epoch 10 s will show an error much less than 0.2 m.

We can conclude that GPS data recorded by the kinematic receiver contains information about the dynamics of the GPS antenna and is affected by some errors (atmospheric delays, ephemeris errors, satellite clock errors ...) and GPS data recorded by the reference receiver contains information about those errors with a very high correlation with the errors affecting the kinematic receiver. In consequence, the recording rate of the kinematic receiver must be chosen according to the dynamics of the kinematic receiver whereas the time variability of the errors that affect both the reference and the rover receivers must be the decisive factor in the choice of the recording rate at the reference station.

The reference receiver is usually set to the same recording rate as the kinematic receiver; nevertheless there are some situations where that is not possible (for instance when the reference receiver belongs to a different organization). There are two possible solutions to this problem: error modeling and carrier phase interpolation.

6.5.1 Error modeling

A possible way of dealing with the above situation is to model the errors canceled by the reference receiver with an additional parameter Λ.

Given a pair of single difference observations from a kinematic receiver k with respect to satellites (s_1, s_r) and from a reference receiver r_1 with respect to the same satellites, the generation and processing of double difference observations (see equation 6.40), will be equivalent to the processing of single difference observations with the additional parameter Λ, as presented in equation 6.41:

$$\lambda_1 \cdot \nabla\Delta\Phi^{s_1,s_r}_{1_{r_1,r_2}} = \nabla\Delta\rho^{s_1,s_r}_{r_1,r_2} + \nabla\Delta\tau^{s_1,s_r}_{r_1,r_2} - \nabla\Delta I^{s_1,s_r}_{r_1,r_2} f_1^{-2} + \lambda_1 \cdot \nabla\Delta N^{s_1,s_r}_{1_{r_1,r_2}}. \tag{6.40}$$

The term $(\nabla\gamma^{s_1,s_r})$ is the satellite clock offset and ζ^{s_1,s_r} the satellite relativistic correction due to the orbit eccentricity effect [PS95b]. If the reference receiver is recording data at a slower frequency than the kinematic receivers, then at epochs where data from the permanent stations r_1 is available, parameter Λ holds equation 6.41:

$$\begin{aligned}
\lambda_1 \cdot \nabla\Phi^{s_1,s_r}_{1_k} - \Lambda &= \nabla\rho^{s_1,s_r}_k + c\cdot(\nabla\gamma^{s_1,s_r}) + c\cdot\zeta^{s_1,s_r} + \nabla\tau^{s_1,s_r}_k - \\
&\quad \nabla I^{s_1,s_r}_k f_1^{-2} + \lambda_1 \cdot \nabla N^{s_1,s_r}_{1_k}, \\
\Lambda &= \lambda_1 \cdot \nabla\Phi^{s_1,s_r}_{1_{r_1}} - \nabla\rho^{s_1,s_r}_{r_1} - c\cdot(\nabla\gamma^{s_1,s_r}) - c\cdot\zeta^{s_1,s_r} + \nabla\tau^{s_1,s_r}_{r_1} - \\
&\quad \nabla I^{s_1,s_r}_{r_1} f_1^{-2} + \lambda_1 \cdot \nabla N^{s_1,s_r}_{1_{r_1}}.
\end{aligned} \tag{6.41}$$

As there is a linear dependence between parameters $(\nabla N_{1_k}^{s_1,s_r}, \nabla N_{1_{r_1}}^{s_1,s_r})$, $(\nabla I_k^{s_1,s_r}, \nabla I_{r_1}^{s_1,s_r})$ and $(\nabla \tau_k^{s_1,s_r}, \nabla \tau_{r_1}^{s_1,s_r})$, it is not possible to estimate both parameters at the same time. Thus, the values of $\nabla N_{1_{r_1}}^{s_1,s_r}$, $\nabla I_{r_1}^{s_1,s_r}$ and $\nabla \tau_{r_1}^{s_1,s_r}$ are fixed to zero and only the parameters corresponding to the kinematic receiver $\nabla N_{1_k}^{s_1,s_r}$, $\nabla I_k^{s_1,s_r}$ and $\nabla \tau_k^{s_1,s_r}$ are estimated (note that, in this case, parameteres $\nabla N_{1_k}^{s_1,s_r}$, $\nabla I_k^{s_1,s_r}$ and $\nabla \tau_k^{s_1,s_r}$ are in fact estimating the double difference ambiguity parameter $\Delta\nabla N_{1_{k,r_1}}^{s_1,s_r}$ and the double difference ionospheric parameter $\Delta\nabla I_{k,r_1}^{s_1,s_r}$). If the reference station is not very far (within 100 km), the same argument may be applied to the double difference tropospheric parameter $\Delta\nabla \tau_{k,r_1}^{s_1,s_r}$. After fixing the parameters to zero, the functional model is therefore

$$\begin{aligned} \lambda_1 \cdot \nabla \Phi_{1_k}^{s_1,s_r} - \Lambda &= \nabla \rho_k^{s_1,s_r} + c \cdot (\nabla \gamma^{s_1,s_r}) + c \cdot \zeta^{s_1,s_r} + \nabla \tau_k^{s_1,s_r} - \\ &\quad \nabla I_k^{s_1,s_r} f_1^{-2} + \lambda_1 \cdot \nabla N_{1_k}^{s_1,s_r}, \\ \Lambda &= \lambda_1 \cdot \nabla \Phi_{1_{r_1}}^{s_1,s_r} - \nabla \rho_{r_1}^{s_1,s_r} - c \cdot (\nabla \gamma^{s_1,s_r}) - c \cdot \zeta^{s_1,s_r}. \end{aligned} \tag{6.42}$$

At epochs with no data from the reference stations, parameter Λ must be estimated. In order to do that, a dynamic model for parameter Λ is employed (the PV or PVA dynamic models described in Chapter 2 can be used.)

6.5.2 Carrier phase interpolation

In some situations it is not possible to add the additional parameters described in the previous section (difficulty in changing the functional model, computational burden not allowing extra parameters to be estimated ...).

Another way to overcome the different observation rates of the kinematic and reference station is to interpolate the GPS observations of the reference station at the kinematic receiver epochs. This interpolation can be done in a preprocessing step; thus, there is no interaction with the main processing algorithm. An example of the error committed when phase observations are interpolated can be seen in figure 6.24, where a static 1Hz file was decimated to a 30 second epoch file and the phase observations interpolated back to 1 second epoch interval. For the interpolation a 3rd degree polynomial was used adjusting the four epochs (at 1/30 Hz) surrounding the epoch to be interpolated.

Once the synthetic data has been created, the double difference algorithm may be utilized as in the usual way. As discussed above, over short time intervals (a few seconds) the dynamics of errors (atmospheric, ephemeris, satellite clocks ...) is smooth enough to allow acceptable interpolation values. The residual value not corrected by the interpolation process will propagate into the computed trajectory.

Special attention must be paid when this technique is combined with ambiguity resolution techniques. The interpolation errors and the correlation between interpolated observations will increase the residuals of the observations and the correct set of ambiguities may not pass the ambiguity validation procedures or lead to a bad ambiguity resolution. There are two possible solutions to the problem. As ambiguity resolution techniques may be used in high dynamics surveys, even if the recording rate is very low, a solution can be to filter the data from the rover receiver at the same recording rate as

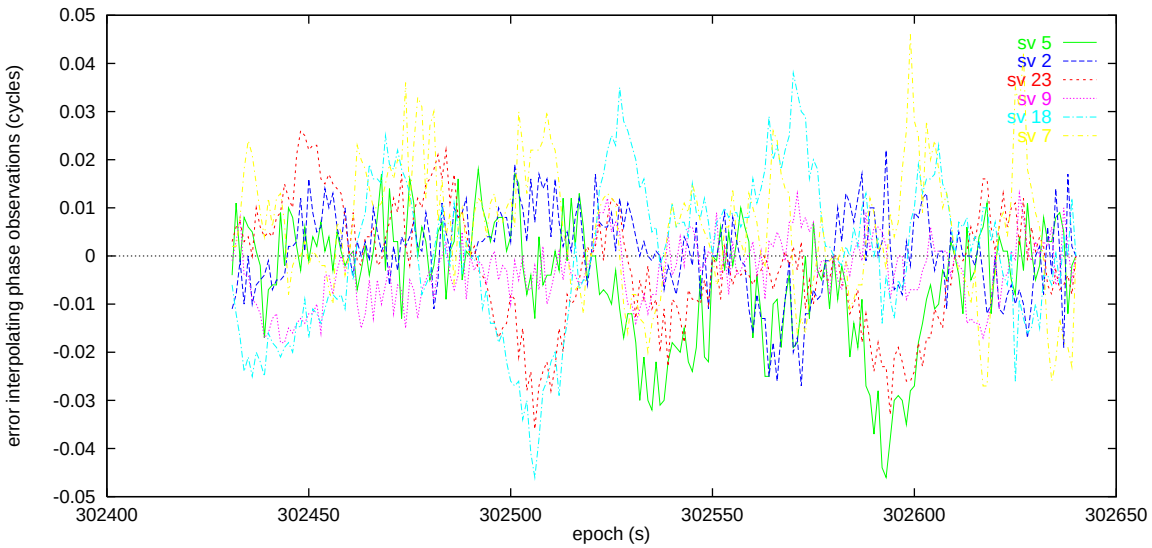

Figure 6.24: Error when phase data recorded at 1/30 Hz is interpolated at 1 Hz (SA off).

that of the reference receiver and then compute the correct set of ambiguity parameters. Once the ambiguities have been solved, the trajectory of the kinematic receiver can be computed using the above technique but fixing the ambiguity parameters to the values obtained in the previous computation. In the global computation, another possibility is, to hide the interpolated epochs from the OTF algorithm; in this way, the ambiguity resolution algorithm will process only the epochs with original data from the reference station.

Three tests (two with SA on and one with SA off) have been done to obtain empirical values on the degradation of the trajectory as the time between observations at the reference station grows.

Tests with SA on

The behavior of the technique with SA on (1994–2000) is much more unpredictable due to the lack of information of the δ-process (error in the satellite clock due to Selective Availability).

Two tests have been carried out under this condition. Both tests were airborne kinematic surveys with very high dynamic environments (especially during turns) and the airborne and the reference receiver recorded data at 1 Hz. The double difference GPS trajectory (computed at 1 Hz) was selected as a reference trajectory. To ensure the quality of the reference trajectory, it was checked against aerial triangulation projection centers. The trajectory was then computed using GPS data recorded in the airplane at 1 Hz and GPS data from a reference receiver decimated to one epoch every 5, 10, 15, 20, 25 and 30 seconds. The observations from the reference receiver were interpolated at 1 Hz in order to perform double difference GPS positioning. The four neighboring epochs were used for the observation interpolation. The set of determined trajectories was compared with

		recording rate at reference station					
		5 s	10 s	15 s	20 s	25 s	30 s
flight 1	horizontal	0.002	0.004	0.011	0.023	0.032	0.060
	vertical	0.002	0.011	0.026	0.055	0.081	0.142
flight 2	horizontal	0.003	0.006	0.012	0.024	0.039	0.055
	vertical	0.010	0.019	0.033	0.060	0.092	0.149

Table 6.2: Error of the kinematic trajectory (SA on). RMS units in m.

		recording rate at reference station					
		5 s	10 s	15 s	20 s	25 s	30 s
flight 1	horizontal	0.008	0.014	0.021	0.024	0.032	0.030
	vertical	0.010	0.021	0.025	0.039	0.059	0.071

Table 6.3: Error of the kinematic trajectory (SA off). RMS units in m.

the reference set computed using real data instead of interpolated data. The RMS of the differences between the trajectories can be seen in table 6.2. It has to be added that the maximum error was 3 to 4 times bigger than the RMS.

Tests with SA Off

On May 2nd 2000, the Selective Availability was switched off. Since then, GPS signals have not been affected by this important source of error. Selective Availability was very annoying in GPS processing not only due to the magnitude of the induced error (30–50 meters 1 sigma) but also because of the uncertainty of its dynamics, which made useless any attempt to model its effect.

As can be seen in table 6.3, when SA is off, carrier phase interpolation gives better results, as expected.

From the test in tables 6.2, 6.3, we can conclude that the interpolation of GPS observations from a reference station is a valid option which does not degrade the quality of the GPS derived trajectory significantly (at least for interpolation steps of less than 15 seconds).

6.5.3 Mixing reference stations recording at different rates

As explained in section 6.3, using multiple reference stations can provide important additional information in kinematic processing. However, in order to maintain low deployment and operational costs, existing permanent GPS networks should be used (logistics for deploying a network of GPS stations surrounding the area of the survey can be very complicated.) As permanent GPS networks are operated by different institutions, data from stations may have been recorded at different rates. For example, a typical situation could be to deploy one permanent GPS station recording at 1 Hz and to use the data from the EUREF network (see image 6.25) which records data every 30 seconds (some

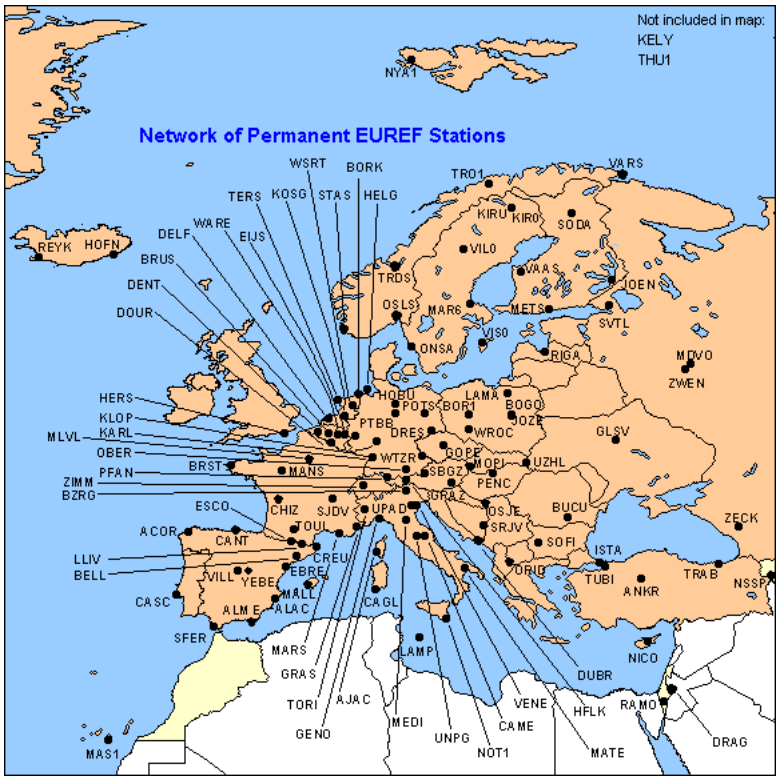

Figure 6.25: EUREF network of permanent GPS stations.

EUREF stations record at 1 Hz, but not all).

This situation (having access to multiple reference stations, one recording at the same frequency as the kinematic receiver and the rest at lower frequency) is also an acceptable scenario for a kinematic survey. In this case, the processing strategy could be to produce pseudo-observations by interpolating the original observations from the reference station at the kinematic receiver epochs, or to perform a two step computation as follows: first, the double difference ambiguities and atmospheric parameters between the reference stations are computed processing the data at the lowest frequency of each station pair. Second, all the data available from all reference and kinematic receivers is processed together with the auxiliary information (double difference ambiguity, ionospheric, and tropospheric parameters) computed in the first step (as described in section 6.3). There are two kinds of epochs during the computation of the trajectory: multireference epochs (epochs with information from more than one reference station) and single reference epochs (epochs with information from only one reference station). This situation has the advantage of reducing the computations burden while keeping the modeling capability of a network of GPS receivers. Calculations are reduced since the design matrix at the single reference epochs is much smaller than the design matrix at the multi reference epochs. However, some aspects of the multiple reference stations are lost at the single reference epochs such as multipath reduction.

6.6 Summary

In this Chapter, several processing strategies have been presented in order to improve the reliability of kinematic surveys.

Most kinematic surveys do not need to be processed in real time; therefore, as explained in section 6.1, the best strategy is to apply a global processing scheme and use all the available data to allow the auxiliary parameters (atmospheric delays, ambiguities ...) to converge in a reliable way and to select the most favorable part of the survey (when nearest to the reference station) in order to fix the ambiguity parameters.

One of the limiting factors for high precision kinematic GPS positioning is ionospheric delays. High precision local ionospheric models can deal with the problem. However, they are costly (in terms of reference station deployment) and still under study. Global and regional ionospheric models can mitigate the problem but the residual ionospheric delays (not corrected by the model) must also be modeled. Section 6.2 proposes the use of stochastic ionospheric parameters instead of ionospheric free synthetic observables, which are very sensitive to the loss of lock on the L2 frequency and do not allow the ambiguity parameters to be fixed. The main advantages of the proposed stochastic parameters lie in the flexibility obtained in the trajectory processing and in the possibility of using some information about the dynamics of the ionospheric effects in the computation.

In certain areas, there are already several reference receivers that can be used in kinematic GPS processing. In order to increase the robustness of kinematic surveys, the use of multiple reference receivers is studied in section 6.3. When the double difference observation models 2.3 are used, the double difference observations from additional reference stations are correlated and special care must be taken to use the correct covariance matrices. In order to take full advantage of kinematic network computation, constraints between ambiguity and atmospheric stochastic parameters are introduced. The improvement observed in internal and external reliability ranges from 60% to 90% if the bias occurs in one reference station, and from 30% to 40% if the bias occurs in the kinematic receiver, thus affecting all the double difference observables.

In section 6.4, the use of multiple kinematic receivers for trajectory determination is explored. Two different approaches are studied. The least robust and easiest to implement, distance constraint, where the two kinematic receivers are processed independently but imposing that epoch by epoch the distance between them must remain constant. The other approach, vector constraint, where the vector between the two kinematic antennas is derived by using an additional sensor (IMU), and the observations from both kinematic receivers are used together to compute the trajectory of only one kinematic antenna is more robust and difficult to implement. The observed improvement in internal and external reliability by using the proposed vector constraint approach can reach 60% for a bias affecting one kinematic receiver. A multiple kinematic antennas configuration for overcoming satellite occlusions is also presented and studied. This approach can be used to bridge satellite gaps during turns.

During the last decade the different mapping organizations have been deploying networks of permanent GPS stations over different countries. Using this data in kinematic

surveys would provide a big advantage in trajectory determination; however, very few of those permanent GPS station are recording data at the required frequency for kinematic positioning (< 1 Hz). In section 6.5, the possibility of using data recorded at low frequency is studied and two approaches are proposed: interpolating the carrier phase observations from reference stations and modeling the errors corrected by reference station observations. Both cases open the possibility of using the available data from permanent reference stations in kinematic trajectory determination and of applying the methods described in section 6.3 for increasing survey reliability.

Chapter 7

Using external information from oriented sensors

In real life applications, operational issues play an important role in kinematic GPS positioning. In order to apply some of the procedures described in Chapter 6, some field deployment must be carried out (deployment of a network of reference stations), but this is not always possible due to economic, logistic and time constraints. It is also well-known that satellite constellation also plays an important role in the achievable accuracy. Although the complete GPS constellation has been fully operational for several years there are certain time windows where only four satellites are visible and with very bad geometry (PDOP > 10).

Taking a real life example, figure 7.1 shows the number of visible satellites and the corresponding PDOP value while figure 7.2 shows the distribution of the satellites in the sky at a place near Barcelona in late 2001. As can be observed, there is a window between 13:45 and 14:15 where the number of satellites is only four, and for most of the time, the PDOP is greater than 10. If we look at the skyplot plotted in 7.2, we can see that the three higher satellites (prn: 5, 9 and 30) are practically aligned (therefore being redundant) while the remaining satellites are very close or below the cutoff angle, thus being very vulnerable to obstructions.

The situation can be even worse if the survey is carried out in an area with obstructions such as urban canyons. The constellation visible from a vehicle doing mobile mapping in urban areas is very poor. Most of the times less than four satellites are visible, and if four satellites were visible from a street, they would be aligned and providing almost redundant information, making little contribution to positioning. In such a situation, it is clear that the contribution of an IMU is required for positioning. However, in order to compensate the errors of their gyroscopes and accelerometers, inertial sensors need to be calibrated from time to time using a precise position. The role of GPS in GPS/IMU positioning is to provide precise trajectories, at least in some parts of the survey, to calibrate the IMU sensors.

The ADOP value defined in 2.2.5 can be used for illustrating the effects of bad satellite geometry. Figure 7.3 shows the ADOP value on the y axis as a function of the number of epochs processed (x axis). As can be seen, the ADOP value falls under 0.2 (a reference value for a successful validation of the ambiguities) after processing 33 epochs. Figure 7.4 shows the ADOP of a survey with the satellite geometry displayed in figures 7.1 and 7.2. As can be observed, even after processing 1800 epochs the ADOP is greater than 0.2 cycles, which means that it is unlikely that any ambiguity resolution algorithm is able to validate ambiguity parameters with an acceptable level of confidence. As a consequence, we face a survey where it would be very difficult to obtain a precise/reliable kinematic

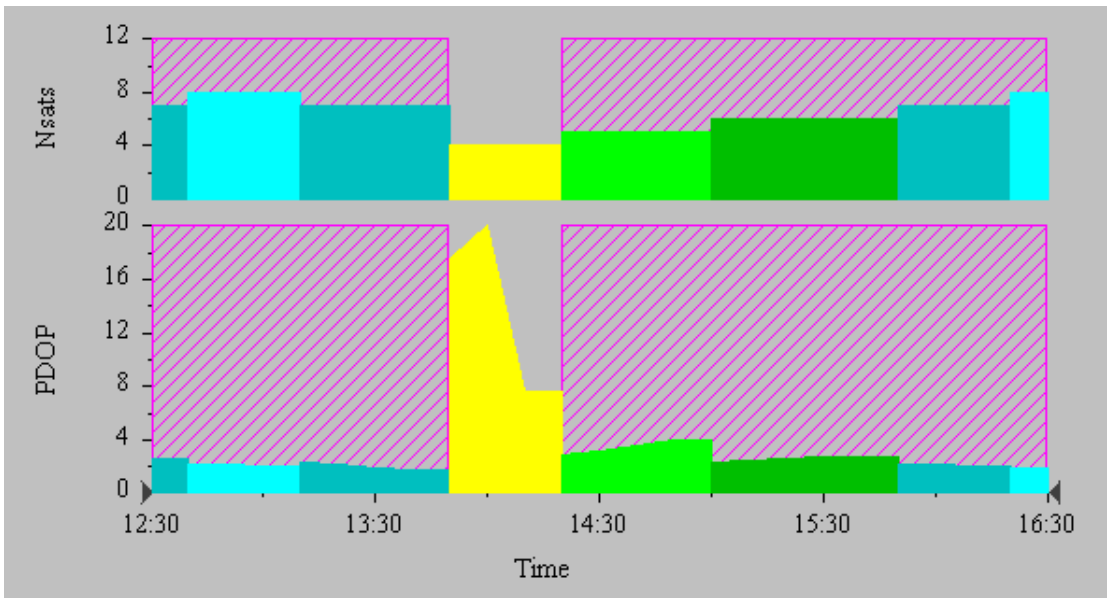

Figure 7.1: Satellite constellation, number of satellites and PDOP.

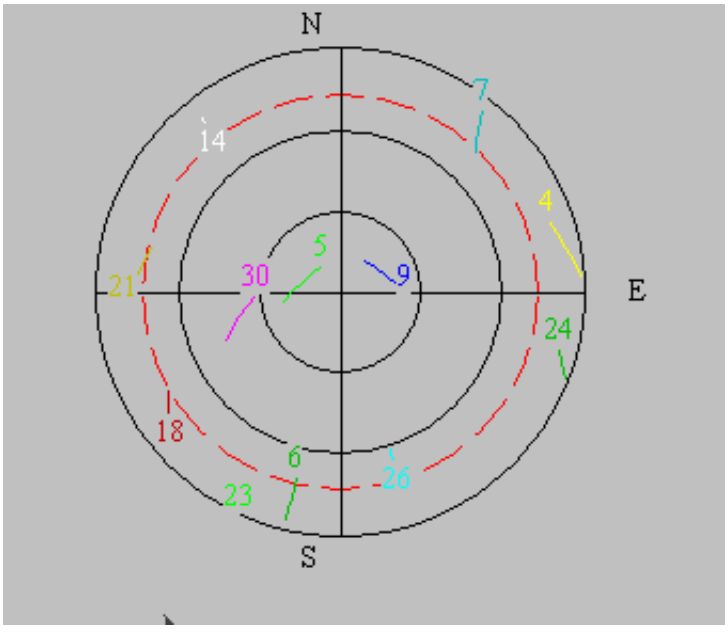

Figure 7.2: Satellite constellation: skyplot.

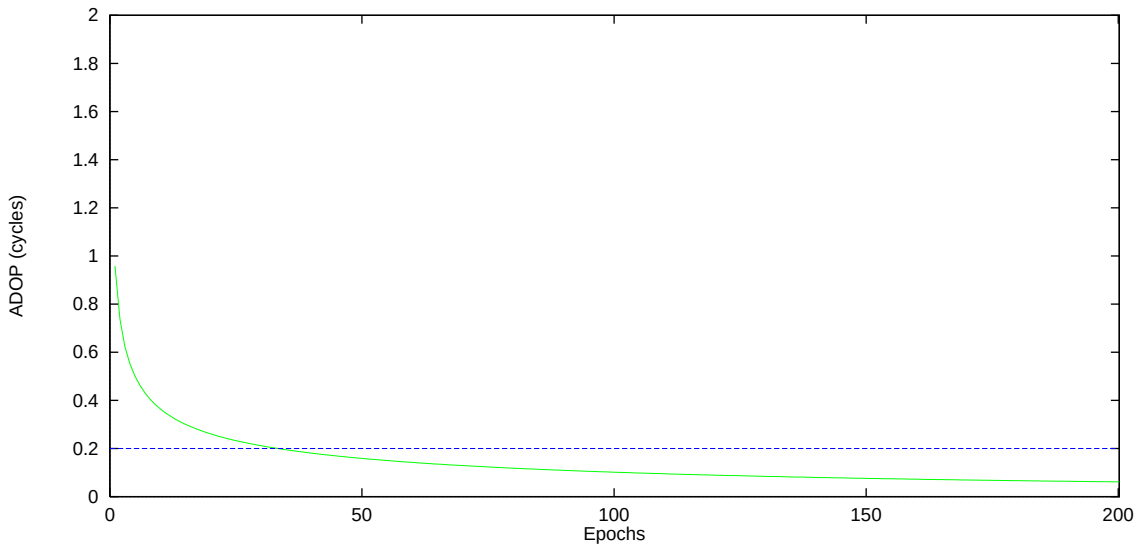

Figure 7.3: ADOP of a survey with good GPS constellation.

trajectory.

In operational conditions, a robust algorithm must be able to overcome, or at least minimize, these situations. Even if the survey has been carefully planned, a satellite can be switched off (for maintenance) or maneuver from one orbit to another. In such eventualities, the only way of producing high precision kinematic positioning is to use additional positioning information in the computation.

If the observations of the existing GPS constellation are not enough to determine a precise/reliable trajectory the only solution is to add more information coming from outside the GPS system. Observations coming from an IMU can be very useful when we need to bridge some gaps in the trajectory, but affordable inertial systems have big errors on their sensors (gyroscopes and accelerometers), and therefore the precision of the trajectory degrades very rapidly.

The sensors used for Earth observation need to be oriented in order to normalize their observations in a common reference frame (usually known as mapping reference frame). In other words, the observations need to be translated from the sensor reference frame (c-frame in figure 7.5) to the mapping reference frame (e-frame in figure 7.5). After normalizing both systems to the same linear units (scale factor), the transformation from the c-frame to the e-frame can be achieved by a rotation R_c^e and a translation T_c^e of the c-frame.

Usually, in sensor orientation the GPS antenna is kept fixed in the sensor frame (c-frame), and the GPS derived trajectory is used for determining the translation T_c^e from the c-frame to the e-frame.

Certain types of sensors can also be oriented indirectly. This is the case of photogrammetric sensors, where the identification in an image of three points with known coordinates in the e-frame allows the rotation R_c^e and the translation T_c^e to be determined. The indirect orientation of sensors opens the possibility of determining the position of the

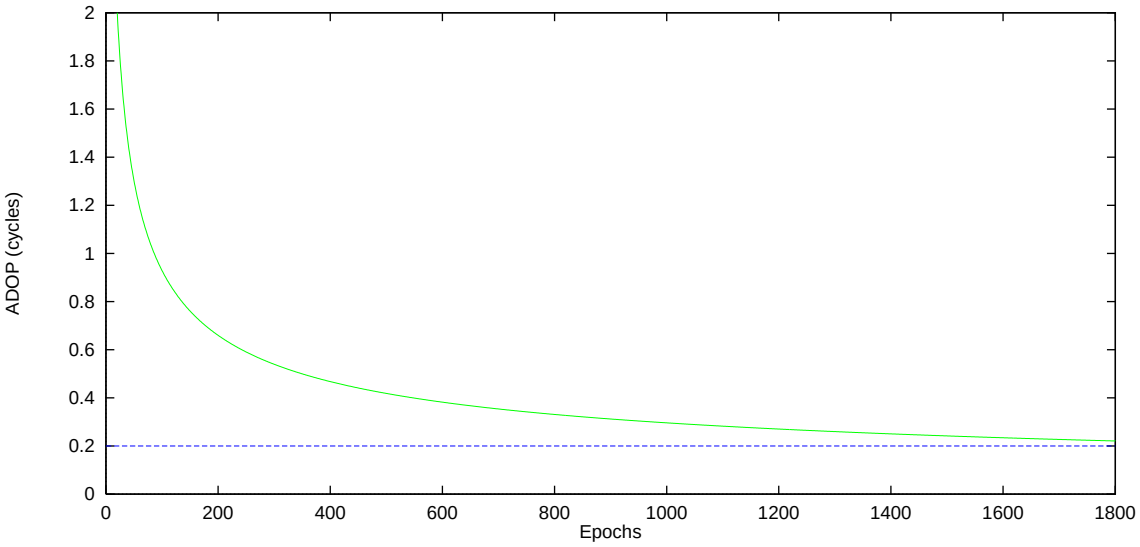

Figure 7.4: ADOP of a survey with bad GPS constellation.

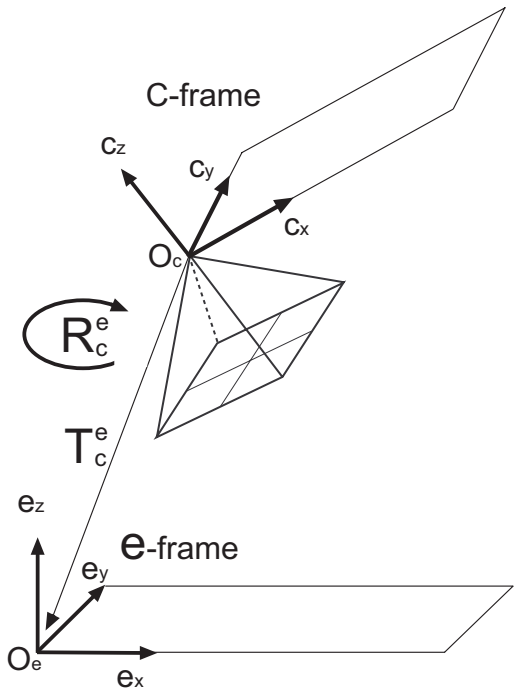

Figure 7.5: Relations between the sensor and mapping reference frames.

	Photo scale					
	1:3500	1:5000	1:15000	1:22000	1:32000	1:60000
Horizontal(m)	0.03	0.04	0.14	0.19	0.22	0.56
Vertical (m)	0.04	0.06	0.18	0.21	0.26	0.64

Table 7.1: Empirical precision of the determination of the projection centers.

GPS antenna at a certain instant. This is the additional information proposed to help in GPS trajectory determination under a weak GPS constellation.

The use of GPS positioning to orient Earth observation sensors is usually cheaper than the use of indirect methods. However, in an operational environment, if a flight has already been made under bad GPS constellations, it might be possible to georeference some frames, lines or pulses (sensor measurements) by indirect methods and then use that information in GPS trajectory computation to correctly solve ambiguities. Subsequently, the trajectory of the complete flight would be accurately determined, (with the help of indirect orientation), and whole survey could be oriented resulting in an enormous cost saving.

The possibility of using indirect measurements depends on the type of sensor employed. Different sensors provide different accuracies of their measurements and therefore, the instant positions to be used by the GPS processing also show different accuracies. In the following sections, two different sensors are studied. The first is a photogrammetric sensor that can be used in aerial and terrestrial surveys while the second is an airborne laser sensor.

7.1 Aerial photogrammetry

Photogrammetry is defined by [STH80] as the art, science and technology of obtaining reliable information about physical objects and the environment, through processes of recording, measuring and interpreting images and patterns of electromagnetic radiant energy and other phenomena. In mapping, field work is replaced by measurements in stereoscopic pairs of photographs (two photographs of the same area taken from different camera stations to provide the binocular vision).

In order to compile maps, the photographs must be oriented in the space, i.e. their exterior orientation (geographic position of the exposure center and the three angles defining the attitude of the focal plane) needs to be determined.

Exterior orientation of a stereo pair can be indirectly determined (see figure 7.6) by identifying five elements in both photographs (relative orientation) and knowing the coordinates in the e-frame of at least three points. The precision of the exposure center of each photograph (O_c in figure 7.5) depends on the quality of the photographs, flight scale, quality of the observations, focal length... Table 7.1 shows the precision of the determination of exposure projection centers in normal real life projects, assuming that the photographs were taken by a last generation analog camera with a focal length of about 150 mm and with point measurement precision of 6 microns.

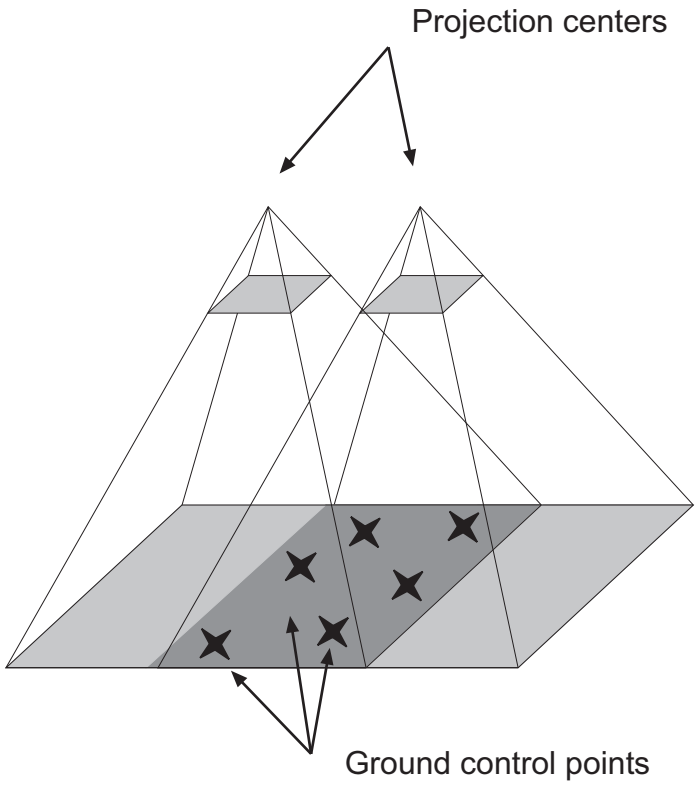

Figure 7.6: Indirect orientation of a stereo pair.

If the production survey consists of a photogrammetric flight where tens (or even hundreds) of aerial photos have been taken and there is a problem in the GPS constellation that prevents the GPS trajectory from being precisely/reliably computed, it would be very helpful to indirectly orient some photographs and then use the derived projection centers as observations in the computations of the complete trajectory of the airplane.

7.1.1 Implementation

An issue to be addressed in order to implement the method proposed in the previous section is that the time at which the photograph has been taken is not synchronized with the time at which the GPS receiver records the observations. If the receiver is taking the measurements at times $t_1, t_2, t_3, t_4, t_5, t_6 \ldots$ and the shutter of the camera has been released at time t_s between epochs t_3 and t_4, the difference in synchronization will be the minimum of $\Delta_{t_3}^{t_s} = t_s - t_3$ and $\Delta_{t_s}^{t_4} = t_4 - t_s$. If the kinematic receiver is recording at 1 Hz, the difference in synchronization can be up to 0.5 seconds. Therefore, the Kalman filter must accept variable time steps and also compute antenna velocities at each epoch of the flight. When computing the position of the airplane at time t_4 (using the position at time t_s and the velocity derived by the Kalman filter) the error is be equivalent to the error made when interpolating a continuous trajectory of the aircraft from a discrete trajectory (1 Hz). The error of interpolating a 1 Hz trajectory at the middle point between epochs and comparing it to a 2 Hz trajectory is shown in figure 7.7. The time distance between

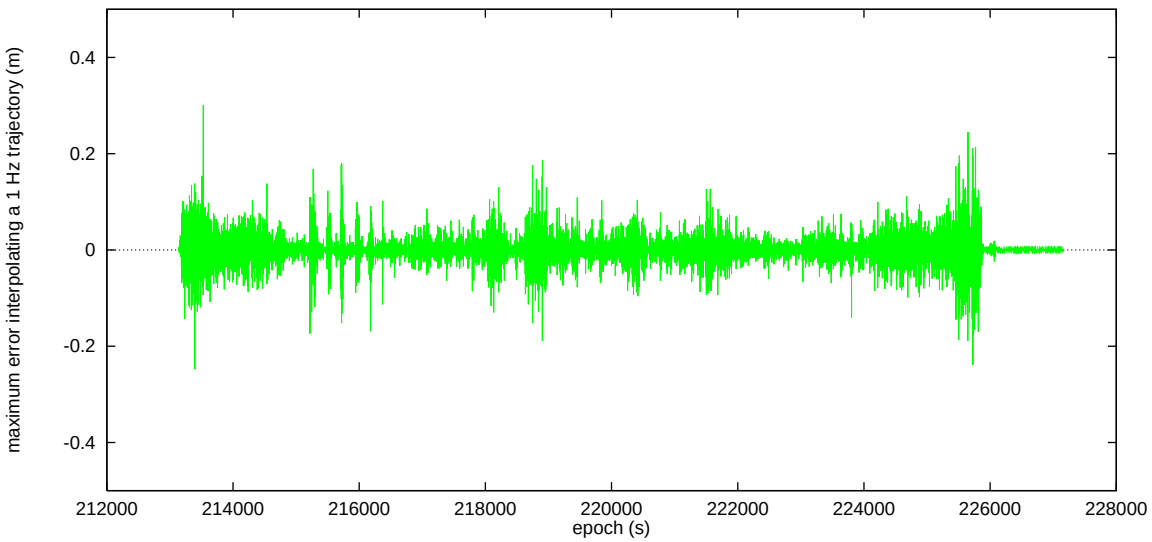

Figure 7.7: Error interpolating an airborne trajectory.

the interpolated points and the points with GPS information is 0.5 seconds; this is the maximum possible time distance between a GPS observation and the time with external information. The RMS is 2.7 cm and it must be taken into account that the bigger errors correspond to the part of the flight when the aircraft was maneuvering and not during the smooth production part of the flight.

The position of the projection center needs be transformed into the position of the GPS antenna by using the following formula:

$$X_k = X_p c + r_c^e(\omega, \phi, \kappa) V_{offset}, \tag{7.1}$$

where

$$\begin{aligned} X_k &= \text{coordinates of the GPS antenna at the time of photograph,} \\ X_p c &= \text{coordinates of the photograph's projection center,} \\ r_c^e(\omega, \phi, \kappa) &= \text{rotation matrix between the camera frame (c-frame) and the e-frame,} \\ V_{offset} &= \text{antenna offset between the GPS antenna and the projection center.} \end{aligned} \tag{7.2}$$

Vector V_{offset} can be measured prior to the flight while the indirect orientation of the photograph allows $X_p c$ and $r_c^e(\omega, \phi, \kappa)$ to be determined.

The Kalman filter should be prepared to fix the trajectory of the GPS antenna at time t_s to the position computed by the indirect orientation of the photogrammetric camera. The precision of the fixed position depends on the characteristics of the flight (see table 7.1). In small scale flights, the determination of the projection centers, by photogrammetric techniques, is not very accurate; however, the quality requirements for trajectory determination are also more relaxed and easier to achieve even without fixing the ambiguities. Once the projection center coordinates are available, the Kalman filter predicts (extrapolates) the position at the neighboring GPS epoch by using the projection

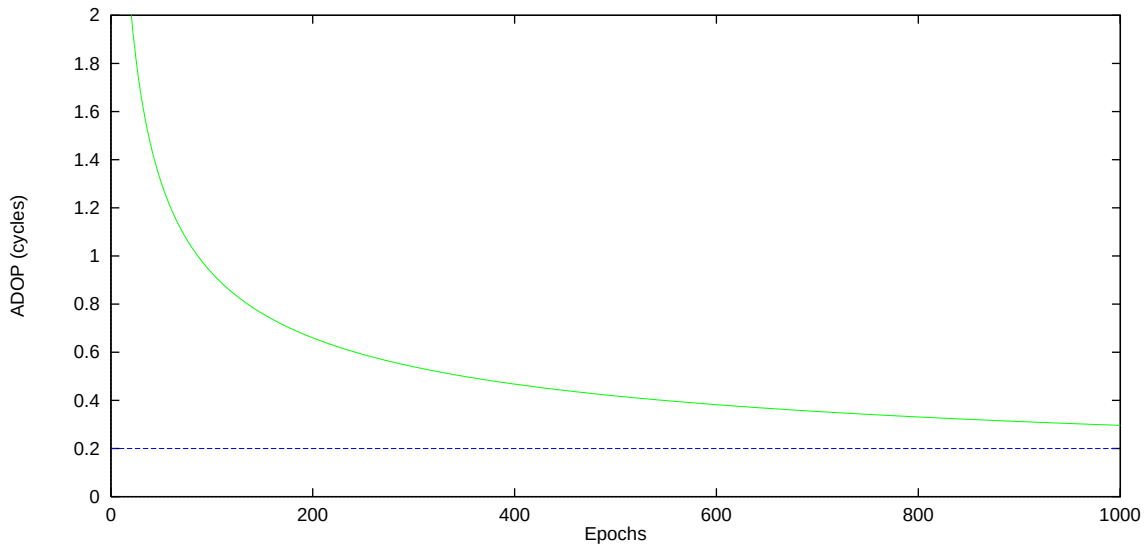

Figure 7.8: ADOP of a survey with bad GPS constellation.

center derived position and the antenna velocity computed by the Kalman filter. At the following GPS epoch, the precision of the predicted position is much higher and this helps the ADOP parameter to converge, thus enabling the ambiguity parameters to be solved and validated.

In order to apply the suggested technique, all the camera components must be calibrated to prevent unmodeled parts of the sensor from propagating into the determination of the projection center coordinates (e.g. an error in the focal length will propagate into an erroneous determination of the projection center height.) If the sensor calibration is not possible, then the projection center coordinates will not be reliable. Such a situation could be partially overcome by using the difference between projection center determinations, where the constant effect of sensor calibration vanishes.

7.1.2 Simulation

Figure 7.8 shows the ADOP corresponding to 1000 epochs of a survey (1:5000 photogrammetric flight mission) with a bad GPS constellation. As can be observed, the ADOP is always above 0.2 cycles, and therefore it is very difficult to validate any ambiguity solution. However, if three ground control points are observed in one image, it can be oriented indirectly and its projection center is determined with 5 cm accuracy. Fixing the position of the GPS antenna to the value derived from the projection center improves the ADOP dramatically (around epoch 200 in figure 7.9). If the same ground control points are used to orient two photographs belonging to one stereo pair, two projection centers are available for the Kalman filter to use. The two-step improvement (spaced 10 seconds apart) can be observed in figure 7.9. In this example, the ADOP shows an improvement of 75%, thus proving that, in certain satellites configurations, using positioning data provided by photogrammetric sensors can be very helpful.

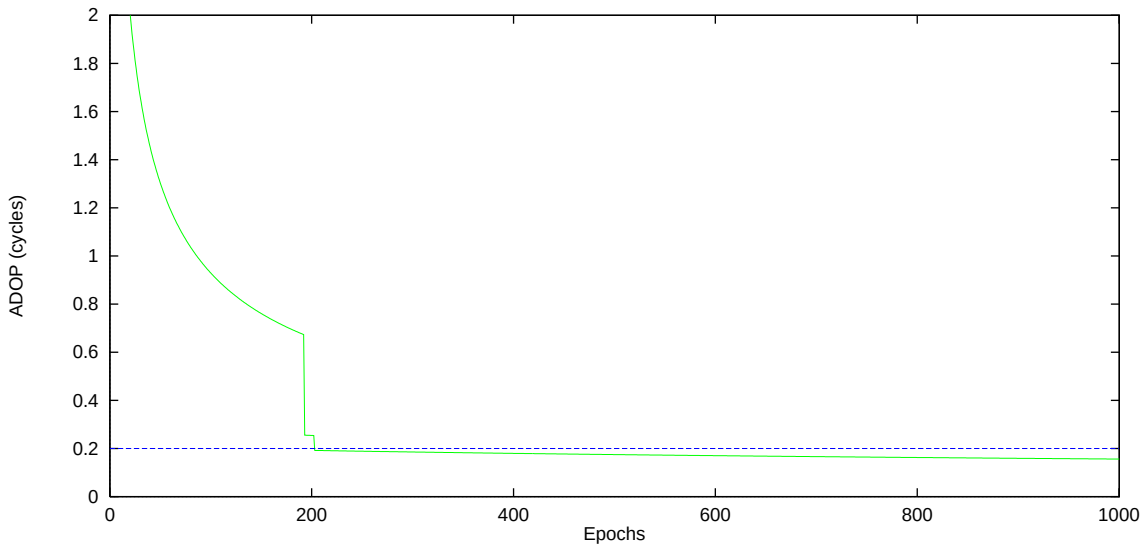

Figure 7.9: ADOP where the position is fixed at two epochs.

7.2 Laser scanning

Since the early 90's the technology of laser scanning has been massively used as an Earth observation sensor for DTM generation. The principle of airborne laser scanning consists of range measurements based on the pulsed laser time of flight. While flying over an area, the sensor sends laser pulses downwards. An optical sensor detects the reflected pulses and computes the time that the laser pulse has needed to travel all the way from the airplane to the ground and backwards. This time is used to derive the two-way distance to the ground by multiplying it by the speed of light. The laser has a rotating mirror for illuminating different areas while the airplane is flying. The laser sends hundreds of pulses per second (2000-50000 pulses depending on the model), thus obtaining the same number of terrain height measurements. In order to compute the ground height from laser raw measurements, a precise orientation (position and attitude) of the laser sensor is needed. Orientation of airborne laser scanning is achieved directly by a combination of GPS and IMU measurements.

In a laser scanning flight, the situation is much worse than in the photogrammetric case because each laser pulse has it own orientation parameters unlike the photo frame, where all the pixels of a photograph ($\approx$ 225 million if scanned at 15 microns) have the same orientation parameters. In laser scanning, it is not possible to compute external orientation parameters using an indirect method. However, as the attitude of the laser sensor is derived with IMU data regardless of the GPS constellation the height of the airplane may be determined with ground control points chosen in a flat area close to the vertical of the airplane (where attitude does not play a critical role).

Using a few ground control points in a laser flight, the height of the aircraft trajectory can be fixed at the instant when these points are measured with the laser. This extra information can be used in GPS processing as extra information to improve reliability in production flights (particularly in flights with low GPS coverage).

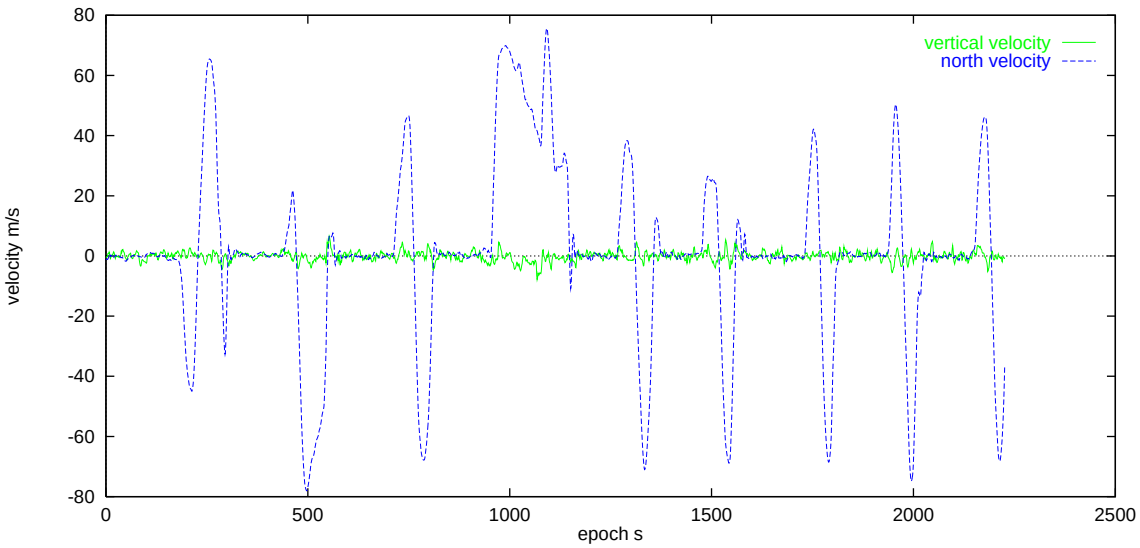

Figure 7.10: Vertical and North velocity in a flight (strips East-West).

7.2.1 Implementation

As in the previous section, the time at which the height information (provided by the laser sensor) is available is not synchronized to the time at which the receivers have observed the GPS signals. Consequently, in order to simplify their inclusion in the computation, the former time must be transferred to the time when a GPS observation is present. During an Earth observation flight, the altitude of the airplane is usually kept as constant as possible (sometimes there is a gradual and constant change in height.) Therefore, the change in vertical velocity is very small, (see figure 7.10) and the height of the GPS antenna at time t_s can be transferred to the height of the antenna at the closest GPS epoch by using the vertical velocity provided by GPS.

Should a 1Hz trajectory be available, it is reasonable to assume that the maximum interpolation error would occur when interpolating at the time corresponding to the middle point between two epochs (x.5 s). An empirical estimation of the interpolation error can be determined by measuring an airplane trajectory at 2 Hz and taking it as the reference, and then interpolating the middle epoch using only one every second epoch as input data. In figure 7.7, the plot of the empirical error from one flight can be seen. The plot corresponds to the complete flight (maneuvers + productive flight), and the maximum errors are correlated with turns of the aircraft.

Depending on the coordinate parameterization used in the Kalman filter computation, there are different implementation possibilities. If the computations are carried out in a local system, it would be very easy to fix the height to the value observed by the airborne laser. However, in most implementations, GPS computations are performed in a geocentric cartesian coordinate system. In this case, in order to simplify the formulation, a suggested approach is to consider the distance to the geocenter as observation. Indeed, as the earth is not spherical, this approach is not error free, but the induced error is tolerable.

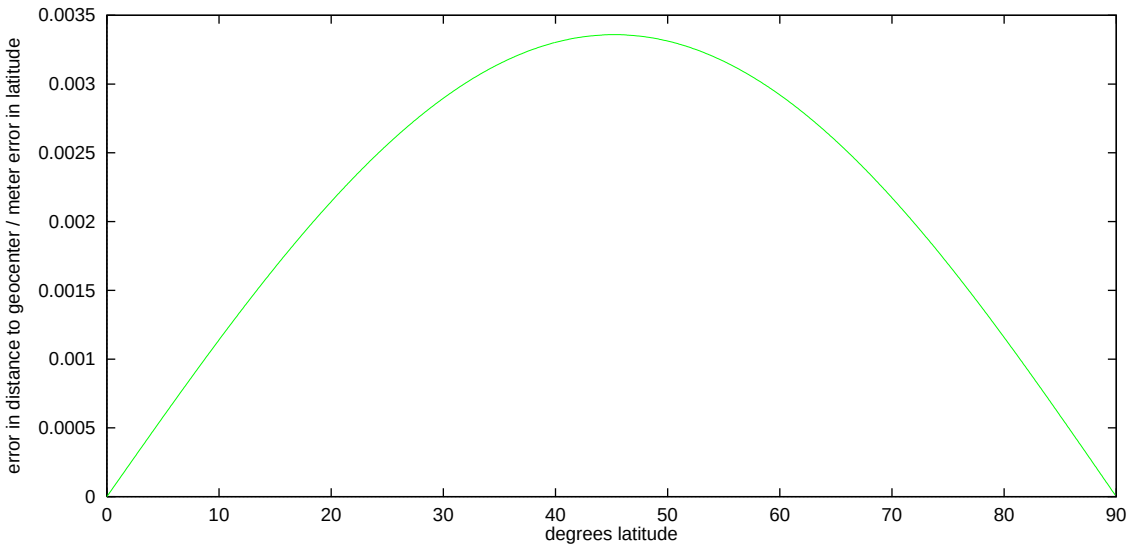

Figure 7.11: Error when assuming distance to geocenter constant.

Let (λ, ϕ, h) be the ellipsoidal coordinates of a point on the Earth's surface with geocentric coordinates (X, Y, Z). As the laser sensor is very precise in height but not in planimetry, the question is what would the error be if we had a precise h and only approximate λ, ϕ and we apply $\sqrt{X^2 + Y^2 + Z^2} = const$ as a restriction. When we look at the transformation equations between geocentric and ellipsoidal coordinates the following equivalence holds:

$$\sqrt{X^2 + Y^2 + Z^2} = \sqrt{(N + h)^2.cos^2(\phi) + sin^2(\phi)[(1 - e^2) * N + h]^2}, \tag{7.3}$$

where

$$\begin{aligned} \lambda, \phi, h &= \text{ellipsoidal coordinates,} \\ X, Y, Z &= \text{equivalent geocentric coordinates,} \\ e &= \text{first numerical eccentricity of the reference ellipsoid,} \\ N &= \text{radius of curvature of the prime vertical,} \\ N &= \frac{a}{\sqrt{1 - e^2 sin^2(\phi)}}, \\ a &= \text{semi-major axis of the reference ellipsoid.} \end{aligned} \tag{7.4}$$

As can be seen in equation 7.3, the error does not depend on the longitude λ. In order to evaluate the error, a gradient has been computed. In figure 7.11 the gradient depending on the latitude is shown. At a given latitude (x-axis) and for each meter error (in latitude) in the assumed position, fixing the distance to the geocenter (and not fixing the height) will introduce an error in the computation of the value shown on the y-axis. The figure also shows that an error of less than 3 meters in the north component (easily achievable with code DGPS) implies an error of less than 1 cm if the distance to geocenter is constrained instead of the height. The accuracy of airborne laser systems is on the order of 5-10 cm, so the error can be considered negligible.

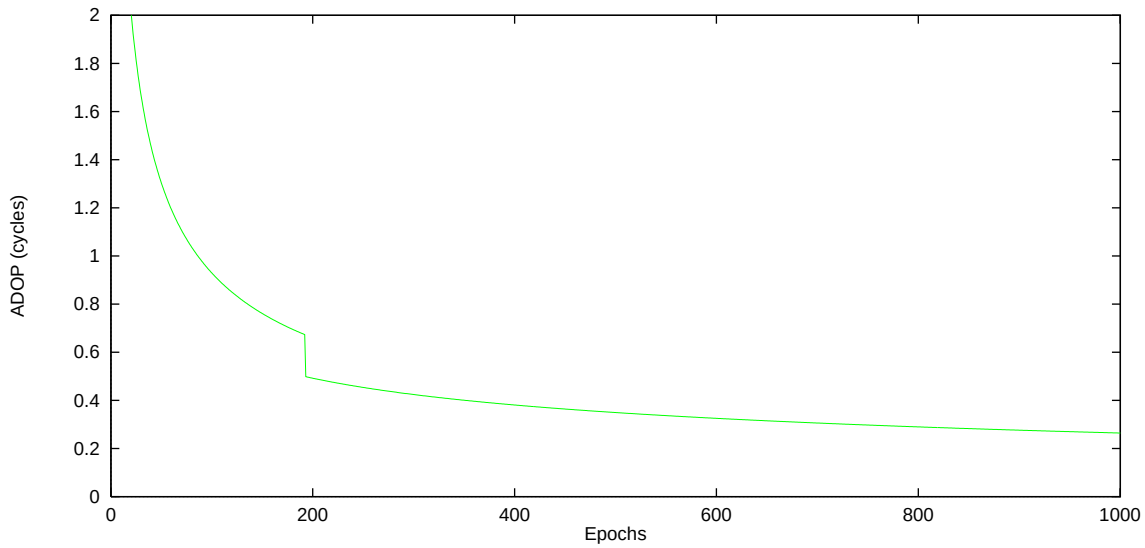

Figure 7.12: ADOP fixing the height at one epoch.

7.2.2 Simulation

A simulation has been made with the same data used in the previous section. In this case, the distance to the geocenter ($\approx h$ fixed) was fixed with a precision of 10 cm for one epoch. The value of h can be observed by measuring the terrain height of a flat area without vegetation. The ADOP corresponding to the first 1000 epochs is shown in figure 7.12. It can be observed that there is a jump at epoch 200 (the epoch where the height has been fixed): the ADOP jumps from an initial value of 0.7 cycles to a value of 0.5 cycles. There is an improvement of about 30% from the initial value. In this example, the resulting ADOP (after fixing the height at one epoch) is however still far from the reference value of 0.2 cycles.

Measuring ground control points in the field is an expensive task; nonetheless, once the field deployment has been done, measuring extra ground control points is much more economical. Therefore, if a production laser flight is made with a bad GPS constellation and it is planned to measure ground control points to improve the robustness and reliability of the trajectory determination, then several ground control points might be measured. These points would be used for fixing the height of the kinematic receiver at several epochs during the GPS trajectory computation. Figure 7.13 shows the ADOP value corresponding to the first 1000 epochs after fixing the height at five different epochs. As can be seen, at the first epoch where the height has been constrained, the ADOP shows an improvement of about 30% but the rest of the epochs where the height has been constrained show very little improvement in the ADOP value, about less than 10% with the second ground control point and less than 4% with the fifth height constraint.

It can be concluded that if only the height is constrained (e.g. using ground control points in a laser scanning flight) there is a significant improvement of the ADOP, but this improvement is much smaller than that obtained if the complete position is constrained (photogrammetric case). In the example presented in this section and plotted in 7.12 and

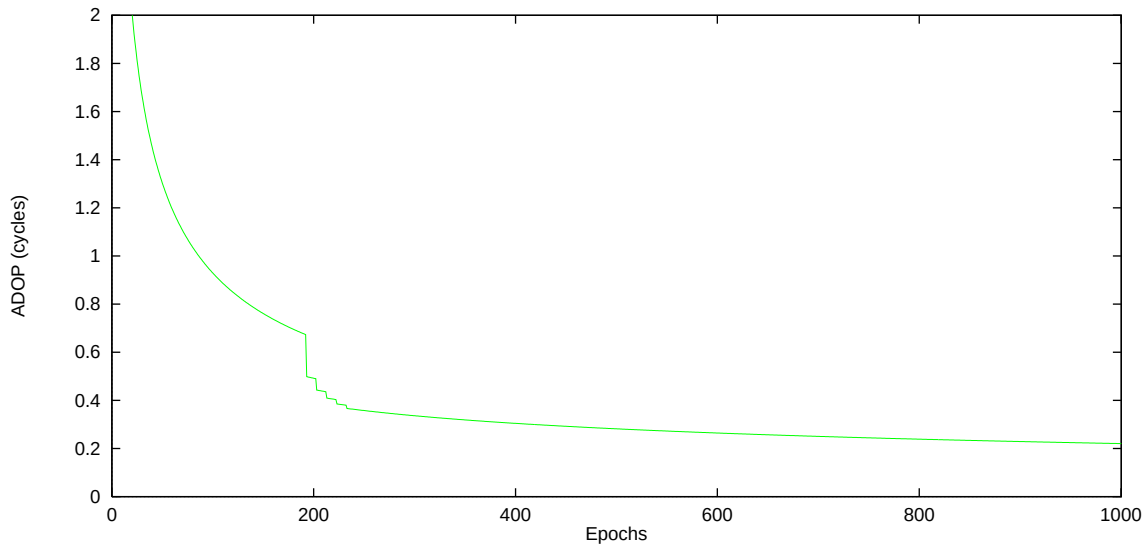

Figure 7.13: ADOP fixing the height at five epochs.

7.13, the resultant ADOP is far above the reference value of 0.2 cycles and in this particular case, finding reliable ambiguity parameters would be very difficult. However, this approach of constraining the height can be very helpful in cases with a GPS constellation slightly better than the one in the example.

7.3 Summary

GPS precise kinematic positioning is widely used in sensor orientation. However, due to operational constraints (mainly a bad GPS constellation), some surveys need additional information in order to compute precise kinematic trajectories.

For each Earth observation sensor, there are some ways to study the impact of a bad GPS trajectory determination in georeferenced data. Therefore, if some control field measurements are made it is possible to orient the sensor (at least partially) in an indirect way and compute some components of the sensor position. This Chapter covers the impact of this external information in GPS precise trajectory determination. In particular, the cases of a photogrammetric camera and a Laser sensor have been studied.

Special care must be taken in the model used for sensor orientation. It must be ensured that the model is not a simplification where the position parameters are lumped together with additional parameters (e.g. height component of the sensor and focal length error). Hence, the model should be strict and the sensor should be calibrated.

Chapter 8
GNSS Modernization

Within the next few years the Global Navigation Satellite Systems (GNSS) scenario will change dramatically. The present GPS constellation will suffer a complete modernization to improve its capabilities and a complete new satellite constellation (Galileo) from the EU will be deployed.

In regard to the future GNSS a question related to this work that immediately arises is: how would these new satellite navigation systems improve the reliability and robustness of precise kinematic positioning?

To have an idea of the changes, today high-end receivers have 24 channels to track 12 satellites on the L1 and L2 frequencies; in a few years these receivers will need at least 72 channels to track GPS and Galileo signals. Although it will take more than a decade to have both systems fully operational, some studies have already been done and still more will come to give us a clear idea of what the implications of the new systems will be: changes in algorithms, workflows, methodologies, applications ...

This Chapter does not attempt to cover all aspects and possible processing improvements with the new GNSS. A completely new thesis could be written by performing an exhaustive analysis of the impact of the third civil frequency, new ranging codes and the autonav capability of the new GPS satellites as well as of the influence of the additional Galileo satellites and their new generation signals. The scope of this Chapter is to provide some ideas about the implications of the most important items of the improved GPS (a third civil frequency) and Galileo (more available satellites) systems.

Therefore, this Chapter will include some studies about internal and external reliability of kinematic surveys by using simulated three frequency GPS data and a hybrid GPS/Galileo constellation.

8.1 Modernized GPS

After two decades of successful operation, there are plans from the IGEB (Interagency GPS Executive Board) to modernize the GPS constellation [STS00]. The modernization will consist of upgrading the operational control segment, adding capabilities to civil as well as military users [FCS01].

The ground control network will upgrade the GPS monitor stations adding new additional stations from the NIMA (National Imagery and Mapping Agency). This increase in the number of monitor stations will reduce the GPS clock and ephemeris errors; therefore, their contribution to the UERE (User Equivalent Range Error) will decrease from 2.3 meters to 1.25 meters.

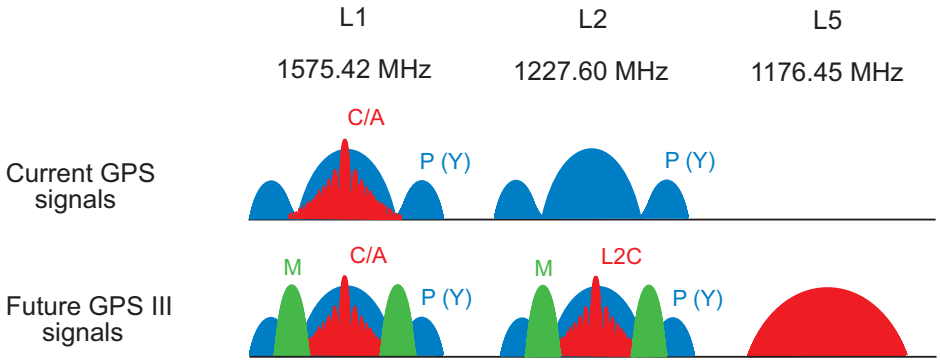

Figure 8.1: Current and modernized signal structures [STS00].

For civil users, the main advantages will be the modulation of an unencrypted civil signal (L2CS) on the current L2 frequency and the availability of a third frequency (called L5) at 1176.45 MHz. The comparison between the present and the new scenarios can be seen in figure 8.1. For civil users, the L2CS code on L2 will provide better observation capability of the L2 frequency (and therefore better immunity to interferences).

The new L2CS code on L2 will be much better than the current C/A code on L1 (stronger signal, lower crosscorrelation and probably no navigation data will be modulated on it) and the L2 carrier phase will have a better signal to noise ratio [FCS01], reducing the likelihood of loss of lock.

As for the military improvements of the GPS constellation, the military will have the possibility of locally denying access to GPS signals. Additionally, a new military code referred to as M-code will be modulated on the current L1 and L2 frequencies to improve cryptographic protection.

8.1.1 Third civil frequency

As explained above, a new civil code will also be broadcast on the L2 frequency, and a completely new civil frequency at 1176.45 MHz will be available to the geodetic community.

A completely new signal (uncorrelated to L1 and L2 measurements) would be very welcome by the surveying community. New observations on the L5 frequency will provide an increase in robustness and better accuracy, and will speed ambiguity resolution algorithms.

Nevertheless, the long satellite life shown by the current GPS constellation and the number of satellites already developed will delay the availability of the new improvements significantly. The satellite modernization schedule, according to [STS00], is shown in table 8.1.

This latter implementation implies that, although the first satellites with the new L5 signal will be delivered at the beginning of 2005, the initial operation capability of the L5 signal will be delayed until 2012, while the declaration of full operation capability for the new L5 signal is not expected until 2014.

Enhancements	Implementation Dates
GPS IIR - L2CS code on L2 - M-code on L1 & L2	2003-2006
GPS IIF - L2CS code on L2 - M-code on L1 & L2 - L5	2005-2010
GPS III - L2CS code on L2 - M-code on L1 & L2 with greater power - L5	2010 - to be determined

Table 8.1: GPS Modernization Schedule.

8.1.2 Simulation

To study the impact of the new civil frequency, a set of simulated data was created. As explained before, notice that only the effect of a third frequency will be studied without considering the additional items that will be modernized in the GPS constellation.

Data from a static measurement was used for the simulation. The idea was to artificially generate data from the L5 frequency, and afterwards evaluate the improvement on reliability that these extra observations introduce in the kinematic computation of files (the static receiver is processed as if it were a kinematic one.) In the first step, the position of the static receiver is kept fixed while the carrier phase ambiguities from both frequencies, the ionospheric and tropospheric delays are computed. Thus, after the first step all the parameters in 8.1 are known:

$$\begin{aligned} \lambda_1 \cdot \nabla\Delta\Phi_{1_{k,r}}^{s_i,s_r} &= \nabla\Delta\rho_{k,r}^{s_i,s_r} + \nabla\Delta\tau_{k,r}^{s_i,s_r} - \nabla\Delta I_{k,r}^{s_i,s_r} f_1^{-2} + \lambda_1 \cdot \nabla\Delta N_{1_{k,r}}^{s_i,s_r}, \\ \lambda_2 \cdot \nabla\Delta\Phi_{2_{k,r}}^{s_i,s_r} &= \nabla\Delta\rho_{k,r}^{s_i,s_r} + \nabla\Delta\tau_{k,r}^{s_i,s_r} - \nabla\Delta I_{k,r}^{s_i,s_r} f_2^{-2} + \lambda_1 \cdot \nabla\Delta N_{2_{k,r}}^{s_i,s_r}. \end{aligned} \tag{8.1}$$

In the second step, for each epoch and satellite pair s_i, s_r the synthetic observable $\nabla\Delta\Phi_{5_{k,r}}^{s_i,s_r}$ was computed by using the following formula:

$$\lambda_5 \cdot \nabla\Delta\Phi_{5_{k,r}}^{s_i,s_r} = \nabla\Delta\rho_{k,r}^{s_i,s_r} + \nabla\Delta\tau_{k,r}^{s_i,s_r} - \nabla\Delta I_{k,r}^{s_i,s_r} f_5^{-2}, \tag{8.2}$$

where f_5 is the new third civil frequency of GPS (1176.45 MHz) and λ_5 is the corresponding wavelength (≈ 0.25 m).

All the parameters in 8.2 could be computed or obtained from 8.1. Therefore, there was no problem in building $\nabla\Delta\Phi_{5_{k,r}}^{s_i,s_r}$. A small random part of less than 1% of the wavelength was added to the synthetic observation. Notice that the observation was generated with

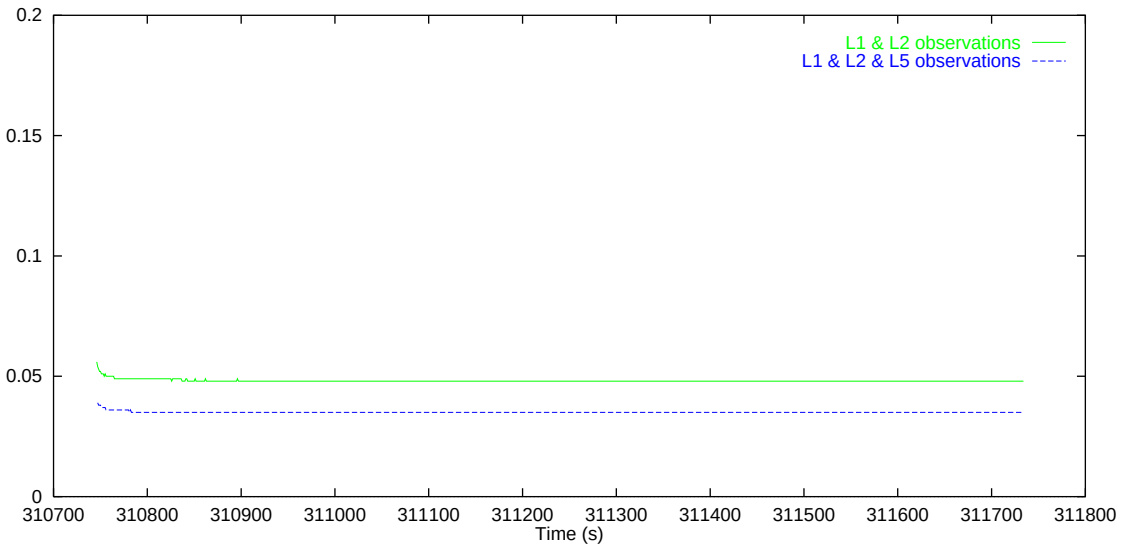

Figure 8.2: Internal reliability of the L1 observable.

its corresponding ambiguity equal to zero, but this had no effect at all because in the processing of the $\nabla\Delta\Phi_{5_{k,r}}^{s_i,s_r}$ observable the corresponding ambiguity parameter $\nabla\Delta N_{5_{k,r}}^{s_i,s_r}$ was also estimated.

Once the data from the GPS third frequency had been simulated, an empirical study was carried out to quantify the improvement in internal and external reliability for the current main observable of precise kinematic positioning (L1 phase observable).

Figure 8.2 shows the improvement in internal reliability corresponding to satellite 9. The computation was performed estimating the ionosphere with stochastic parameters. The upper line shows the MDB when processing only the present L1 and L2 phase observables while the lower line shows the MDB when the L1, L2 and the simulated L5 data are processed simultaneously. It can be seen that in this particular case the improvement is about 30%.

The external reliability is shown in figure 8.3. In this case, the upper line represents the external reliability of satellite 9 when L1 and L2 observations are processed. The lower line shows the external reliability of the same satellite when the phase observations (L5) of the modernized GPS constellations are used. In this case, the improvement is about 55%.

The availability of a third frequency for civil use will be of great importance for kinematic positioning. TCAR (Triple Carrier phase Ambiguity Resolution) techniques could be very successful as the determination of ionospheric delays would be much easier [HPJSC02]; however, as far as robustness of the computations is concerned, an extra observation would be of much help. The above examples show the improvement in reliability in non-optimal survey conditions, that is with only four satellites. It is clear that in a situation where GPS constellations were optimal (more than six satellites in view), the redundancy of current GPS observations could be sufficient to keep the MDB very low, but the aim is to have a truly all weather, all time reliable positioning system.

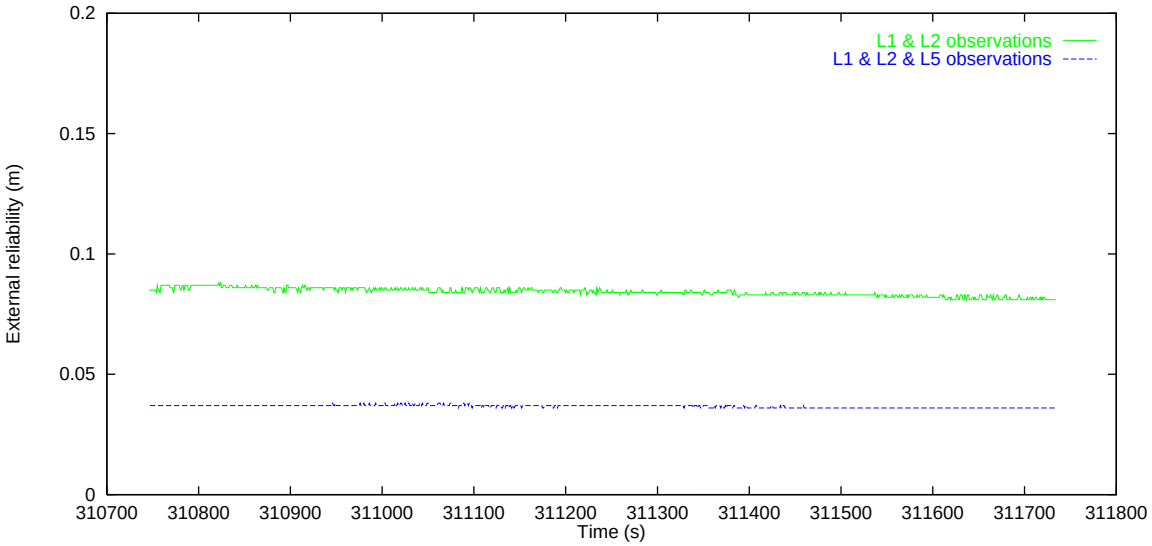

Figure 8.3: External reliability of the L1 observable.

Signal	Frequency (MHz)	Chip rate (Mchip/s)	Data rate (bps)
E5	1202.025	15.345	1000/0
E6	1278.750	5.115	1000
E2	1561.098	3.096	1000/0
E1	1589.742	3.096	1000/0

Table 8.2: Galileo navigation frequencies according to [DLM+01].

8.2 Galileo

Europe has recognized the strategic applications of the satellite positioning system and has decided to contribute to GNSS with the Galileo program in order to guarantee satellite signal availability and performance.

According to [BL01], the Galileo system will consist of several components: Galileo global components consisting in the space segment (30 satellites) and the ground segment for managing the satellite constellation; regional and local components for enhancing Galileo accuracy, integrity ...in a regional or local area; the user segment consisting of different types of user receivers and the service centers providing an interface between Galileo service providers and the users.

According to the planned constellation [LHD+00], the Galileo constellation will comprise 27 satellites (plus 3 in orbit spare satellites) distributed over three planes (54 degrees inclination) MEO circular orbits at 23616 km altitude. The Galileo satellites will transmit 4 navigation signals with ranging codes and data modulated on different carriers. Although the frequency plan can still undergo some changes, there will be 4 different navigation frequencies on the L-Band. These frequencies are described in table 8.2 according to [DLM+01].

The Galileo system will cover a wide range of mass market, governmental, commer-

cial and safety of life applications. The Galileo system will provide full earth coverage with an accuracy of 5 meters standalone. Observations of the carrier phase signals from the 4 frequencies will allow for a variety of carrier phase combinations that will assist in integer ambiguity determination. TCAR and MCAR (Multiple Carrier phase Ambiguity Resolution) techniques will play an important role in high precision positioning while new generation codes will provide a theoretical code tracking accuracy of a few cm [ETPH02]. One may wonder if carrier phase positioning will still be used in presence of centimetric accuracy code observations however, as multipath errors are much larger in code observations than in carrier phase observations, it can be predicted that carrier phase positioning will still be more precise and reliable.

The Galileo system has ended the definition phase and the detailed system design is under development. The first in orbit validation satellites will be launched in 2004 according to schedule, while the Galileo system should be completely deployed by 2008.

8.2.1 Simulation

For this simulation a dual (GPS+Galileo) receiver was considered. As according to Galileo specifications the system must be fully compatible with GPS, it was assumed that Galileo and GPS time reference systems were synchronized and that GPS and Galileo orbits were also in the same reference system.

The simulated data consisted of two files with GPS and Galileo observations. A file from a static GPS survey was used as a seed to make the GPS/Galileo survey. Once the simulated data had been generated, the survey was treated as it were a kinematic survey and the increase in robustness was studied.

Like in the simulation of GPS L5 observations, in the first step the position of the static receiver is kept fixed while the carrier phase ambiguities from both frequencies, the ionospheric and tropospheric delays are computed. Thus, once again after the first step all the parameters in 8.3 are known.

$$\begin{aligned} \lambda_1 \cdot \nabla\Delta\Phi_{1_{k,r}}^{s_i,s_r} &= \nabla\Delta\rho_{k,r}^{s_i,s_r} + \nabla\Delta\tau_{k,r}^{s_i,s_r} - \nabla\Delta I_{k,r}^{s_i,s_r} f_1^{-2} + \lambda_1 \cdot \nabla\Delta N_{1_{k,r}}^{s_i,s_r}, \\ \lambda_2 \cdot \nabla\Delta\Phi_{2_{k,r}}^{s_i,s_r} &= \nabla\Delta\rho_{k,r}^{s_i,s_r} + \nabla\Delta\tau_{k,r}^{s_i,s_r} - \nabla\Delta I_{k,r}^{s_i,s_r} f_2^{-2} + \lambda_1 \cdot \nabla\Delta N_{2_{k,r}}^{s_i,s_r}. \end{aligned} \tag{8.3}$$

The orbits of Galileo satellites were taken as the nominal planned Galileo constellation. The satellite with the highest elevation was taken as the reference satellite. At each epoch and from each Galileo satellite above the horizon, the double difference phase observation was generated following the equation:

$$\lambda_j \cdot \nabla\Delta\Phi_{j_{k,r}}^{galileo_i,galileo_r} = \nabla\Delta\rho_{k,r}^{galileo_i,galileo_r} + \nabla\Delta\tau_{k,r}^{galileo_i,galileo_r} - \nabla\Delta I_{k,r}^{galileo_i,galileo_r} f_j^{-2}, \tag{8.4}$$

where $\nabla\Delta\rho_{k,r}^{s_i,s_r}$ can be computed from the Galileo satellite orbits and from the station coordinates. The value of the tropospheric delay adjusted in the first step was used for the

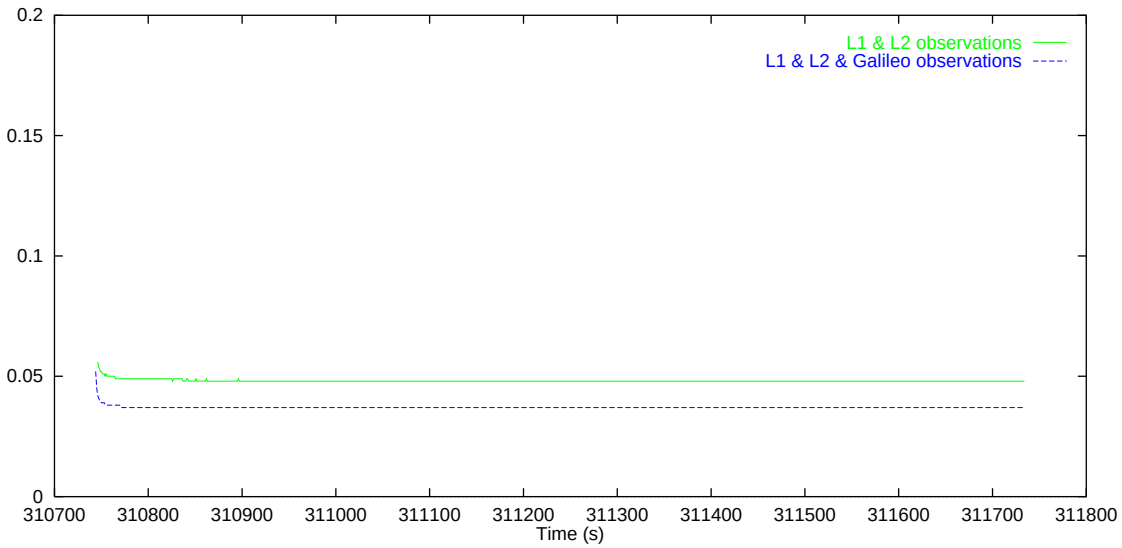

Figure 8.4: Internal reliability of the GPS L1 observable using GPS+Galileo observations.

tropospheric parameter $\nabla\Delta\tau_{k,r}^{galileo_i,galileo_r}$. As for the ionospheric parameter $I_{k,r}^{galileo_i,galileo_r}$, an artificial value was used but maintaining the stochastic properties of the ionospheric parameters computed for the GPS observations $\nabla\Delta I_{k,r}^{s_i,s_r}$. For simplicity, in this simulation only the E1 and E5 frequencies of the Galileo constellation were used. f_j (1589.742MHz and 1202.025MHz) and λ_j (0.189 m and 0.249 m) are the corresponding wavelengths. Considering only two frequencies for Galileo is enough to have an idea of the improvements that the Galileo constellation will introduce in terms of robustness and reliability of GNSS surveys. The use of the Galileo third frequency would provide a more complete overview of the new scenario. However, this frequency is likely to be available under fee; therefore, the recovery of the carrier phase will only be possible if using less robust codeless techniques are used.

Once the synthetic file had been prepared with double difference real GPS observations and double difference simulated Galileo observations, the trajectory of the rover receiver was computed estimating the double difference stochastic ionospheric parameters for each satellite pair, one tropospheric parameter and one double difference ambiguity parameter for each satellite pair and for each frequency used.

A comparison of the survey's internal reliability with only GPS data and with GPS + Galileo data can be seen in figure 8.4. In this plot the upper line also shows the MDB corresponding to GPS satellite 9 when only the present L1 and L2 phase observables are processed, while the lower line shows the MDB when the GPS and simulated Galileo data is processed. As can be seen, the improvement in the internal reliability of satellite 9 is 30%, similar to that obtained with the third frequency.

In regards to the external reliability of GPS satellite 9 if the Galileo simulated data is used, the improvement reaches 80% when compared to the external reliability if only GPS observations are processed. The increase in the number of satellites (4 extra simulated Galileo satellites) provides a better immunity to errors from a particular satellite.

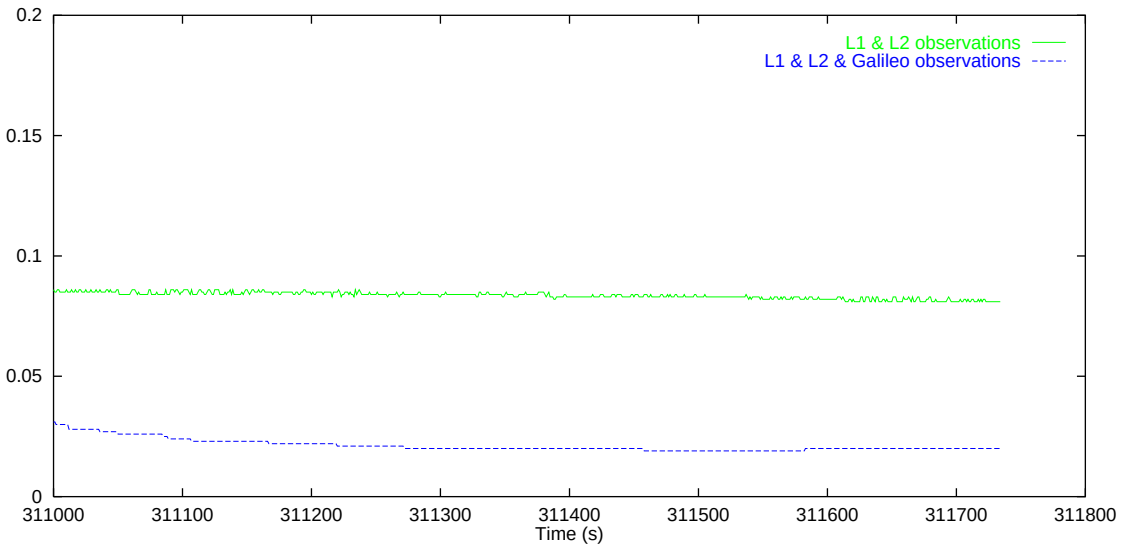

Figure 8.5: External reliability of the GPS L1 observable using GPS+Galileo observations.

Additional satellites for positioning are always very welcome for any user of GNSS systems. The Galileo constellation will be very important for the surveying community, especially in kinematic positioning, because the use of GPS and Galileo satellites will increase the redundancy of observations. Increasing the redundancy of the system always increases its reliability because there are more observations to control the quality of the survey, as has been shown in the previous simulation.

8.3 Summary

Over the next decade the situation of the GNSS scenario will undergo two important changes: the modernization of GPS satellites and the deployment of the new Galileo constellation. The new scenario will bring more satellites, frequencies and codes. The carrier phase signal to noise will benefit from the increased signal strength and the fact that some of the carriers will have no navigation data modulated on it. In addition, the 21st century new code design will provide a theoretical tracking accuracy of a few cm. In this new situation, MCAR techniques will be developed, and robust instantaneous ambiguity resolution methods are likely to be a reality.

However, it will take more than 10 years before both constellations would be fully deployed. Meanwhile, the market needs robust kinematic positioning techniques. The objective of this Chapter is to perform simulations to study the impact of having a third frequency on GPS satellites and of having a duplicate GPS/Galileo constellation in reliability. Both situations represent the most significant improvements of the new GNSS scenario but not the only ones. In ours simulations, the internal reliability improved by approximately 30% while the external reliability improved by more than 50% in both cases. The exhaustive study of the impact of the new situation is beyond the scope of this Chapter.

Chapter 9
Conclusions

The research reported in this Thesis has addressed one of the most challenging and demanding applications of precise point determination with GPS: trajectory determination for the orientation of airborne Earth observation sensors. With the exception of the traditional frame camera sensor —be it analogue or digital— the orientation of modern sensors completely depends on GPS or on GPS/INS. Thus, in this particular application context, GPS point positioning must be precise, accurate and reliable, which is a matter of data —quantity and quality— and of algorithms. In general terms, it can be stated that the algorithms developed over the past decade can provide the required precision and accuracy as long as some (rather expensive) conditions related to GPS infrastructure mission deployment and data processing are met. Reliability —which is achieved through the appropriate and sufficient amounts of data and algorithmic intelligence— has been relegated to a secondary role. Probably, because reliability is less of an academic concept and more of a practical concept. In fact, the significance of reliability goes far beyond a simple "being practical" and reaches a "being productive." In short, reliability is the key to automation in data processing.

To illustrate this, the LWF (Laboratory-Workshop-Factory) paradigm [CN92] for the operation of software systems can be used. The Laboratory mode corresponds to the situation where the software engineer is operating the software for doing development or research (producing a prototype car, for instance); the Workshop mode is defined by an interactive use of the software (producing a Ferrari) and the Factory mode is the automatic use of the software (producing a SEAT). Under this description, it can be said that at the current stage, high precision kinematic GPS software lays between the Laboratory and Workshop modes with several parameters that need to be tuned by skilled operators and several runs of the software needs to be done to obtain acceptable results. The only way to design factory-grade precision kinematic GPS software is to improve the current robustness standards, as long as there is room for such an improvement with the current GPS signals.

The presented research shows that such a room does exist both by its algorithmic and mission configuration findings.

As stated in Chapter 1, the objective of this Thesis is to propose algorithms and methods for increasing the reliability and robustness of GPS kinematic positioning, while doing studies on the reliability of already existing methods.

Chapter 6 shows the increment in reliability of several algorithms and procedures presented, some of the algorithms are already in use by the GPS community while others 6.4, 6.5 proposing the use of existing sensors (IMU, reference stations) are showing increments

of more than 50% on the reliability of the computation. It has to be mentioned that the possibility to merge two reference stations together with two kinematic receivers (linked by an IMU) opens the possibility to obtain two GPS trajectories nearly independent. The implementations of those procedures results in the possibility to overcome satellite occlusions during turns and in a remarkable better chances for automating the airborne kinematic trajectory computation in a production environment.

Sensor orientation is the main application of airborne high precision GPS positioning. In case of a bad GPS constellation or frequent loss of lock during the survey, it might be impossible to determine a trustful GPS trajectory. Therefore, a very expensive airborne survey can be worthless due to the impossibility to obtain a precise trajectory for orienting the sensor. Chapter 7 presents some ideas for the integration between sensor orientation and GPS trajectory determination. In this Chapter it is proven that a successful integration can be done ending with better chances to solve the carrier phase ambiguity parameters and incrementing the possibility to determine a trustful GPS trajectory.

The research would not be complete if it had not given an outlook on the future of GNSS (GPS and Galileo) trajectory determination. One of the implicit messages of the Thesis is the need for more and better signals. The future of GPS III and Galileo signals is, at least, as clear as these modernization/deployment efforts are. Considering the circumstances, it does not make much sense to work beyond simulating the reliability of a combined use of GPS and Galileo satellites. Chapter 8 does this analysis and proves that the external reliability improves by more than 50%. Although the final implemented signals are likely to differ from the current planned ones, these results must be taken into account for any long term GNSS development effort.

The author believes that implementing the findings of this research will lead to an increase of reliability —ultimately "quality for automated data processing in big quantities"— , which will largely compensate the marginal implementation costs.

Chapter 10
Recommendations for future research

Applying the algorithms and methods presented in this thesis would significantly improve the reliability of kinematic GPS positioning and facilitate the automation of kinematic GPS processing. In this Chapter, some recommendations for future research are given in order to further improve the robustness of kinematic GPS determination.

- Further studies must be carried out to fully understand the improvements due to the use of atmospheric models provided by IGS Troposheric and Ionospheric working groups.
- In the field of Earth observation sensor orientation, the use of inertial sensors (IMU) is becoming very popular. More studies covering a deeper integration of GPS/IMU sensors should be conducted. The implications of the tightly coupled integration of the GPS/IMU technology are little known, especially in relation to reliability and ambiguity resolution strategies.
- The reliability of MCAR algorithms in the context of new GPS III and Galileo signals and frequencies should also be carefully studied in order to be prepared for the new scenario.
- Some research should also focus on the use of undifferenced absolute/relative kinematic positioning by using auxiliary IGS GPS products (precise satellite clocks)and PPP (Precise Point Positioning) techniques, especially in the presence of frequent signal blockages.
- In Chapter 7, some ideas for a deeper integration of sensor orientation and GPS trajectory determination have been contributed. Further lines of work may include integration with other Earth observation sensors (SAR, gravimeters ...).
- The use of new accurate code observables of Galileo and GPS III in precise kinematic positioning needs to be investigated to know the limits of these observables, particularly when combined with new multipath mitigation antennas.

Bibliography

[Abi93] H.Z. Abidin. *Computation and geometrical aspects of On-The-Fly ambiguity resolution.* PhD thesis, Department of Surveying Engineering, University of New Brunswick, Fredericton, New Brunswick, Canada, 1993.

[ABT01] R. Alamús, A. Baron, and J. Talaya. Integrated sensor orientation at ICC, mathematical models and experiences. In *OEEPE-Workshop, Integrated Sensor Orientation*, September 2001.

[AS93] F. Ackermann and H. Schade. Application of GPS for aerial triangulation. *Photogrammetric Engineering and Remote Sensing*, 59(11):1625–1632, 1993.

[AT00] R. Alamús and J. Talaya. Airborne sensor integration and direct orientation of the CASI system. In *Proceedings of the XIXth Congress of the International Society for Photogrammetry and Remote Sensing (ISPRS)*, July 2000.

[Bak98] H.C. Baker. *GPS water vapour estimation for meteorological applications.* PhD thesis, Institute of Engineering Surveying and Space Geodesy, University of Nottingham, United Kingdom, 1998.

[BCT94] D. Barrot, I. Colomina, and A. Térmens. On the reliability of block triangulation with GPS aerial control. In *Proceedings of the Commission III, International Society for Photogrammetry and Remote Sensing (ISPRS) Symposium*, September 1994.

[Beu] G. Beutler. The impact of the International GPS Geodynamics Service (IGS) on the surveying and mapping community. In *1992 IGS workshop.* IGS International GPS Geodynamics Service.

[BH92] R.G. Brown and P.Y.C. Hwang. *Introduction to random signals and applied Kalman filtering.* John Wiley and Sons, Inc., New York, second edition, 1992.

[Bie77] G.J. Bierman. *Factorization Method for Discrete Sequential Estimation.* Academic Press, Inc., San Diego, California, 1977.

[BL01] J. Benedicto and D. Ludwig. Galileo system architecture and services. In *V GNSS International Symposium (GNSS2001)*, May 2001.

[Bru00] A.M. Bruton. *Improving the Accuracy and Resolution of SINS/DGPS Airborne Gravimetry*. PhD thesis, Department of Geomatics Engineering, University of Calgary, Canada, 2000.

[CE98] O.L. Colombo and A.G. Evans. Testing decimeter-level, kinematic, differencial gps over great distances at sea and on land. In *ION-98, 11th International Technical Meeting of the Satellite Division of the Institute of Navigation*, September 1998.

[CHPJ+99] O.L. Colombo, M. Hernandez-Pajares, J.M. Juan, J. Sanz, and J. Talaya. Resolving carrier-phase ambiguities on-the-fly, at more than 100 km from nearest reference site, with help from ionospheric tomography. In *ION-99, 12th International Technical Meeting of the Satellite Division of the Institute of Navigation*, September 1999.

[CHTT92] I. Colomina, M. Hernández, J. Talaya, and A. Térmens. Experiences and results of the GPS aerial triangulation Test Urgell. In *International Archives of Photogrammetry and Remote Sensing. Vol.XXIX, Part B1*, pages 283–290, August 1992.

[CL96] P. Collins and R. Langley. Mitigating tropospheric propagation delay errors in precise airborne GPS navigation. In *IEEE Position, Location and Navigation Symposium*, April 1996.

[CL97] J.P. Collins and R.B. Langley. Estimating the residual tropospheric delay for airborne differential GPS positioning. In *ION-97, 10th International Technical Meeting of the Satellite Division of the Institute of Navigation*, September 1997.

[CN92] I. Colomina and J. Navarro. About the LWF model. Oral communication, 1992.

[Col89] I. Colomina. Combined adjustment of photogrammetric and GPS data. In *Proceedings of the 42. Photogrammetric Week*, pages 313–328. Universität Stuttgart, September 1989.

[Col92] O.L. Colombo. Precise, long-range aircraft positioning with GPS: the use of data compression. In *Sixth international geodetic symposium on satellite positioning*, pages 640–649. OSU–DMA, March 1992.

[Col93] I. Colomina. A note on the analytics of aerial triangulation with GPS aerial control. *Photogrammetric Engineering and Remote Sensing*, 59(11):1619–1624, 1993.

[Col99] I. Colomina. GPS, INS and aerial triangulation: what is the best way for the operational determination of photogrammetric image orientation. September 1999.

[Cra99] M. Cramer. Direct geocoding – is aerial trinagulation obsolete? In *Proceedings of the 47. Photogrammetric Week*. Universität Stuttgart, September 1999.

[CRD00] M.E. Cannon, J.K. Ray, and J. Deschamps. Attitude determination using multipath mitigation on multiple closely-spaced antennas. In *ION-00, 13th International Technical Meeting of the Satellite Division of the Institute of Navigation*, September 2000.

[CTB95] I. Colomina, J. Talaya, and X. Baulies. The NOSA project and concept for integrated sensor orientation. In *Proceedings of the 3rd International Worshop High Precision Navigation*, pages 239–246. Universität Stuttgart, April 1995.

[DBBS+03] C. Dunn, W. Bertiger, Y. Bar-Sever, S. Desai, B. Haines, D. Kuang, G. Franklin, I. Harris, G. Kruizinga, T. Meehan, S. Nandi, D. Nguyen, T. Rogstad, J. Brooks Thomas, J. Tien, L. Romans, M. Watkins, S. Wu, S. Bettadpur, and J. Kim. Instrument of Grace: GPS augments gravity measurements. *GPS World*, 14(2):16–28, 2003.

[DLM+01] R. Dellago, F. Luongo, M. Marinelli, J. Hahn, and R. Lucas. Galileosat: System architecture and design status. In *V GNSS International Symposium (GNSS2001)*, May 2001.

[ETPH02] B. Eissfeller, C. Tiberius, T. Pany, and G. Heinrichs. Real-Time kinematic in the light of GPS modernization and Galileo. *Galileo's World*, pages 28–34, Autumn 2002.

[FCS01] R.D. Fontana, W. Cheung, and T. Stansell. The modernized L2 civil signal. *GPS World*, 12(9):28–34, 2001.

[FKH96] Y. Feng, K. Kubik, and S. Han. A long-range dynamic GPS processing system for aircraft navigation and positioning. In *International Archives of Photogrammetry and Remote Sensing. Vol.XXXI, Part B1*, pages 65–71, July 1996.

[Fot00] G Fotopoulos. Parametrization of DGPS carrier phase errors over a regional network of reference stations. Master's thesis, Department of Geomatics Engineering, The University of Calgary, Calgary, Alberta, Canada, 2000.

[Fri90] P. Frieβ. *Kinematische Positionsbestimmung für die Aerotriangulation mit dem NAVSTAR Global Positioning System.* Col. C, Vol. 359. Deutsche Geodätische Komission, München, 1990.

[Fri98] P. Frieβ. About ionospheric parameters. Oral communication, 1998.

[GA93] M.S. Grewal and A.P. Andrews. *Kalman Filtering: Theory and Practice.* Prentice-Hall, Inc., New Jersey, 1993.

[Gel74] A. Gelb, editor. *Applied optimal estimation*, Cambridge, Massachusetts, 1974. Massachusetts Institute of Technology, The MIT Press.

[GY95] C. Goad and M. Yang. Precise GPS positioning in a mobile environment. In *Proceedings of the 1995 Mobile Mapping Symposium*, pages 123–132. The Ohio State University, May 1995.

[Han97] S. Han. *Carrier phase-based long-range GPS kinematic positioning.* PhD thesis, School of Geomatic Engineering, University of New South Wales, Sydney, NSW 2052 Australia, 1997.

[Hat82] R. Hatch. The synergism of GPS code and carrier measurements. In *Proceedings 3rd International Geodetic Symposium on Satellite Doppler Positioning*, pages 1213–1232, 1982.

[HPJS99] M. Hernandez-Pajares, J.M. Juan, and J. Sanz. New approaches in global ionospheric determination using ground GPS data. *Journal of Atmospheric and Solar Terrestrial Physics*, 61:1237–1247, 1999.

[HPJSC99] M. Hernandez-Pajares, J.M. Juan, J. Sanz, and O.L. Colombo. Precise iononspheric determination and its application to real-time GPS ambiguity resolution. In *ION-99, 12th International Technical Meeting of the Satellite Division of the Institute of Navigation*, September 1999.

[HPJSC02] M. Hernandez-Pajares, J.M. Juan, J. Sanz, and O.L. Colombo. Impact of real-time ionospheric determination on improving precise navigation with GALILEO and next-generation GPS. In *ION-02, 15th International Technical Meeting of the Satellite Division of the Institute of Navigation*, September 2002.

[HSF] U. Hugentobler, S. Schaer, and P. Fridez, editors. *Bernese GPS Software Version 4.2.* Astronomical Institute, University of Berne.

[HSG] R. Hatch, T. Sharpe, and P. Galyean. Starfire: A global high accuracy differential GPS system. In *NavCom Technology, Inc.*

[HWLC94] B. Hoffman-Wellenhof, H. Lichtenegger, and J. Collins. *GPS: theory and practice.* Springer-Verlag, Wien, third edition, 1994.

[Lei90] G. Leick. *GPS satellite surveying.* John Wiley and Sons, Inc., 1990.

[LHD+00] R. Lucas, J.H. Hahn, S. Dinwiddy, M. Lugert, G. Gatti, and J. Benedicto. Galileo space and ground segment definition: System and performance. In *ION-2000, 13th International Technical Meeting of the Satellite Division of the Institute of Navigation*, September 2000.

[MBSBS01] R.J. Muellerschoen, Y.E. Bar-Sever, W.I. Bertiger, and D.A. Stowers. NASA's global DGPS for High-Precision Users. *GPS World*, 12(1):14–20, 2001.

[MCL95] V.B. Mendes, P. Collins, and R. Langley. The effect of tropospheric propagation delay errors in airborne GPS precision positioning. In *ION-95, 8th International Technical Meeting of the Satellite Division of the Institute of Navigation*, September 1995.

[Nie96] A.E. Niell. Global mapping functions for the atmosphere delay at radio wavelengths. *Journal of Geophysical Research*, 101(B2):3227–3246, 1996.

[Odi02] D. Odijk. *Fast precise GPS positioning in the presence of ionospheric delays.* PhD thesis, Mathematical Geodesy and Positioning, Faculty of Civil Engineering and Geosciences, Delft University of Technology. The Netherlands, 2002.

[Ou96] J. Ou. *Atmosphere and its effects on GPS surveying.* Number 14 in LGR. Delft Geodetic Computing Centre, 1996.

[PS95a] B.P.. Parkinson and J.J. Spilker. *Global Positioning System: Theory and Applications. Volume II.* Number 164 in Progress in Astronautics and Aeronautics. American Institute of Aeronautics and Astronautics, Inc., 1995.

[PS95b] B.P.. Parkinson and J.J. Spilker. *Global Positioning System: Theory and Applications. Volume I.* Number 163 in Progress in Astronautics and Aeronautics. American Institute of Aeronautics and Astronautics, Inc., 1995.

[Raq98] J.F. Raquet. *Development of a method for kinematic GPS carrier phase ambiguity resolution using multiple reference receivers.* PhD thesis, Department of Geomatics Engineering, The University of Calgary, Canada, 1998.

[RL97] J. Raquet and G. Lachapelle. Long-distance kinematic carrier-phase ambiguity resolution using a reference receiver network. In *ION-1997, 10th International Technical Meeting of the Satellite Division of the Institute of Navigation*, pages 1747–1756, September 1997.

[RSMB95] M. Rothacher, S. Schaer, L. Mervart, and G. Beutler. Determination of antenna phase center variations using GPS data. In *1995 IGS workshop.* IGS International GPS Geodynamics Service, May 1995.

[RTCfMsscN98] Radio Technical Commission for Maritime services special commitee No. 104. RTCM recommended standards for differential GNSS service. Technical Report 11-98/SC104-STD, 1998.

[Saa73] J. Saastamoinen. Contributions to the theory of atmaspheric refraction. *Bulletin Géodésique*, (105, 106, 107):279–298,383–397,13–34, 1973.

[SBE94] D.B. Sauer, G. Beutler, and H.J. Euler. Phase measurements in kinematic GPS applications. Theory and summary of processing strategies. In M.E. Cannon and G. Lachapelle, editors, *Proceedings of the International Symposium on Kinematic Systems in Geodesy, Geomatics and Navigation*, pages 255–263, Calgary, September 1994. Department of Geomatics Engineering, The University of Calgary.

[SBM+95] S. Schaer, G. Beutler, L. Mervart, M. Rothacher, and U. Wild. Global and regional ionosphere models using the GPS double difference phase observable. In *1995 IGS workshop*. IGS International GPS Geodynamics Service, May 1995.

[SC94] J. Shi and M.E. Cannon. Precise airborne DGPS positioning with a multi-receiver configuration: Data processing and accuracy evaluation. In M.E. Cannon and G. Lachapelle, editors, *Proceedings of the International Symposium on Kinematic Systems in Geodesy, Geomatics and Navigation*, pages 393–402, Calgary, September 1994. Department of Geomatics Engineering, The University of Calgary.

[Sch01] B.M. Scherzinger. Robust inertially-aided RTK position measurement. In *Proceedings of the International Symposium on Kinematic Systems in Geodesy, Geomatics and Navigation KIS2001*, pages 265–272. UoC, ION, June 2001.

[See93] G. Seeber. *Satellite Geodesy*. Walter de Gruyter, Berlin, 1993.

[SHN] T. Sharpe, R. Hatch, and F. Nelson. John Deere's StarFire System: WADGPS for Precision Agriculture. In *NavCom Technology, Inc.*

[SLW94] K.P. Schwarz, Y. Li, and M. Wei. The spectral window for airborne gravity and geoid determination. In M.E. Cannon and G. Lachapelle, editors, *Proceedings of the International Symposium on Kinematic Systems in Geodesy, Geomatics and Navigation*, pages 445–456, Calgary, September 1994. Department of Geomatics Engineering, The University of Calgary.

[STH80] C.C. Slama, C. Theurer, and S.W. Henriksen, editors. *Manual of Photogrammetry*. American Society of Photogrammetry, 1980.

[STS00] K. Sandhoo, D. Turner, and M. Shaw. Modernization of the Global Positioning System. In *ION-00, 13th International Technical Meeting of the Satellite Division of the Institute of Navigation*, September 2000.

[SW94] K.P. Schwarz and M. Wei. Some unsolved problems in airborne gravimetry. In *Proceedings of the IAG Symposium Gravity and Geoid*, 1994.

[SW95] K.P. Schwarz and M. Wei. *Inertial geodesy and INS/GPS integration.* Department of Geomatics Engineering, University of Calgary, Calgary, Alberta, Canada, 1995. Partial lecture notes for ENGO623.

[Tal00] J. Talaya. Robust GPS kinematic positioning for direct georeferencing. In *Proceedings of the XIXth Congress of the International Society for Photogrammetry and Remote Sensing (ISPRS)*, July 2000.

[TB99] J. Talaya and E. Bosch. CATNET, a permanent GPS network with real time capabilities. In *ION-99, 12th International Technical Meeting of the Satellite Division of the Institute of Navigation*, September 1999.

[Teu98] P.J.G. Teunissen. Minimal detectable biases of GPS data. *Journal of Geodesy*, 72:236–244, 1998.

[TK98] P.J.G. Teunissen and A. Kleusberg, editors. *GPS for Geodesy.* Springer-Verlag, 1998.

[TO97] P.J.G. Teunissen and D. Odijk. Ambiguity dilution of precision: definition, properties and application. In *ION-97, 10th International Technical Meeting of the Satellite Division of the Institute of Navigation*, pages 891–899, September 1997.

[WBD+87] D.E. Wells, N. Beck, D. Delikaraoglou, A. Kleusberg, E.J. Krakiwsky, G. Lachapelle, R.B. Langley, M Nakiboglu, K.P. Schwarz, J.M. Tranquilla, and P. Vanicek. *Guide to GPS positioning.* Canadian GPS Associates, Fredericton, New Brunswick, Canada, 1987.

[Wei97] S.D. Weisenburger. Effect of constrains and multiple receiversfor on-the-fly ambiguity resolution. Master's thesis, Department of Geomatics Engineering, The University of Calgary, Calgary, Alberta, Canada, 1997.

[WM01] L. Wanninger and M. May. Carrier-phase multipath calibration of GPS reference stations. *Journal of the Institute of Navigation*, 48(2):113–124, 2001.

[Wüb89] G Wübbena. The GPS adjustment software package GEONAP, concept and models. In *5th Int. Geod. Symp. Satellite Positioning*, pages 452 – 461, 1989.

Appendix A

Kinematic GPS software

A kinematic GPS processing software has been developed to carry out the studies covered by this dissertation. The software, called TraDer, is intended to be very flexible to allow several processing modes: multiple reference stations, stations recording data at different observational rates, multiple kinematic GPS receivers, angular data to use the vector constraint approach explained in Chapter 6. In this appendix, some details of the software implementation which are relevant to the performed research are given.

A.1 Object-Oriented software

The software has been written in C++ following the Object-Oriented methodology in order to be as modular as possible. Therefore, each process or data will have its own class. Each class will have its own precondition and postcondition to guarantee maximum robustness of the software. Interaction between classes is achieved through module interfaces. The Object-Oriented methodology provides great flexibility, in particular the software processes the data in postprocessing but has been designed to allow a real time operation of the filtered solution without big changes in the program.

The classes have been written in a hierarchical structure: the core of the software corresponds to a general Kalman filter class, there is an intermediate layer consisting in a specialized GPS class while the most external layer is composed of the input, output, quality control and management classes, as can be seen in figure A.1.

A.2 Discrete Kalman filter

The use of stochastic variables and dynamical models suggested the implementation of a discrete Kalman filter algorithm.

Let x be the state vector and P the associated covariance; then the discrete Kalman filter equations [GA93] at epoch k are:

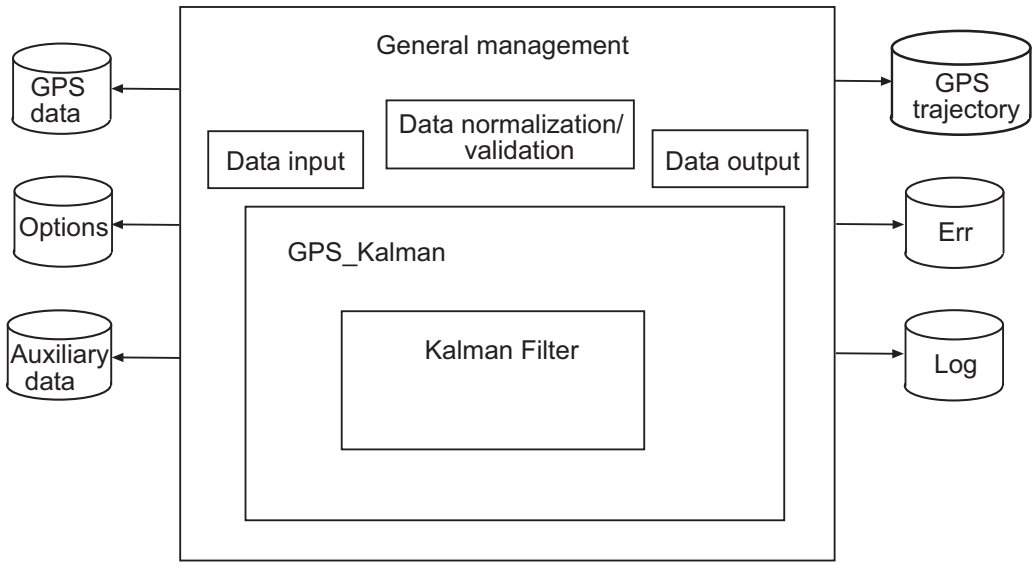

Figure A.1: Basic software architecture

$$
\begin{array}{ll}
\text{Initial Conditions} & E[x(0)] = x_0; \quad E[(x(0)-x_0)(x(0)-x_0)^T] = P_0, \\
\text{System Model} & x_k = \Phi_{k-1}x_{k-1} + w_{k-1}; \qquad w_k \sim N(0, Q_k), \\
\text{Measurement Model} & z_k = H_k x_k + v_k; \qquad v_k \sim N(0, R_k), \\
\text{Other Assumptions} & E[w_k v_j^T] = 0 \text{ for all j,k}, \\
 & \\
\text{State Estimate Extrapolation} & x_k(-) = \Phi_{k-1}x_{k-1}(+), \\
\text{Error Covariance Extrapolation} & P_k(-) = \Phi_{k-1}P_{k-1}(+)\Phi_{k-1}^T + Q_{k-1}, \\
\text{State Estimate Update} & x_k(+) = x_k(-) + K_k[z_k - H_k x_k(-)], \\
\text{Error Covariance Update} & P_k(+) = [I - K_k H_k]P_k(-), \\
\text{Kalman Gain Matrix} & K_k = P_k(-)H_k^T[H_k P_k(-)H_k^T + R_k]^{-1},
\end{array}
\tag{A.1}
$$

with $x_k(-)$ being the prediction of the state vector at epoch k and $x_k(+)$ being the state estimation at epoch k.

Therefore, the Kalman filter can be described by the four different steps shown in A.2.

The Kalman filter consists in either a forward filter (with positive time increments between steps) or a backward filter (with negative time increments between steps).

At each epoch, the state vector and the associated covariance matrix are stored in a file in order to allow the solution to be smoothed. A smoother is simply an epoch by epoch weighted mean of the forward and backward solution.

As explained in chapter 6:

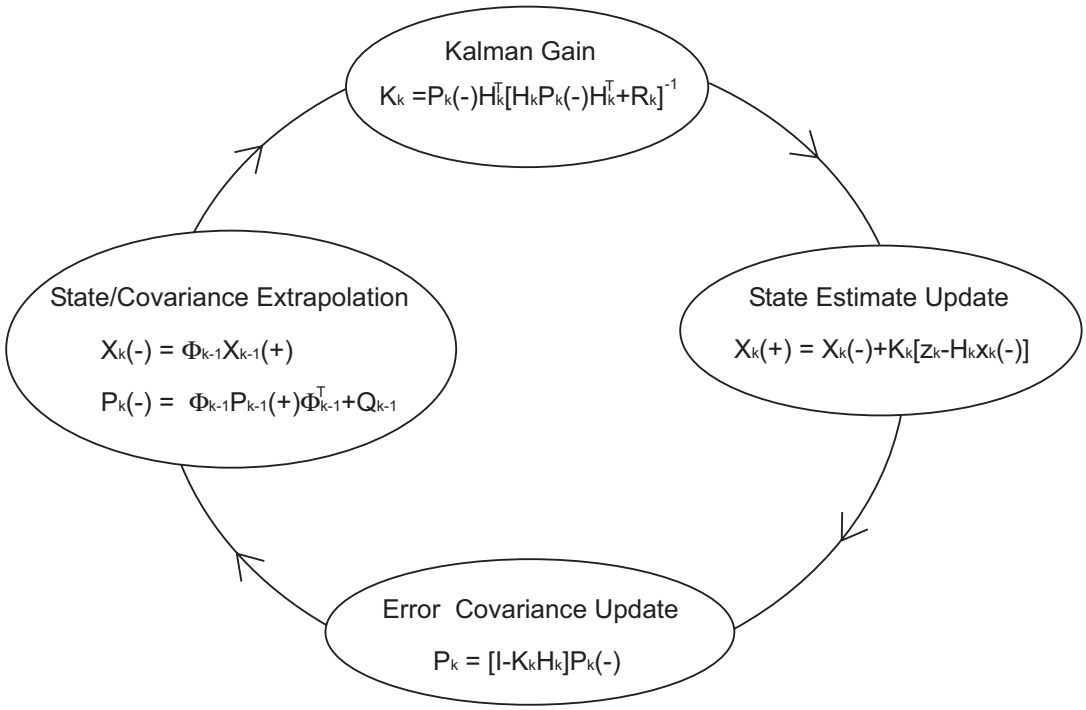

Figure A.2: The four steps describing a general Kalman Filter

$$\begin{array}{ll} \hat{x}_f & \text{forward estimate at epoch t,} \\ P_f & \text{forward error covariance at epoch t,} \\ & \\ \hat{x}_b & \text{backward estimate at epoch t,} \\ P_b & \text{backward error covariance at epoch t,} \\ & \\ \hat{x}(t/T) & \text{smoothed estimate at epoch t,} \\ P(t/T) & \text{smoothed error covariance at epoch t.} \end{array} \tag{A.2}$$

Then the smoothed solution is,

$$\begin{aligned} P(t/T) &= \frac{1}{\frac{1}{P_f}+\frac{1}{P_b}} = \frac{P_bP_f}{P_b+P_f}, \\ \hat{x}(t/T) &= P(t/T)(\frac{\hat{x}_f}{P_f}+\frac{\hat{x}_b}{P_b}). \end{aligned} \tag{A.3}$$

A.2.1 Parameter elimination

When a new satellite rises, it is clear that the state vector increases its size as new parameters need to be estimated (ambiguity parameters, ionospheric parameters). If a loss of lock to a given satellite occurs (a rather common situation in kinematic surveys), a new ambiguity parameter needs to be estimated as well. Therefore, the state vector needs to increase its size by estimating new parameters. It is also desirable to decrease its size (in order to maintain the computational burden as low as possible) by not maintaining useless parameters such as ambiguity parameters from satellites no longer in view.

If x is the state vector and P its associated covariance of dimensions n and nxn, respectively, the inclusion of one additional parameter is rather simple. The new state and covariance matrix is:

$$\tilde{x} = \begin{pmatrix} x_1 \\ \vdots \\ x_n \\ x_{n+1} \end{pmatrix} \tag{A.4}$$

$$\tilde{P} = \begin{pmatrix} & & 0 \\ & P_{(nxn)} & \vdots \\ & & 0 \\ 0 & \cdots & 0 \; \sigma^2_{n+1} \end{pmatrix} \tag{A.5}$$

If the state vector contains n parameters and the last parameter must be eliminated from the state vector and associated covariance, then the state vector must decrease its size while the covariance matrix must be resized by taking the corresponding submatrix. If x is the state vector and P its covariance matrix, the transformed matrix is:

$$\tilde{x} = \begin{pmatrix} x_1 \\ \vdots \\ x_{n-1} \end{pmatrix} \tag{A.6}$$

$$\tilde{P} = C_{11} \tag{A.7}$$

with

$$P = \left(\begin{array}{c|c} C_{11} & C_{12} \\ \hline C_{21} & C_{22} \end{array}\right) \quad \begin{array}{lcrcl} C_{11} & \rightarrow & (n-1) & \text{x} & (n-1) \\ C_{12} & \rightarrow & (n-1) & \text{x} & 1 \\ C_{21} & \rightarrow & 1 & \text{x} & (n-1) \\ C_{22} & \rightarrow & 1 & \text{x} & 1 \end{array} \tag{A.8}$$

In case the parameter that needs to be eliminated is not the last one of the state vector, a reordering of the state vector and covariance matrix must be performed prior to the parameter elimination. The reordering is achieved through the following transformation (substituting parameter i for parameter j):

$$\begin{aligned} \tilde{x} &= x \cdot M, \\ \tilde{P} &= M^T \cdot P \cdot M, \end{aligned} \tag{A.9}$$

where M is

$$M = \begin{pmatrix} 1 & & & & & & & & \\ & \cdot & & & & & & & \\ & & 1 & & & & & & \\ & & & 0_{i,i} & & 1_{i,j} & & & \\ & & & & 1 & & & & \\ & & & & & \cdot & & & \\ & & & & & & 1 & & \\ & & & 1_{j,i} & & 0_{j,j} & & & \\ & & & & & & & 1 & \\ & & & & & & & & \cdot \\ & & & & & & & & & 1 \end{pmatrix} \tag{A.10}$$

A.2.2 Covariance matrix decomposition

At each step the Kalman filter starts with a state vector and its associated covariance matrix. Because of the high correlation between the estimated parameters and of numerical problems it is not unusual that the main properties of the covariance matrix (symmetry and positive definiteness) are no longer maintained. Therefore, if the procedures described in A.2 are applied, the system will not be convergent.

The best way of maintaining the properties of the covariance matrix P is by using the Cholesky factorization of P into an upper triangular (U) and diagonal matrix (D), so that the covariance matrix will read:

$$P = UDU^T. \tag{A.11}$$

Given an upper triangular (U) and diagonal matrix (D), the composition UDU^T is always a symmetrical, positive-definite matrix. Then, a way of guaranteeing numerical stability is to use the Cholesky factorization in the Kalman filter estimator instead of the original P matrix.

Optionally, TraDer can perform the computations using either the standard Kalman filter equations or the UDU^T estimate covariance updating algorithm from Beirman [Bie77].

For covariance prediction, the block triangular aspect of the transfer function Φ permits the following implementation:

$$\tilde{U} = \Phi U. \tag{A.12}$$

Then the error covariance extrapolation is

$$UDU_k^T(-) = \tilde{U}D\tilde{U}^T + \sigma a a^T, \tag{A.13}$$

where σ is the noise associated to the state parameters and a is the process noise associated to the time since the update.

For the error covariance update, the relevant equations are

$$\begin{array}{lcl} K & = & UDU^T(-)H^T[HUDU^T(-)H^T + R]^{-1}, \\ UDU^T(+) & = & UDU^T(-) - KHUDU^T(-). \end{array} \tag{A.14}$$

There are several algorithms for computing the above equations maintaining the UDU^T factorization of the covariance matrix, for instance the modified Cholesky decomposition explained in [GA93].

The factorization of the covariance matrix ensures that the properties of this matrix (symmetry and positive definiteness) are maintained. In addition, since U is upper triangular, there exist very efficient algorithms for the computation of the required values.

Appendix B

Photogrammetric approach for the determination of the vector between primary and secondary kinematic antennas

GPS derived trajectories have been used in photogrammetry for many years in the determination of photograph projection centers [Col93]. Nowadays, direct orientation of airborne sensors is becoming more popular and the number of flights with GPS/IMU data is increasing every year [ABT01]. Taking the trajectory and attitude of the aircraft as observations, the observational model used in photogrammetry is

$$X^e_{k_1}(t) = X^e_{pc}(t) + r^e_n(\lambda(\mathrm{t}), \phi(\mathrm{t}))r^n_b(\Phi(\mathrm{t}), \Theta(\mathrm{t}), \Psi(\mathrm{t}))r^b_c(d)V_{off}, \tag{B.1}$$

where

$$\begin{aligned}
X^e_{k_1}(t) &= \text{coordinates of the GPS antenna i at time t in an ECEF frame (e-frame),} \\
X^e_{pc} &= \text{coordinates of the projection center at time t,} \\
r^e_n(\lambda(\mathrm{t}), \phi(\mathrm{t})) &= \text{matrix depending on the geographical position } \lambda, \phi, \\
r^n_b(\Phi(\mathrm{t}), \Theta(\mathrm{t}), \Psi(\mathrm{t})) &= \text{attitude provided by the IMU (Roll} = \Phi, \text{ Pitch}=\Theta, \\
&\quad \text{Heading} = \Psi), \\
r^b_c(d) &= \text{misalignment matrix between the IMU frame and the aircraft frame (c-frame),} \\
V_{off} &= \text{antenna offset between the GPS antenna and the projection center in the aircraft frame.}
\end{aligned} \tag{B.2}$$

Assuming the camera does not move during a flight, the value V_{off} is a constant vector in the airplane fixed reference system (c-frame) measured with high precision (a few millimeters) prior to the flight; $r^b_c(d)$ is a matrix for correcting the difference in orientation between the c-frame and the instrumental frame of the IMU (b-frame). As the IMU is kept fixed to the aircraft, this matrix is also constant and can be determined in a calibration flight with an accuracy of 10 arcseconds; $r^n_b(\Phi(\mathrm{t}), \Theta(\mathrm{t}), \Psi(\mathrm{t}))$ is the rotation matrix between the b-frame and the navigation frame (n-frame) determined by the IMU measurements. Finally, the $r^e_n(\lambda(\mathrm{t}), \phi(\mathrm{t}))$ matrix is a matrix for correcting the difference in orientation between the n-frame and the ECEF (Earth-Centered-Earth-Fixed) frame also known as e-frame. This matrix is computed from the position of the aircraft $(\lambda(\mathrm{t}), \phi(\mathrm{t}))$. Having the approximate position of the airplane, this matrix can be computed with enough accuracy (a 30 m error in the position used for the computation implies a 1 arcsecond error in the determination of the $r^e_n(\lambda(\mathrm{t}), \phi(\mathrm{t}))$ matrix.)

If we have two antennas k_1 and k_2 in the aircraft and we generalize equation B.1, we obtain

$$\begin{array}{rcl} X^e_{k_1}(t) & = & X^e_{pc}(t) + r^e_n(\lambda(\mathrm{t}), \phi(\mathrm{t}))r^n_b(\Phi(\mathrm{t}), \Theta(\mathrm{t}), \Psi(\mathrm{t}))r^b_c(d)V_{off_1}, \\ X^e_{k_2}(t) & = & X^e_{pc}(t) + r^e_n(\lambda(\mathrm{t}), \phi(\mathrm{t}))r^n_b(\Phi(\mathrm{t}), \Theta(\mathrm{t}), \Psi(\mathrm{t}))r^b_c(d)V_{off_2}, \end{array} \tag{B.3}$$

where $X^e_{pc}(t)$ is the projection center of the camera at time t. Thus, if at every epoch of the flight equations B.3 are subtracted, we have determined the vector between antennas k_1 and k_2 at every epoch in an ECEF system:

$$X^e_{k_2}(t) - X^e_{k_1}(t) = r^e_n(\lambda(\mathrm{t}), \phi(\mathrm{t}))r^n_b(\Phi(\mathrm{t}), \Theta(\mathrm{t}), \Psi(\mathrm{t}))r^b_c(d)(V_{off_2} - V_{off_1}). \tag{B.4}$$

The expression of $(V_{off_2} - V_{off_1})$ corresponds to the vector between the primary and secondary antennas in the aircraft reference frame (c-frame)$\upsilon_{c\,(k_2,k_1)}$. Substituting it in equation B.4 we obtain equation 6.33:

$$X^e_{k_2}(t) - X^e_{k_1}(t) = r^e_n(\lambda(\mathrm{t}), \phi(\mathrm{t}))r^n_b(\Phi(\mathrm{t}), \Theta(\mathrm{t}), \Psi(\mathrm{t}))r^b_c(d)\upsilon_{c\,(k_2,k_1)}, \tag{B.5}$$

with $X^e_{k_2}(t) - X^e_{k_1}(t)$ being $\upsilon_{e\,(k_2,k_1)}(t)$, the vector between the kinematic antennas at time t in an ECEF frame.

The constant matrix $r^b_c(d)$ in B.5 must be determined to compute the vector between kinematic antennas $X^e_{k_2}(t) - X^e_{k_1}(t)$. Note that this matrix is the same one used in the photogrammetric model equation B.1. Therefore, it can be computed by performing an aerial triangulation from a calibration flight.

Appendix C

List Abbreviations

ADOP	Ambiguity Dilution Of Precision
AS	Anti Spoofing
AT	Aerial Triangulation
C/A	Clear Acquisition Code
CODE	Center for Orbit Determination in Europe
DGPS	Differential Global Positioning System
DTM	Digital Terrain Model
ECEF	Earth Centered Earth Fixed
EKF	Extended Kalman Filter)
EUREF	European Reference Frame
FAA	Federal Aviation Administration
GAGE	Group of Astronomy & Geomatics
GDGPS	Global Differential GPS
GNSS	Global Navigation Satellite System
GPS	Global Positioning System
GRACE	Gravity Recovery and Climate Experiment
ICC	Institut Cartogràfic de Catalunya
IG	Institut de Geomàtica
IGDG	Internet based Global Differential GPS
IGEB	Interagency GPS Executive Board
IGS	International GPS Service
IMU	Inertial Measurement Unit
LEO	Low Earth Orbit
LWF	Laboratory-Workshop-Factory
MCAR	Multiple Carrier phase Ambiguity Resolution
MDB	Minimal Detectable Bias
MEO	Medium Earth Orbit
NASA	National Aeronautics and Space Administration
NAVSTAR	Navigation System with Time and Ranging
NIMA	National Imagery and Mapping Agency
OTF	On The Fly
PDOP	Position Dilution Of Precision
PPM	Parts Per Million
PPP	Precise Point Positioning
RMS	Root Mean Square
RTK	Real Time Kinematic
SA	Selective Availability

SAR	Synthetic Aperture Radar
TCAR	Triple Carrier phase Ambiguity Resolution
TEC	Total Electron Content
UERE	User Equivalent Range Error
UPC	Universitat Politècnica de Catalunya
WAAS	Wide Area Augmentation System
WADGPS	Wide Area Differential GPS
WG	Working Group
WGS84	World Geodetic System 1984
WVR	Water Vapor Radiometer
TEC	Total Electron Content
UERE	User Equivalent Range Error

Acknowledgements

I would like to express my gratitude for the support of many people that helped me write this Thesis.

To my parents, for their dedication and encouragement throughout my education years.

To my wife and my little children, Alba, Inés and Biel, for supporting and understanding me all this time.

To Jaume Miranda and Josep Lluís Colomer (Director and Deputy Director of the ICC), responsible for my continuous work in the field of Geodesy, for encouraging me in the search of new ideas and developments. In addition, ICC provided all the data used for this work.

To Manuel Hernández-Pajares, tutor of this Thesis at the UPC.

Finally, to my supervisor Ismael Colomina, who introduced me to the amazing world of Geodesy and GPS positioning and supervised this Thesis.

Mataró, March 2003.